Charles University

Faculty of Science

Study programme: Physical Chemistry

mgr inż. Rafał Łukasz Konefał

Interactions in solutions and gels of stimuli-responsive polymer systems investigated by NMR spectroscopy

Ph.D. Thesis

Supervisor: RNDr. Jiří Spěváček, DrSc.

Institute of Macromolecular Chemistry AS CR

Department of NMR Spectroscopy

PRAGUE 2018

Univerzita Karlova

Přírodovědecká fakulta

Studijní program: Fyzikální chemie

mgr inż. Rafał Łukasz Konefał

INTERAKCE V ROZTOCÍCH A GELECH NA PODNĚTY REAGUJÍCICH POLYMERNÍCH SYSTÉMŮ STUDOVANÝCH NMR SPEKTROSKOPIÍ

Dizertační práce

Školitel: RNDr. Jiří Spěváček, DrSc.

Ústav makromolekulární chemie AV ČR, v.v.i.

NMR Spektroskopie

PRAHA 2018

Declaration:

I declare that I have written this thesis independently under the supervision of RNDr. Jiří Spěváček, DrSc. I did not submit this work, or a part of it, to obtain another university degree. To the best of my knowledge, I have cited all the sources I have used.

Prague 22.01.2018

Signature

"A scientist in his laboratory is not a mere technician: he is also a child confronting natural phenomena that impress him as though they were fairy tales."

Maria Skłodowska-Curie

Acknowledgments

First of all, I would like to thank to my supervisor RNDr. Jiří Spěváček, DrSc. for his support, patience, time and worth advices on NMR.

I would like to thank to all my colleagues from the NMR Department at the Institute of Macromolecular Chemistry AS CR, v. v. i. for their help and support.

This work would not exist without colleagues from Institute of Macromolecular Chemistry AS CR, v. v. i. who synthesized; Eva Čadová, Peter Černoch, Eliézer Jäger, Svetlana Petrova, Beata Strachota and analyzed by DLS and SEC (Peter Černoch, Eliézer Jäger), studied compounds used in this dissertation.

Special thanks belong to my family for their faith and support not only during my Ph. D. studies.

Table of Contents

Abstract

Stimuli-responsive (stimuli-sensitive, intelligent, or smart) polymers are polymer materials which, after small external stimuli, evidently change their physical or chemical properties. Smart polymers can be classified according stimuli they respond to such as: temperature changes, mechanical stress, light irradiation, ultrasonic treatment, application of external magnetic as well as electric field, changes of pH, ionic strength, addition of the chemical agents and presence of biomolecules and bioactive molecules. Stimuli-responsive synthetic polymer systems has attracted considerable attention due to wide range of applications, i.e. controlled drug delivery and release systems, diagnostics, tissue engineering and 'smart' optical systems, as well as biosensors, microelectromechanical systems, coatings, and textiles. Among the types of stimuli for this dissertation temperature, pH and reactive oxygen species (ROS) responsive polymer systems were studied. In case of thermoresponsive polymers, when polymer chains are molecularly dissolved in a good solvent, changes (increasing or decreasing) of temperature result in insolubility (globular nanoparticles formation) of polymer chains, called temperature induced phase-separation. pH responsive polymers change properties such as: solubility, volume (gels), chain conformation as well as which bonds can cleavage upon changes in pH of environment. The ROS responsivity results in changes in solubility, hydrolysis, phase transition, and/or degradation of polymer chains.

In this work ^{1}H NMR spectroscopy was applied for structure and temperature induced phase transition characterization (during gradual heating and/or cooling) of various thermoresponsive polymer systems based on: poly(2-ethyl-2-oxazoline), poly(*N*-isopropylacrylamide), poly(vinyl methyl ether), as well as for study of the: interactions between the reaction mixture components, behavior of reaction mixture during the cooling processes (to freezing) and for following the course of polymerization reaction *in situ* in poly(*N*-isopropylacrylamide)/Laponite XLS cryogels. Moreover ^{1}H (and/or ^{13}C) NMR were used for polymer structure and degradation products characterization of novel MPEO-PCL diblock copolymers with acid labile ketal group as a block linkage (pH responsive), pinacol-type boronic ester self-immolative and biodegradable polyoxalate prodrug based on the anticancer chemotherapeutic hormone analog diethylstilbestrol (ROS-degradable). For thermoresponsive polymers ^{1}H spin-spin relaxation times (temperature and time dependences) were measured to follow the changes in interactions and molecular motions of polymer, water and/or additive in solution. Additionally, in case of copolymers for characterization of conformational changes of polymer chains 2D NOESY spectra were recorded.

Keywords: stimuli-responsive, phase transition, temperature, pH, ROS, copolymers, cryogel, PNIPAm, PEO, PVME, PEOx, PCL, ^{1}H NMR, ^{1}H spin-spin relaxation times, 2D NOESY

Abstrakt

Na podněty reagující (na podněty citlivé nebo inteligentní) polymery jsou polymerní materiály, které na malé vnější podněty očividně mění své fyzikální nebo chemické vlastnosti. Inteligentní polymery lze klasifikovat podle podnětů, na které reagují, jako jsou změny teploty, mechanické namáhání, ozáření světlem, aplikace ultrazvuku, aplikace vnějšího magnetického či elektrického pole, změny pH, iontové síly, přidání chemických činidel a přítomnost biomolekul či bioaktivních molekul. Na podněty reagující systémy syntetických polymerů přitahují značnou pozornost díky širokému spektru aplikací, jako jsou systémy pro řízené dodávání a uvolňování léčiv, diagnostiku, tkáňové inženýrství a "inteligentní" optické systémy, stejně jako biosenzory, mikroelektromechanické systémy, nátěry a textilie. V této disertaci byly studovány polymerní systémy reagující na teplotu, pH a reaktivní kyslík (ROS). V případě termoresponsivních polymerů, kdy jsou v dobrém rozpouštědle polymerní řetězce molekulárně rozpuštěny, se změnami teploty (zvýšení nebo pokles) dochází k teplotou-indukované fázové separaci a tvorbě globulárních nanočástic. Polymery reagující na pH mění své vlastnosti, jako jsou rozpustnost, objem (gely), konformace řetězce, jakož i vazby, které se mohou při změnách pH štěpit. ROS-responzivita může vést ke změnám rozpustnosti, k hydrolýze, fázovému přechodu a/nebo degradaci polymerních řetězců.

V této práci byla ^{1}H NMR spektroskopie použita k strukturní charakterizaci u teplotou-indukovaného fázového přechodu (při postupném ohřevu a/nebo chlazení) u různých termoresponsivních polymerních systémů na bázi poly(2-etyl-2-oxazolinu), poly(N-isopropylakrylamidu) a polyvinylmetyléteru, jakož i ke studiu interakcí mezi složkami reakční směsi, chování reakční směsi během ochlazování (vymražování) a ke sledování polymerizační reakce in situ u systémů poly(N-isopropylakrylamid)/Laponit XLS. Kromě toho ^{1}H (a/nebo ^{13}C) NMR spektroskopie byla využita i k charakterizaci polymerních struktur a degradačních produktů nových dvoublokových kopolymerů MPEO-PCL s labilní ketalovou skupinou tvořící spojku mezi bloky (pH-citlivé), polymerů pinakolového typu boronového esteru a biodegradovatelných polyoxalátů na bázi protinádorového chemoterapeutického hormonového analogu diethylstilbestrolu (ROS-responzivní). Ke sledování změn v interakcích a molekulárních pohybech polymeru, vody a/nebo přísady byly u roztoků termoresponsivních polymerů měřeny ^{1}H spin-spinové relaxační doby (teplotní a časové závislosti). V případě kopolymerů byla k charakterizaci konformačních změn polymerních řetězců měřena též 2D NOESY spektra.

Klíčová slova: na podněty reagující polymery, fázový přechod, teplota, pH, ROS, kopolymery, kryogel, PNIPAm, PEO, PVME, PEOx, PCL, ^{1}H NMR, ^{1}H spin-spinové relaxační doby, 2D NOESY

LIST OF ABBREVIATIONS

APS	ammonium persulfate
D_2O	deuterated water
DEB	diethylstilbestrol
DLS	dynamic light scattering
DMF	dimethylformamide
DMSO	dimethyl sulfoxide
EOx	2-ethyl-2-oxazoline
IMK	3-methyl-2-butanone
LCST	lower critical solution temperature
MEK	methyl ethyl ketone
MOx	2-methyl-2-oxazoline
NIPAm	*N*-isopropylacrylamide
NMR	Nuclear Magnetic Resonance
NOESY	Nuclear Overhauser Effect Spectroscopy
NPs	nanoparticles
PBS	Phosphate-buffered saline
PCL	poly(ε-caprolactone)
PEO	poly(ethylene oxide)
PEOx	poly(*2*-ethyl-2-oxazoline)
PMOx	poly(*2*-methyl-2-oxazoline)
PNIPAm	poly(*N*-isopropylacrylamide)
PVME	poly(vinyl methyl ether)
ROS	reactive oxygen species
SEC	size-exclusion chromatography
T_2	spin-spin relaxation time
TBMK	*t*-butyl methyl ketone
TEMED	*N,N,N',N'*-tetramethylethylenediamine

1 Introduction

1.1 NMR Spectroscopy

From the first observation of proton magnetic resonance in water and in paraffin at 1940s[1,2] **N**uclear **M**agnetic **R**esonance (NMR) spectroscopy becomes one of the most important analytical method and excellent tool not only for the chemical structure characterization, but also for investigation of molecular interactions, as well as molecular motions of plenty of studied materials, inter alia thermoresponsive polymers[3].

NMR spectroscopy takes advantage of the magnetic properties of different nuclei to provide information on molecular structure. Only the nuclei which possess non-zero nuclear magnetic momentum are suitable for NMR spectroscopy. When this kind of nuclei will be placed in strong external magnetic field they align themselves relative to the field in quantized number of orientations. Each of them corresponds to the same number of energy levels involved. The transitions between energy levels can occur by applying magnetic field with correct frequency ν resulting from the resonance condition (see Fig. 1.1)[4];

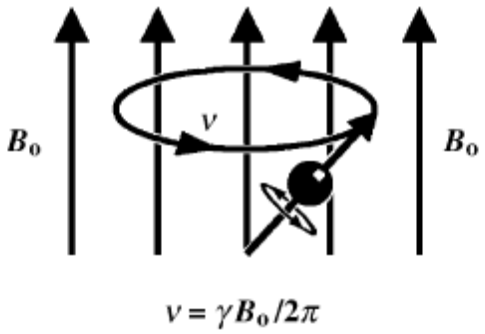

Fig. 1.1 Representation of the precession of the magnetic momentum about the axis of applied magnetic field B_0.

where the term γ is the gyromagnetic ratio, which is a constant value characteristic for the particular nucleus, and B_0 is applied external magnetic field. Gyromagnetic ratio is a crucial parameter for NMR detection sensitivity, higher value of γ results in better observation. The importance of NMR spectroscopy is based on its ability to recognize a particular nucleus according its environment in the molecule. This is related to the fact that applied magnetic field B_0 induces electron cloud surrounding the nucleus, and the local field of nucleus is

different than the applied field. This effect is called magnetic shielding, and nuclei with different chemical environment are differing in the value of resonance frequency. The most popular and widely used nuclei in NMR measurements are: ^{1}H, ^{13}C, ^{15}N, ^{19}F, ^{29}Si and ^{31}P. The majority of them has spin one half, and they are frequently main components of organic or macromolecular compounds. Important factor related to effective sensitivity of NMR measurements is natural abundance of "NMR visible" isotope. For example, by taking into account natural abundance and molar receptivity of ^{1}H (99.98%, 1) and ^{13}C nucleus (1.07%, 0.0159); ^{1}H is around 5700 times more sensitive than ^{13}C, which leads to different times required to record good quality NMR spectra of those nuclei.

The chemical shift δ is the variation of resonance frequency with shielding and can be expressed as a difference between the resonance frequency of the sample ν_s and frequency of reference compound ν_{ref}, as follows:

$$\delta = \frac{\nu_s - \nu_{ref}}{\nu_{ref}} \times 10^6$$

The chemical shift is dimensionless quantity always given in parts per million (ppm). The values of chemical shift are typical for different types of chemical groups where a lower field resonance = higher value of chemical shift.

Second important information about molecular structure is obtained from indirect spin-spin coupling (^{n}J-coupling). This phenomenon describes the interaction between nuclei via *n* chemical bonds. Basically this is an influence of neighboring spins on multiplicity of peaks in the spectrum. The coupling constant *J* which describes the measure how powerfully nuclear spins influence each other, is a distance between the two peaks for the resonance of one nucleus split by another, and is measured in hertz (Hz). Values of *J* represent an interaction through bonds (2-5 covalent bonds in homonuclear proton coupling), and are independent of external magnetic field. *J*-coupling is a helpful parameter to gain information about bond strengths or steric arrangements.

The integral intensity of the signal is the area under the signal curve. By comparison of the intensities in a spectrum, the ratios of the protons in the molecule are obtained. Signal intensities are important in structure determination, as well as to make possible quantitative analysis of the mixtures. In macromolecular chemistry integral intensities are widely used in molecular weight determination (end-group analysis), copolymer composition, and polymer chain structure or conformation characterization.

The nuclear Overhauser effect (NOE) arises from direct through-space magnetic interactions between nuclear spins. The NOE is using a transfer of nuclear spin polarization

from the one Boltzman nuclear spin population distribution to the other one, by cross-relaxation. No *J* coupling need to be present between the nuclei. This effect has great utility in three-dimensional structure determination, and can be detected between nuclei in distance in space less than 5 Å[5].

1.1.1 NMR Experiments

1.1.1.1 1D NMR Experiments

➔^{1}H NMR

The vast majority of organic compounds such as polymers contain hydrogen atoms. Observation of transitions between magnetic energy levels of the most widespread (99.98%) hydrogen isotope ^{1}H (spin number I = ½) is done by ^{1}H NMR spectroscopy. Nowadays proton NMR spectroscopy belongs to the most welcome and frequently used instrumental analytical method in structural analysis of organic compounds. The advantages of the method are: easiness of sample preparation, low concentration of the sample and short time of measurements (usually few minutes). The result of ^{1}H NMR experiment (single pulse sequence) is spectrum with measuring range ≈ 15 ppm (see Fig. 1.2).

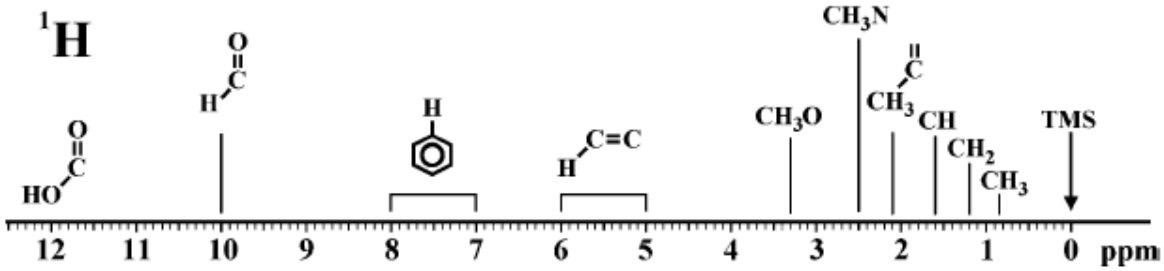

Fig. 1.2 Representation of proton chemical shifts[4].

In general ^{1}H NMR spectrum can be divided in three main regions. Starting from standard tetramethylsilane (TMS) with chemical shift equal to zero, aliphatic protons signals are observed till around 2 ppm. Second region (≈ 2-5 ppm) is covered by signals of protons with electronegative atoms neighborhood (O, N, etc.). The low-field area of the spectrum (≈5-12 ppm) is related to signals of protons attached to unsaturated groups (C=C, C=O, aromatic).

➔ ^{13}C NMR

The direct observation of carbon skeleton of organic compounds is possible by ^{13}C NMR spectroscopy measurements. In comparison to ^{1}H NMR, ^{13}C carbon isotope has low natural abundance (1.07%), and ^{13}C NMR experiment requires much more scans (long time of experiment). Typical ^{13}C NMR measurement is provided by using single pulse sequence with proton decoupling (to avoid splitting of carbon signals). Due to fact that ^{13}C NMR spectrum has broader range (≈ 220 ppm, see Fig. 1.3) than proton one, probability of peaks overlapping is smaller. Similar to proton NMR, ^{13}C NMR spectrum can be divided in three regions with dependency described above.

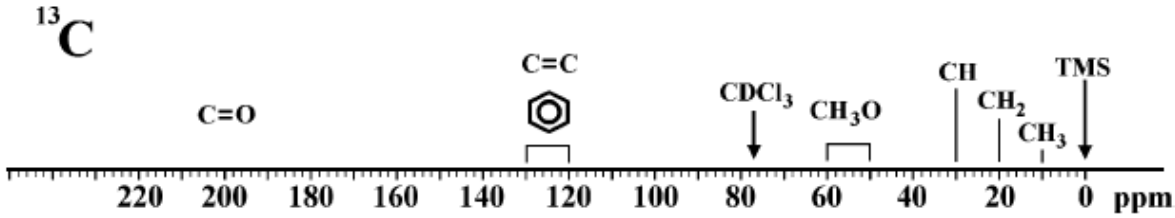

Fig. 1.3 Representation of carbon chemical shifts[4].

1.1.1.2 2D NMR Experiments

In two-dimensional (2D) NMR both abscissa and ordinate are frequency axes. The first frequency dimension is direct measurement of frequency, and in second frequency dimension, magnetic interactions between nuclei through structural connectivity (COSY, HMBC, HSQC), spatial proximity (NOESY, ROESY), or kinetic exchange (EXSY) are shown.

➔ 2D NOESY

The **N**uclear **O**verhauser **E**ffect **S**pectroscop**y** (NOESY) is showing correlation between protons close in space to each other by using their homonuclear NOE interactions. At NOESY spectrum diagonal signals represent ^{1}H NMR spectrum, and cross-peaks are related to pairs of protons with spatial proximity in limited distance ≤ 5 Å. The cross-peaks intensity decreases with a six power distance between nuclei. The NOESY spectra are extremely valuable to clarify conformational problems of macromolecules.

1.1.1.3 Relaxation Experiments

In the NMR experiment radio frequency pulse is applied, and by this action thermal equilibrium of the spin system is disturbed. Following this action, the population ratios are changing, and transverse magnetic field components (M_x and M_y) appears. When the perturbation stops, the system relaxes to re-establish equilibrium condition. They are two relaxation processes: first is characterized by time constant *spin-lattice* (*longitudinal*) *relaxation time* T_1, the relaxation in the applied field direction, and second one is characterized by time constant *spin-spin* (*transverse*) *relaxation time* T_2, relaxation perpendicular to the field direction. A measurement of relaxation times gives important information about mobility in studied compounds.

➔Spin-spin Relaxation (T_2)

The spin-spin relaxation time determines the decay of the *x, y* magnetization and is related to the line-width. Spin-spin relaxation time T_2 constant characterizes molecular mobility which depends on size and/or interactions between solute and solvent. Temperature as well as time measurements allow us to characterization of interactions changes caused by time or some external stimuli. The measurement of spin-spin relaxation time T_2 is carried by using the Carr-Purcell-Meiboom-Gill (CPMG) pulse sequence (see Fig. 1.4 left)[5].

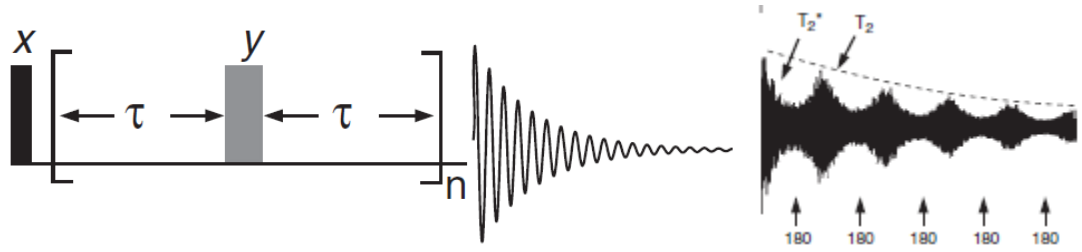

Fig. 1.4 The diagram of Carr-Purcell-Meiboom-Gill (CPMG) pulse sequence (left), and time domain spectrum (right)[5].

The *x* and *y* are $90°_x$ and $180°_y$ pulses, and τ is a delay between $180°_y$ pulse repeating *n* times. T_2 can be determining by performing series of experiments with increasing $2\tau n$ (i.e. 2τ, 4τ, 6τ ... etc.) and record data after the last even echo peak in each case. The decay in intensities of these echoes is determined only by spin-spin relaxation (see Fig. 1.4 right). In solids, viscous liquids, or large molecules in solution T_2 relaxation is fast (short T_2 values) and gives broad signals. In these cases T_2 values can be determined from the *half-height linewidth* $\Delta\nu_{1/2}$, by using the relation[5];

$$\Delta_{\nu_{1/2}} = \frac{1}{\pi T_2^*}$$

1.2 Stimuli-responsive polymers

Polymer materials which, after small external stimuli, significantly change their physical or chemical properties, are called stimuli-responsive (stimuli-sensitive, intelligent, or smart) polymers [6–9]. Stimuli-responsive polymers can be classified according to their physical forms, as well as by the types of stimuli they respond. Based on physical forms these polymers can be divided into: polymeric solutions, covalently crosslinked and physical gels, surfaces and interfaces, and also polymeric solids[10–16]. The types of stimuli can be systematized in three categories of responses: physical, chemical and biochemical (biological)[17]. The physical stimuli is caused by external effects such as temperature changes, mechanical stress, light irradiation, ultrasonic treatment, or application of external magnetic as well as electric field[17–22]. Chemical stimuli includes: changes of pH, ionic strength, or addition of the chemical agents[23–25]. A biochemical stimulus contains presence of biomolecules and bioactive molecules such as enzymes, antigens/antibodies, proteins and glucose[26,27] (see Fig 1.5). The changes cause by the stimuli depends on its type and can be either reversible or irreversible. In addition one stimuli can result in more than one response, and also after multiple stimuli follows one or more responses[28,29]. Furthermore, different responses are expected for various types of stimulus, or physical state. Examples of such responses are connected with changes in polymer-polymer, polymer-solvent interactions (ionic, hydrophobic, van der Waals and hydrogen bonding), conformational changes, micellar formation, swelling/collapsing, change in shape, simple chemical reactions (cross-linking, degradation)[14,30–35].

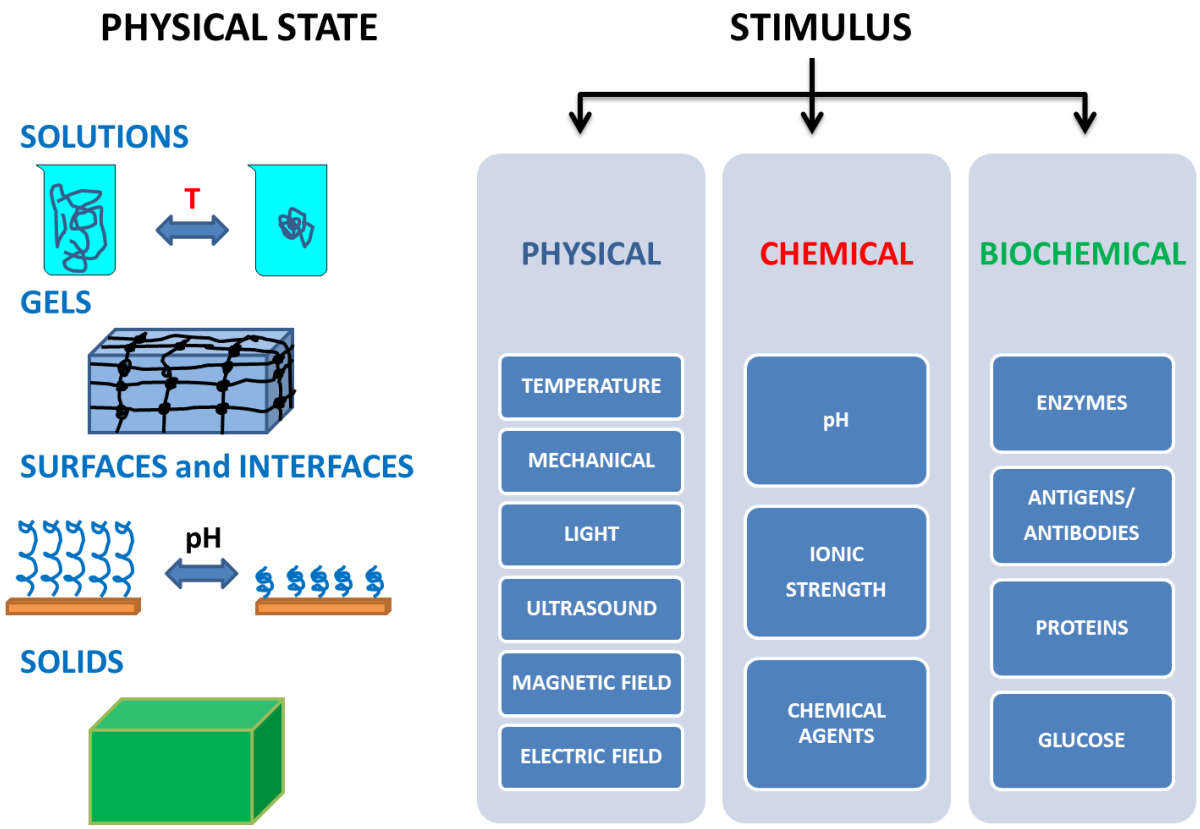

Fig. 1.5 Schematic representation of stimuli-responsive polymers classification according: physical state (left), and types of stimuli (right).

Design and development of stimuli-responsive polymers has great interest due to the wide range of applications such as: control drug and gene delivery systems, bioseparation, sensors and actuators, tissue engineering, chemical valves, membranes with controlled porosity, electronic systems, diagnostics, optical systems, artificial muscles, coatings, textiles, as well as, biocatalysts and gas oil industry[7–12,17,36–50].

From the aforementioned stimuli, in the following, temperature as a most frequently used stimulus will be discussed. Among others pH and reactive oxygen species (ROS) responsive polymers will be briefly reviewed.

1.2.1 Temperature responsive polymers

Among the miscellaneous stimuli aforementioned, due to non-invasive application, temperature is the most extensively employed. Moreover, thermoresponsive behavior of polymer solutions, gels, and surfaces is often completely reversible[51–53]. It is well known that

polymers in solution are sensitive to changes in the temperature, which mostly results in coil size variations[54]. Therefore, according the aforementioned definition of stimuli-responsive polymers, temperature responsive polymers are only those which considerably change their properties with small change in temperature. These changes are typically coil - globule transition in solutions, and volume transition in gels[31,55]. In case of thermoresponsive polymers, when polymer chains are molecularly dissolved in a good solvent, changes (increase or decrease) of temperature result in insolubility (precipitation) of polymer. In other words, the binary polymer/solvent mixture undergoes a temperature induced phase separation from one-phasic to the bi-phasic system (two phases in equilibrium)[56,57]. They are two main types of thermoresponsive polymers; the first, when phase separation occurs as a result of increasing in temperature of solution, system exhibits a lower critical solution temperature (LCST) behavior, and second is the reverse case, when phase separation is observed during decreasing temperature, which is called upper critical solution temperature (UCST) type behavior. As is shown at Figure 1.6 LCST and UCST are critical temperature points of phase separation.

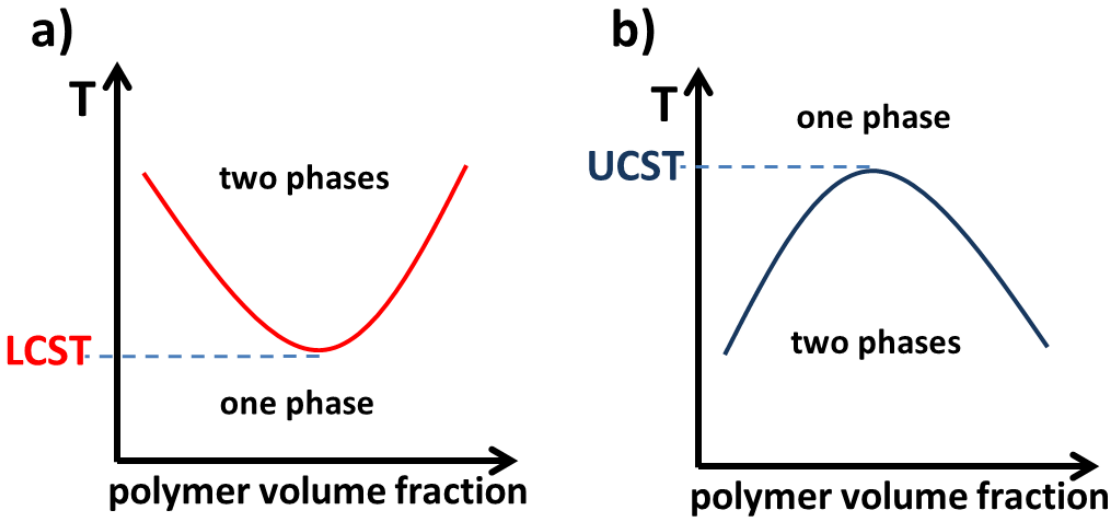

Fig. 1.6 Schematic illustration of phase diagrams for polymer solutions: (a) lower critical solution temperature (LCST) behavior, and (b) upper critical solution temperature (UCST) behavior.

Non-ionic polymers, which exhibit LCST behavior in water, have great interest due to numerous applications. Polymers of this type are hydrophilic and very well soluble at low temperature, but heating results in hydrophobicity of polymer chains. Below the transition temperature of the solution, polymer chains are hydrated, it means that they are forming hydrogen bonds with surrounding molecules of water. Those hydrogen bonds become weaker with increasing temperature, and water molecules are releasing from the polymer structure.

The effect of these changes is dehydration and agglomeration of polymer chains called coil to globule transition of thermoresponsive polymer (Fig. 1.7). From the thermodynamic point of view, using the Gibbs equation $\Delta G = \Delta H - T\Delta S$ (G- Gibbs free energy, H- enthalpy, S- entropy, T- temperature), below LCST hydrogen bonding between water and polymer gives favorable enthalpy contribution due to enhancement ordering of water molecules which interact with the polymer. Consequently, it contributes unfavorably to the entropy of mixing. With increasing of the temperature entropy term becomes prevalent, free energy of mixing gets positive, which is demonstrated in phase separation. In other words, entropy of the water is increasing (water is less ordered when hydrogen bonds between polymer and water are broken) and this is main driving force of the process. This phenomenon is also called "hydrophobic effect"[44,58–60].

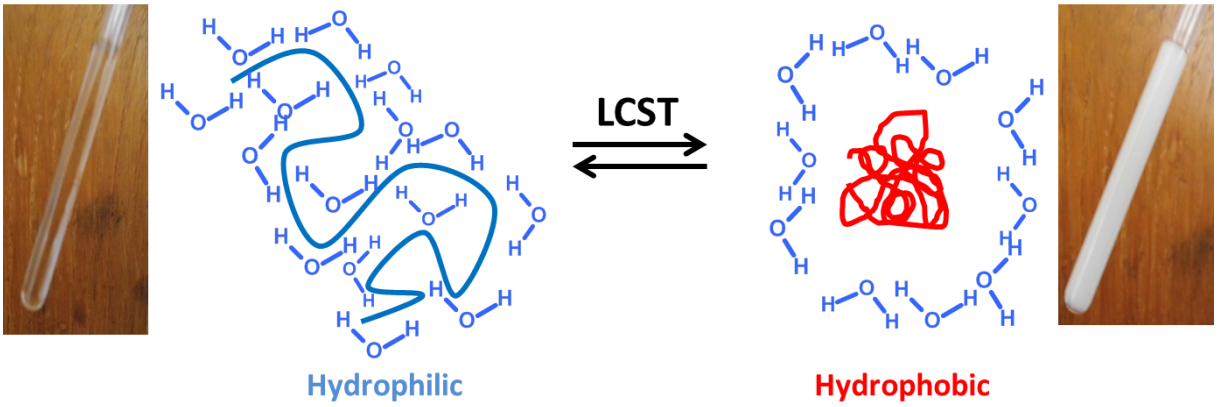

Fig. 1.7 Schematic representation of LCST type coil to globule phase transition, in macroscopic scale observed by turbidity of polymer solution.

Many types of water soluble polymers exhibit LCST type behavior[18,61,62] (examples are shown at Fig. 1.8), according chemical composition those polymers can be divided for three main groups: polymers bearing amide groups, poly(ether)s and phosphorus polymers[60,62]. The most known and widely studied thermoresponsive polymer is poly(*N*-isopropylacrylamide) (PNIPAm), LCST behavior of PNIPAm was firstly reported in 1967-1968, with very sharp transition (with hysteresis during cooling process) and transition temperature around 32°C [63–67]. LCST of PNIPAm is close to human body temperature and can be tuned by incorporation of hydrophilic groups or monomer units, what makes this polymer and its copolymers interesting in biomedical applications[44,68]. PNIPAm belongs to poly(*N*-substituted (meth)acrylamide)s subgroup of thermoresponsive polymers. Other homopolymers from this group with reported LCST are: poly(*N*-n-propylacrylamide) (PNNPAM, LCST≈10°C), poly(*N*-cyclopropylacrylamide) (PNCPAM, LCST≈53°C),

poly(*N,N*-diethylacrylamide) (PDEAM, LCST≈33°C tacticity dependent), poly(*N*-isopropylmethacrylamide) (PNIPMAM, LCST≈43°C), and many others[69–77]. Second subgroup of thermoresponsive polymers bearing amide group are poly(*N*-vinyl amide)s. One of the polymers from this group is poly(*N*-vinyl caprolactam) PVCL, which contains hydrophilic heterocyclic, seven-membered lactam ring. PVCL is non-ionic biocompatible, low toxic, organic and water soluble polymer with phase transition around 31°C. These properties of PVCL, as well as high complexing ability and good film-forming make this polymer interesting for biomedical applications[18,78–82]. From the remaining homopolymers which has amide side chain with the nitrogen directly bonded to the polymer backbone is worth to mention about: poly(*N*-vinyl isobutyramide) (PNVIBA, LCST≈39°C), and poly(*N*-vinyl pyrrolidone) (PVPy, LCST only with the presence of salt)[82,83]. Another class of thermoresponsive polymers are poly(2-alkyl-2-oxazolines) (POx) with nitrogen atom in polymer backbone. Hydrophilicity of POx can be controlled by the length of the side chain of homopolymer: poly(2-methyl-2-oxazoline) (PMeOx) is hydrophilic, thus very well soluble in water, thermoresponsive LCST behavior exhibit poly(2-ethyl-2-oxazoline) (PEOx, LCST≈62°C), poly(2-isopropyl-2-oxazoline) (PiPOx, LCST≈36°C), poly(2-cyclopropyl-2-oxazoline)) (PcPOx, LCST≈30°C) and poly(2-*n*-propyl-2-oxazoline) (P*n*POx, LCST≈36°C) aqueous solutions (critical temperature point depends on molar mass of polymer chains), while polymers with longer side chains are no more soluble in water. Due to their biocompatibility, POx can be used in biomedical applications[38,59,84–87]. Second group of LCST type thermoresponsive polymers constitute poly(ether)s. Poly(ethylene oxide) [or poly(ethylene glycol) (PEO, PEG)], and poly(propylene oxide) [or poly(propylene glycol) (PPO, PPG)] and their copolymers are widely known for their thermoresponsive behavior, especially PEO homopolymer which at high temperatures exhibits both LCST and UCST phase separation called “closed loop”[59]. In PEO-PPO copolymers main driving force for thermoresponsive behavior is amphiphilic balance in the chain structure. Those copolymers depending on composition exhibit cloud points in range 20-85 °C are known as Pluronics, Tetronics, Poloxamers and are commercially available[88–91]. Moreover, short oligo(ethylene glycol) can be used as a side chain. Poly(oligo(ethylene glycol) mathacrylate)s (POEGMA) aqueous solutions exhibit lower values of LCST than high molecular weight linear PEO homopolymers. For example poly(2-(2-methoxyethoxy)ethyl methacrylate) ($PMEO_2MA$) with two ethylene oxide units, and poly(2-[2-(2- methoxyethoxy)ethoxy] ethyl methacrylate) ($PMEO_3MA$) with three ethylene oxide units shows LCST around 26°C and 52°C respectively. Polymers with longer side chains (4-9 ethylene oxide units) exhibit phase

transitions between 60-90°C. Advantage of those polymers is possibility of tuning of the LCST temperature by synthesis of $PMEO_2MA$-*co*- POEGMA copolymers (with variety of monomers ratios)[92–95]. Other type of polymers from this group are poly(vinylether)s. Poly(vinyl methyl ether) (PVME) is the most known and widely studied polymer from this type. PVME exhibits phase transition temperature around 35-36°C, which makes this polymer interesting for biomedical applications. Other thermoresponsive polymers from this type are poly(2-methoxy-ethyl vinyl ether) (PMOVE, LCST≈70°C) and poly(2-(2-ethoxy)ethoxyethyl vinyl ether) (PEOEOVE, LCST≈41°C)[96–98]. Among the polymers bearing phosphorus in monomer repeating unit, homoplymers with reported thermoresponsive behavior can be found. The good examples are biodegradable and biocompatible poly(ethyl ethylene phosphate) (PEP, LCST≈38°C) and poly(isopropyl ethylene phosphate) (PIPP, LCST≈5°C), as well as poly[(alkyl ether) phosphazens] with transitions between 30-80°C[99–102].

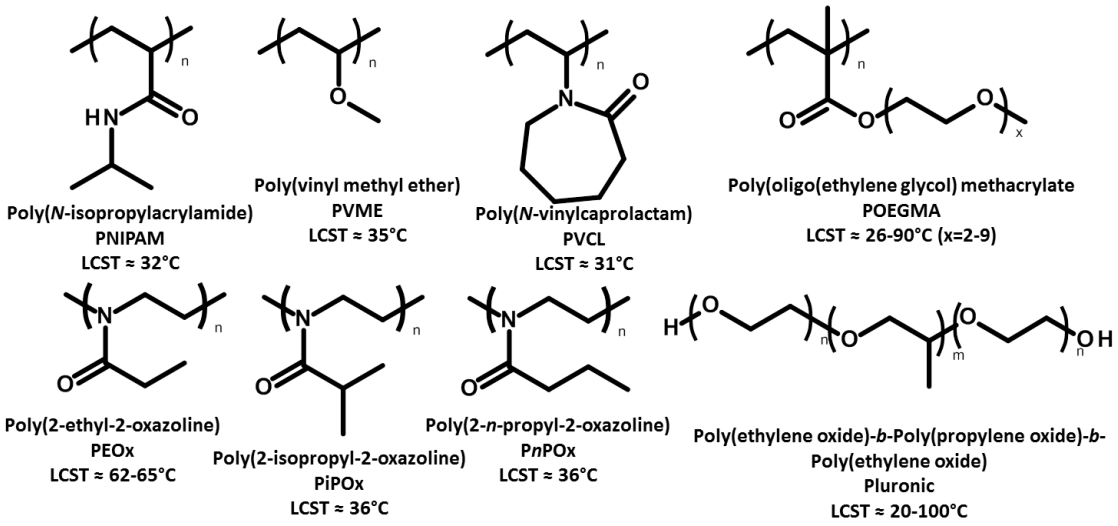

Fig. 1.8 Examples of temperature sensitive polymers and their LCST.

The most common experimental technics for study thermoresponsive polymers are: optical and UV turbidimetry, light scattering, X-ray and neutron scattering, calorimetry, fluorescence, IR spectroscopy, Raman spectroscopy, viscometry, dielectric spectroscopy, theoretical studies, as well as NMR spectroscopy[51,52,82,89,96,103–114]. Among aforementioned methods NMR spectroscopy is giving quantitative information about the LCST phase separation behavior. NMR relaxation time and diffusion experiments can show changes in molecular motions of polymer and water in solution. 2D NOESY measurements give information about conformational changes of polymer chains. To characterize coil to globule phase separation it is required to measure series of ^{1}H NMR spectra during gradual heating or/and cooling processes. When polymer is thermoresponsive like PNIPAm, with increasing

temperature the spectra show a visible reduction in integral intensities of all signals related to the polymer (example for PNIPAm aqueous solution (c=5% wt) is presented at Fig. 1.9 a). This result is evidently related to the fact that with increasing temperature, the mobility of the polymer chains decreases to such an extent that they escape from detection in high-resolution NMR spectra. Next for quantitative characterization of changes occurring during the heating or/and cooling processes, the values of the fraction p for units with significantly reduced mobility can be calculated by using the relation presented at Fig. 1.9c[115], where $I(T)$ is the integrated intensity of given polymer signal in the spectrum at given temperature T and $I(T_0)$ is the integrated intensity of this signal when no phase transition or other reason for the reduced mobility of polymer segments occurs. For T_0 it is necessary to choose the temperature where the integrated intensity of the given signal is the highest and therefore $p(T_0) = 0$. Additionally, in denominator of the equation one should take into account the fact that the integrated intensities should decrease with absolute temperature as $1/T$. In the last step temperature dependence of p- fraction can be obtained (Fig. 1.9b), and phase separation is described by three parameters (Fig. 1.9d): extent of separation (p_{max}) which gives information about how many percent of polymer chains change from coil to globular state, transition width shows temperature range in which phase separation occurs, and LCST - phase transition temperature (point at temperature axis at 0.5 of p_{max}).

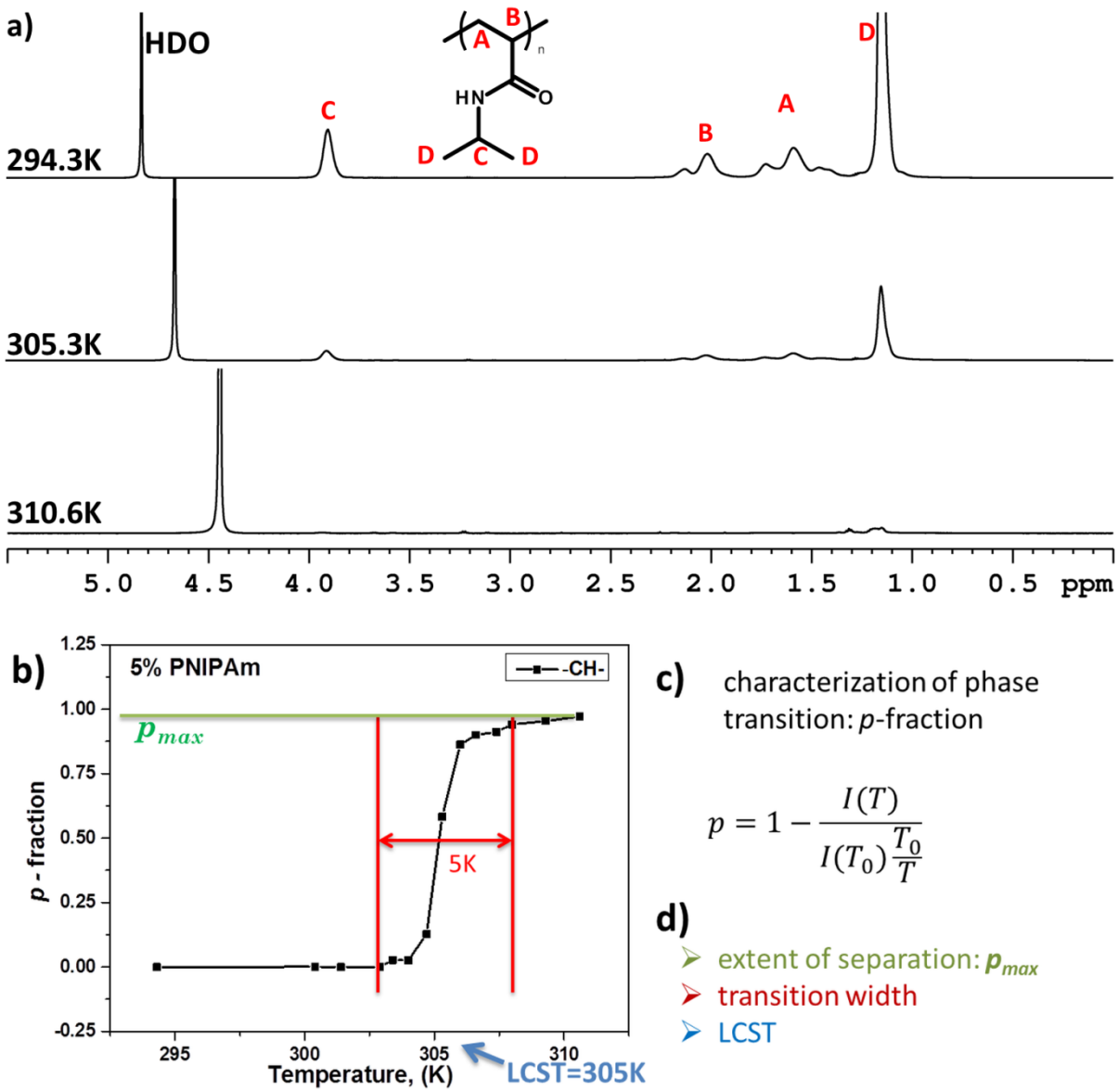

Fig. 1.9 ^{1}H NMR characterization of phase transition: 600.2 MHz ^{1}H NMR spectra of PNIPAm D_2O solution (c=5 wt%) measured at 294.3, 305.3 and 310.6 K under the same instrumental conditions (peak assignments with structure are above top spectrum) (a), temperature dependence of *p*- fraction of PNIPAm aqueous solution (c=5%wt) (CH isopropyl group) (b), *p*- fraction equation (c), and parameters describe phase transition (d).

1.2.2 Other stimuli responsive polymers

➔pH responsive polymers

pH responsive polymers change properties such as: solubility, volume (gels), chain conformation as well as which bonds can cleavage upon changes in pH of environment. Due to the fact that pH values vary in the human body, for example at the tissue level, cancerous

and inflamed tissues have lower pH than healthy tissues; this type of polymers has attracted considerable attention due to potential application as drug delivery agents. Generally pH responsive polymers can be divided into three groups: acidic, basic and pH neutral. Polymers having acidic or basic groups accept or release protons with changes of pH values. Depending on their pK_a values, they obtain polyelectrolyte nature at acidic or basic pH. Therefore this ionic/non-ionic transition change hydrophilicity of polymer in aqueous phase and results in reversible precipitation/solubilization of polymer chains, hydrophilic/hydrophobic behavior of polymeric surfaces and swelling/deswelling in hydrogels. pH responsive acidic group constitute polymers with carboxylic, sulfonic acid, phosphoric acid, aminoacid and boronic acid groups. Group of weak polybases includes polymers with tertiary amine, morpholino, pyrrolidine, piperazine, as well as, pyridine and imidazole groups. Additionally dendrimers such as: poly(amidoamine), poly(ethylene imine) and poly(propylene imine) can be also classified as pH responsive polymers. pH responsive neutral polymers contain in main or side chain acid-labile moieties, which usually degrade under mild acidic conditions. In most cases this kind of bonds is used as a linker between polymer and drug in polymer-drug conjugates. Drug is released in target (i.e. cancerous or inflamed tissue) by cleavage of the linker. Typical pH-labile bonds used in polymer systems are, hydrazone, acetal/ketal, imine, orthoester and others[6,23,43,67,116–119].

➔Reactive oxygen species (ROS) responsive polymers

Reactive oxygen species (ROS) such as hydrogen peroxide (H_2O_2), hydroxyl radicals (HO•), singlet oxygen ($^1O_2$), super oxide radicals ($O_2^{\bullet -}$) are produced by the body as a result of many physiological processes. In healthy cells ROS are produced with low concentration and have crucial role in metabolism (i.e. cell growth, migration, apoptosis). On the other hand, higher ROS production leads to oxidative stress and inflammation events (damage of cellular DNA, protein and lipid molecules) and is correlated to cancer and other diseases. This high local concentration of ROS can be used in design and production of ROS responsive delivery systems. The ROS responsivity results in changes in solubility, hydrolysis, phase transition, as well as, degradation of polymer chains[25,32,43,45,120–122]. The chemical structures of some ROS responsive systems are depicted at Figure 1.10[122].

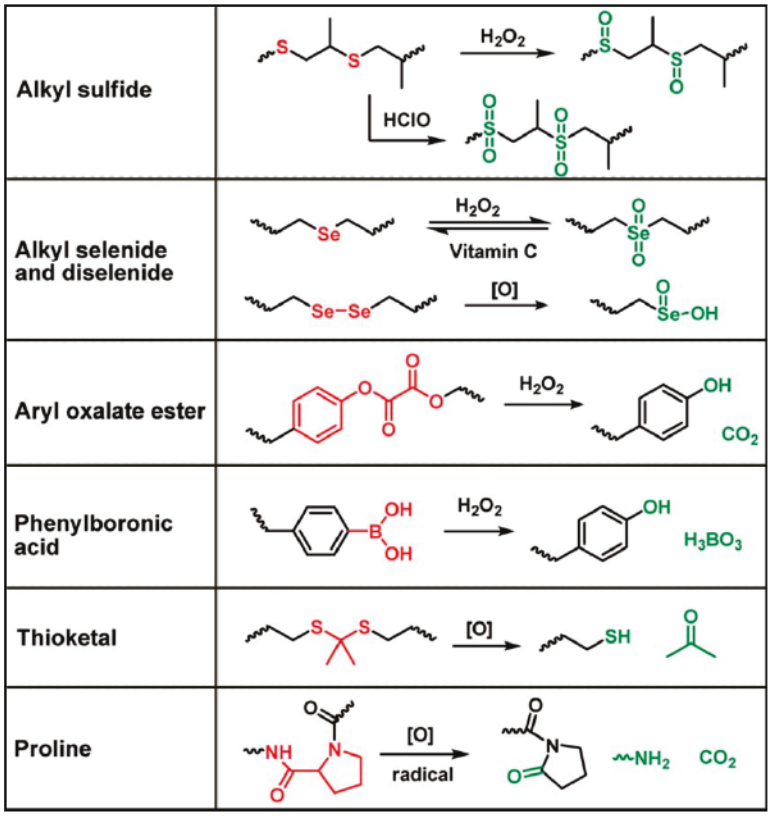

Fig. 1.10 Oxidation-responsive motifs and their oxidation products[122].

2 Aims of the study

The aim of this study is to apply various NMR spectroscopy methods for:

- Characterization of solution behavior of thermoresponsive poly(2-ethyl-2-oxazoline) based homopolymers and copolymers in aqueous solutions.

- Study of thermoresponsive behavior of nanoparticles aqueous solutions of terpolymers containing poly(ethylene oxide), poly(2-ethyl-2-oxazoline) and poly(ε-caprolactone) blocks.

- Characterization of thermoresponsive behavior of aqueous solutions of block copolymers of PEO and PNIPAm.

- Studies of interactions and polymerization kinetics of poly(N-isopropylacrylamide)/clay hydrogels.

- Characterization of additive effects on phase transition and interactions in poly(vinyl methyl ether) solutions.

- The structure determination and responsivity studies of novel pH and ROS responsive polymer systems.

3 List of publications included in the thesis

Publication 1

R. Konefał, J. Spěváček, P. Černoch: *Thermoresponsive poly(2-oxazoline) homopolymers and copolymers in aqueous solutions studied by NMR spectroscopy and dynamic light scattering*

European Polymer Journal 2018, in production

Publication 2

R. Konefał, J. Spěváček, E. Jäger, S. Petrova: *Thermoresponsive behaviour of terpolymers containing poly(ethylene oxide), poly(2-ethyl-2-oxazoline) and poly(ε-caprolactone) blocks in aqueous solutions: an NMR study.*

Colloid and Polymer Science, **2016**, 294, 1717-1726.

Publication 3

J. Spěváček, **R. Konefał**, J. Dybal, E. Čadová, J. Kovářová: *Thermoresponsive behavior of block copolymers of PEO and PNIPAm with different architecture in aqueous solutions: a study by NMR, FTIR, DSC and quantum-chemical calculations.*

European Polymer Journal, **2017**, 94, 471-483.

Publication 4

J. Spěváček, **R. Konefał**, E. Čadová: *NMR study of thermoresponsive block copolymer in aqueous solution.*

Macromolecular Chemistry and Physics, **2016**, 217, 1370-1375.

Publication 5

J. Spěváček, **R. Konefał**, J. Dybal: *Temperature-induced phase transition in aqueous solutions of poly(N-isopropylacrylamide)-based block copolymer.*

Macromolecular Symposia, **2016**, 369, 92-96.

Publication 6

B. Strachota, L. Matejka, A. Zhigunov, **R. Konefał**, J. Spevacek, J. Dybal, R. Puffr: *Poly(N-isopropylacrylamide)-clay based hydrogels controlled by the initiating conditions: evolution of structure and gel formation.*

Soft Matter, **2015**, 11, 9291-9306.

Publication 7

B. Strachota, L. Matějka, A. Sikora, J. Spěváček, **R. Konefał**, A. Zhigunov, M. Šlouf: *Insight into the cryopolymerization to form poly(N-isopropylacrylamide)/clay macroporous gel. Structure and phase evolution.*

Soft Matter, **2017**, 13, 1244-1256.

Publication 8

L. Starovoytova, J. Šťastná, A. Šturcová, **R. Konefał**, J. Dybal, N. Velychkivska, M. Radecki, L. Hanyková: *Additive effects on phase transition and interactions in poly(vinyl methyl ether) solutions.*

Polymers, **2015**, 7, 2572-2583.

Publication 9

S. Petrova, E. Jäger, **R. Konefał**, A. Jäger, C. de Garcia Venturini, J. Spěváček, E. Pavlova, P. Štěpánek: *Novel poly(ethylene oxide monomethyl ether)-b-poly(ε-caprolactone) diblock copolymers containing a pH-acid labile ketal group as a block linkage.*

Polymer Chemistry, **2014**, 5, 3884-3893.

Publication 10

E. Jäger, A. Höcherl, O. Janoušková, A. Jäger, M. Hruby, **R. Konefał**, M. Netopilik, J. Panek, M. Slouf, K. Ulbrich, P. Stepanek: *Fluorescent boronate-based polymer nanoparticles with reactive oxygen species (ROS)-triggered cargo release for drug-delivery applications.*

Nanoscale, **2016**, 8, 6958-6963.

Publication 11

A. Höcherl, E. Jäger, A. Jäger, M. Hruby, **R. Konefał**, O. Janoušková, J. Spevacek, Y. Jiang, P. W. Schmidt, T. P. Lodge, P. Stepanek: *One-pot synthesis of reactive oxygen species (ROS)-self-immolative polyoxalate prodrug nanoparticles for hormone dependent cancer therapy with minimized side effects.*

Polymer Chemistry, **2017**, 8, 1999-2004.

4 Summary of the results

4.1 PEOX homopolymers and gradient copolymers (publication 1)

In this part structural changes during temperature-induced phase transition in D_2O solutions of poly(2-ethyl-2-oxazoline) (PEOx) and P(EOx-*grad*-2-methyl-2-oxazoline (MOx)) copolymers were investigated by ^{1}H NMR spectroscopy, ^{1}H spin-spin relaxation times (temperature and time dependences) and 2D NOESY at various temperatures. Herein obtained results fully reported in **publication 1** (see Appendix) are briefly discussed. Two PEOx homopolymers (with M_n=17200 and 5900), two P(EOx/MOx) gradient copolymers with ≈75/25 ratio of monomer units (M_n= 15100 and 6300), and two P(EOx/MOx) gradient copolymers with monomer ratio ≈50/50 (M_n= 10200 and 7300) were prepared by Peter Černoch using cationic ring-opening polymerization of EOx and MOx in acetonitrile, initiated by methyl p-tosylate.

^{1}H NMR spectra and fraction *p* of units with significantly reduced mobility.

Figures 4.1.1 and 4.1.2 shows high-resolution ^{1}H NMR spectra of a D_2O solution (c=5 wt%) of the PEOx-H homopolymer and P(EOx/MOx)(53/47)-H gradient copolymer measured under the same instrumental conditions at three temperatures. The assignment of resonances to various proton types is shown directly in the spectra measured at 360 K and chemical structure of polymers is shown at the figures. ^{1}H NMR spectra presented in Figures were measured at temperatures below the LCST (down), in the middle of the transition (middle) and above the LCST (up) of studied polymers. The most significant effect observed in the spectra is a visible reduction in integral intensities of all signals related to polymers units. This effect is evidently related to the fact that with increasing temperature, the mobility of the part of polymer segments which form globular-like structures (mesoglobules) decreases to such an extent that they escape detection in high-resolution NMR spectra. Nevertheless, this effect is much weaker in copolymer solution.

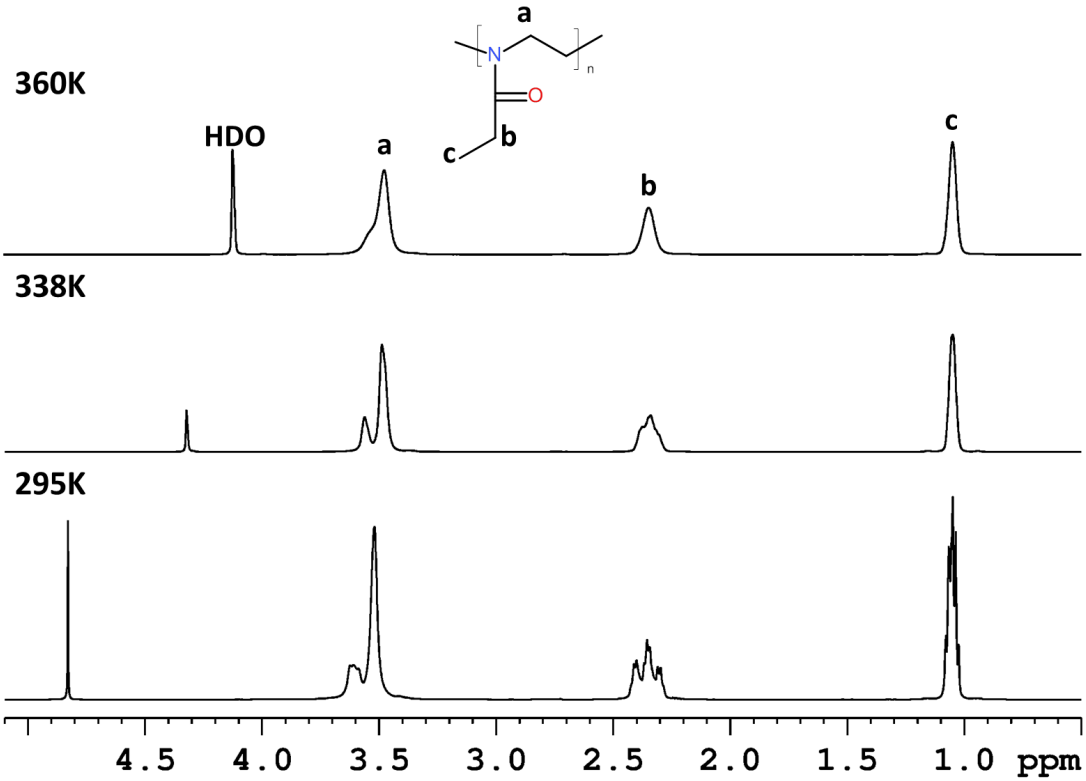

Fig. 4.1.1 600.2 MHz ^{1}H NMR spectra of PEOx-H homopolymer in D_2O solution (c=5 wt%) measured at 295, 338 and 360 K under the same instrumental conditions.

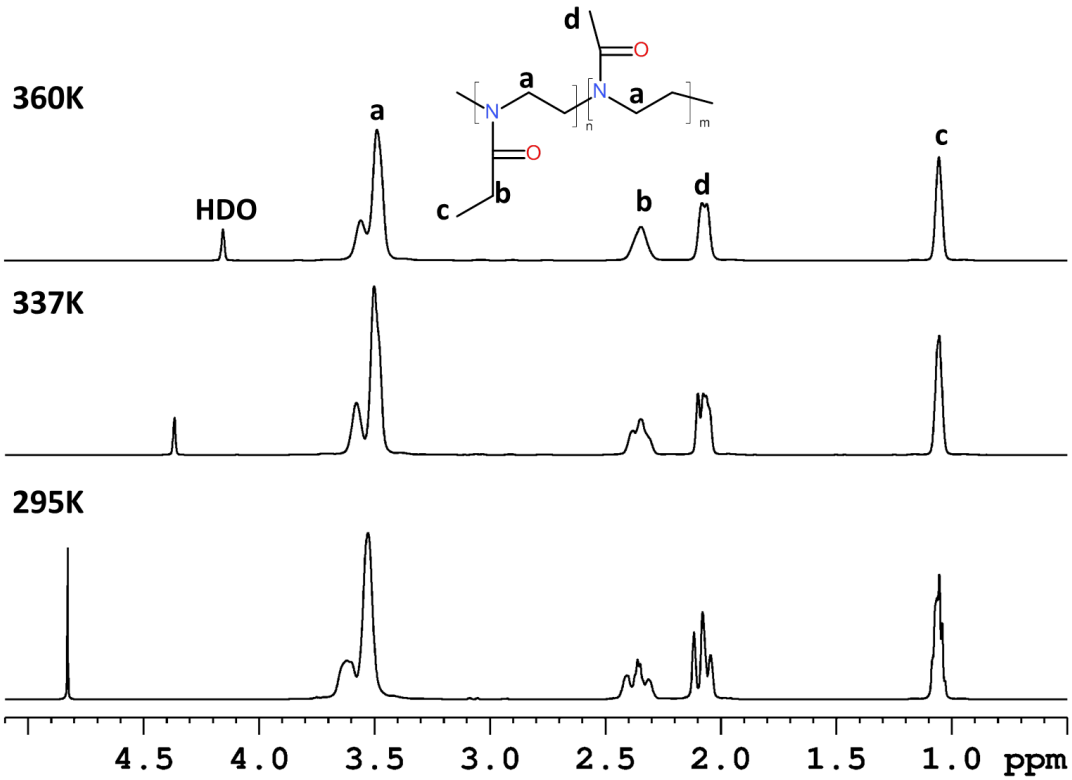

Fig. 4.1.2 600.2 MHz ^{1}H NMR spectra of P(EOx/MOx) (53/47)-H copolymer in D_2O solution (c=5 wt%) measured at 295, 337 and 360 K under the same instrumental conditions.

Quantitative characterization of changes appearing during the heating and cooling process, can be provide from integrated intensities in ^{1}H NMR spectra by calculation the *p*-fraction values of the units with significantly reduced mobility by using equation presented at Fig. 1.9c. Temperature dependences of the fraction *p* of D_2O solutions (c=5 wt %) of all investigated homopolymers and copolymers are shown in Fig. 4.1.3. Additionally for comparison in the Figure is also shown temperature dependence of the *p*-fraction for PNIPAM (M_n = 35480) in D_2O solution (c=5 wt %) (dashed line). In comparison with PNIPAM which exhibit sharp (transition width 2 K) and complete (maximum value of the *p*-fraction, p_{max} = 1) phase transition, the transition of PEOx homopolymers is broader and around 20% ($p_{max} \approx 0.8$) of PEOx units possess high mobility and do not participate in the phase transition. Moreover, much higher (than for PNIPAM) values of LCST (defined as the temperature at $p_{max}/2$) of the PEOx depends on the polymer molecular weight (higher molecular weight - lower LCST). In contrast to PEOx homopolymers, for P(EOx-*grad*-MOx) copolymers D_2O solutions very broad and virtually independent of copolymer composition phase transition is observed. Values of *p*-fraction gradually increase from 315 K without any noticeable jump (transition width at least ≈45 K) and reach much lower maximum values (range of p_{max} = 0.32 – 0.44). Additionally, temperature dependences of the fraction *p* determined from integrated intensities of various PEOx and P(EOx-*grad*-MOx) signals are the same for heating and cooling processes so confirming that *p*-fraction relates to EOx and/or MOx units as a whole.

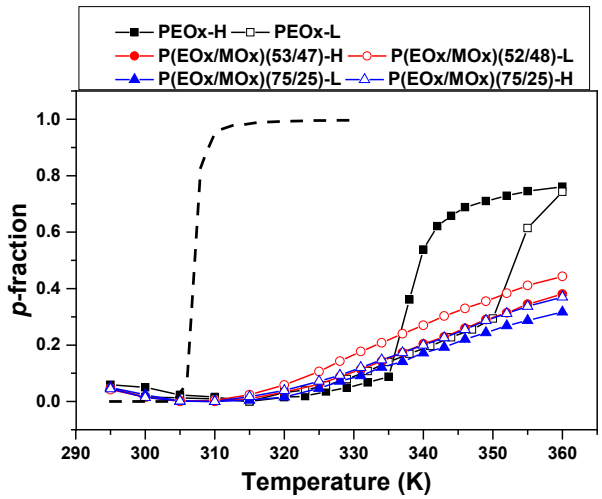

Fig. 4.1.3 Temperature dependences of the fraction *p* of units with significantly reduced mobility in D_2O solutions (*c* = 5 wt%) of PEOx homopolymers (PEOx-H, PEOx-L) and P(EOx-*grad*-MOx) copolymers (P(EOx/MOx)(52/48)-L, P(EOx/MOx)(53/47)-H, P(EOx/MOx)(75/25)-L, P(EOx/MOx)(75/25)-H) during gradual heating. Dashed line shows for comparison temperature dependence of the *p*-fraction for D_2O solution (*c* = 5 wt%) of PNIPAM.

The reversibility of the phase transition was characterized by measurements of the sample during gradual cooling directly after heating process. Figure 4.1.4 shows temperature dependences of the fraction *p* in D_2O solutions (c=5 wt%) of the homopolymer PEOx-H (a)(similar behavior was obtained for PEOx-L homopolymer) and copolymer P(EOx/MOx)(53/47)-H (b) (similar behavior for other copolymers) during gradual heating and subsequent gradual cooling. For the PEOx homopolymer (Fig. 4.1.4a) values of *p*-fraction remain almost unchanged in the whole range of temperatures of measurements during gradual cooling which means that on the molecular level the phase transition of PEOx homopolymer is irreversible. This is in contrast with the fact that the sample of PEOx-H in D_2O was transparent after pulling out from the magnet at 295 K and results obtained by macroscopic cloud point measurements on 0.5 wt% solutions reported in literature. In case of copolymer samples it is observed reversible phase separation with some hysteresis (Fig. 4.1.4b).

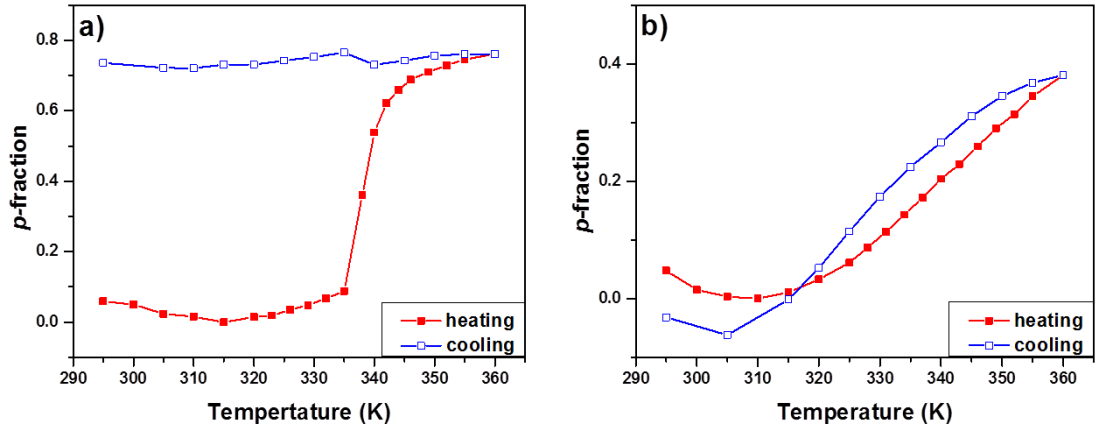

Fig. 4.1.4 Temperature dependences of the fraction *p* of units with significantly reduced mobility in D_2O solutions (*c* = 5 wt%) of PEOx-H homopolymer (a) and P(EOx/MOx)(53/47)-H copolymer (b) during gradual heating and subsequent gradual cooling.

In next step of the investigation, effect of polymer concentration on transition temperatures was studied. For this purpose solutions of the PEOx-H homopolymer and P(EOx/MOx)(53/47)-H copolymer were prepared with three different polymer concentrations *c* = 0.5, 5 and 20 wt%. In Fig. 4.1.5 are shown the *p*-fraction temperature dependences in the PEOx-H (a) and P(EOx/MOx)(53/47)-H (b) solutions recorded for these concentrations during gradual heating. Similarly to 5 wt% concentration samples, all polymer proton types show the same *p*-fraction temperature behavior. It is clearly visible from the Fig. 4.1.5a that for the PEOx-H homopolymer the way of transition for *c* = 0.5 wt% and *c* = 5 wt% is very similar. Completely different character of the transition shows solution with *c* = 20 wt% concentration. In this case higher starting value of the *p*-fraction at 295 K is gradually

increasing from 310 K to 335 K; next it drops to reach the minimum at 345 K and then again rise. Decreasing *p*-fraction values (in 335-345 K) is a result of increasing mobility of polymer segments at these temperatures. PEOx-H solution (c = 20 wt%) is very viscous (jelly-like) at room temperature. We assume that at temperatures 335-345 the respective physical network structure is breaking and reorganizing, and this process was confirmed by DSC measurements. Similar behavior of 20 wt% solution was also obtained for second homopolymer PEOx-L. Figure 4.1.5b shows results obtained for P(EOx/Mox)(53/47)-H copolymer in D_2O solutions. In contrast to homopolymes these dependences are very similar; in all cases the established LCST values somewhat decrease with increasing concentration.

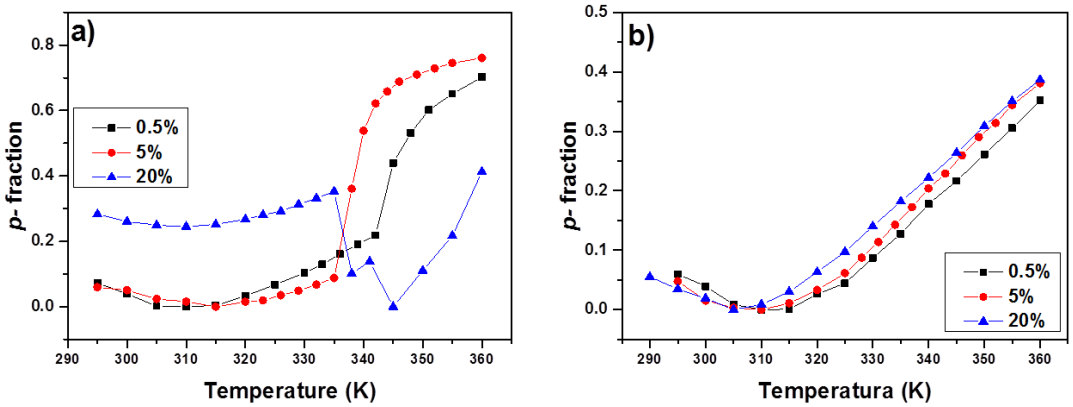

Fig. 4.1.5 Temperature dependences of the fraction p of PEOx-H homopolymer (a) and P(EOx/MOx)(53/47)-H copolymer (b) in D_2O solutions with three polymer concentrations (c = 0.5; 5; 20 wt%) during gradual heating.

Spin-Spin Relaxation Times T_2 of Water (HDO) Molecules

Information on behavior of water molecules and polymer-solvent interactions (hydration) during phase-transition in water solutions was obtained by spin-spin relaxation times T_2 measurements. Experiments were measured at temperatures based on the temperature dependence of the *p*-fraction. Results obtained for PEOx-L homopolymer D_2O solution (c = 5 wt%) are shown in Fig. 4.1.6: temperature dependence (Fig. 4.1.6a) and time dependence at 360 K (Fig. 4.1.6b). Results presented in Fig. 4.1.6a show that while at temperatures below 335 K the T_2 relaxation curves were monoexponential, at $T \geq 335$ K, i.e., in the transition region and above the transition, the relaxation curves were non-exponential and two T_2 components were necessary to fit experimental relaxation curves. These data show the existence of two types of water at temperatures above 335 K. First type is "free water" with longer relaxation times which are similar as T_2 values at lower temperatures (T_2 = 3-4 s) which corresponds to HDO molecules in solution. Second type is "bound" water with T_2

values which are 2 orders of magnitude shorter (T_2= 42 ms at 335 K, T_2= 21 ms at 360 K) which corresponds to HDO molecules bound (confined, entrapped) inside the collapsed globular structures. These values are virtually constant for both types of water molecules showing that arrangement with "free" and "bound" water is stable at least for 12 hrs (Fig. 4.1.6b).

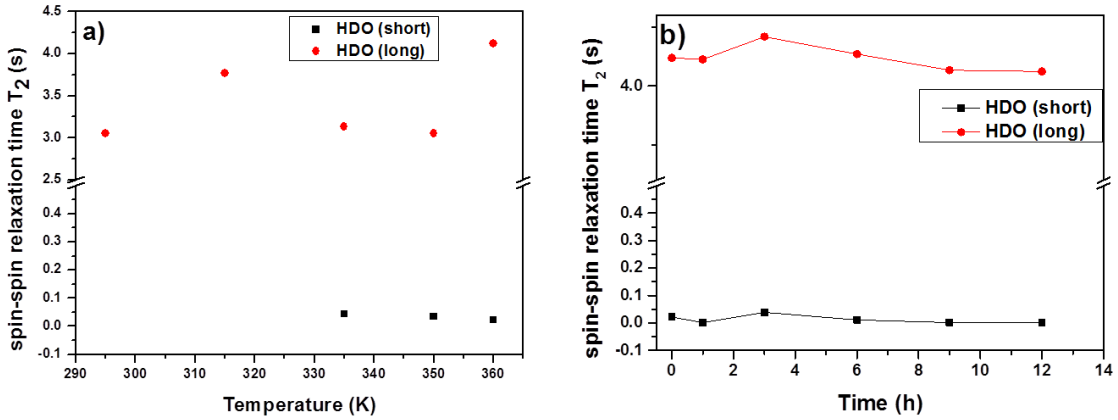

Fig. 4.1.6 Temperature dependence (a) and time dependence at 360 K (b) of ^{1}H spin-spin relaxation times T_2 of HDO in D_2O solution (c = 5 wt%) of the PEOx-L homopolymer.

2D ^{1}H-^{1}H NOESY NMR spectra

To obtain information on spatial proximity between proton groups of EOx and MOx units, on D_2O solutions (c = 5 wt%) of P(EOx/MOx)(75/25)-L and P(EOx/MOx)(53/47)-H copolymers we measured 2D ^{1}H-^{1}H NOESY NMR spectra at three temperatures: at 295 K (below the transition), 340 K (in the middle of the transition) and 360 K (above the transition) (Fig. 4.1.3). These copolymers have relatively low values of the p-fraction (p_{max} = 0.32 and 0.44, respectively) at 360 K and therefore a major part of these copolymers is directly detected in high-resolution NMR spectra at this temperature. NOESY spectra recorded for the P(EOx/MOx)(75/25)-L sample are shown in Fig. 4.1.7. In spectrum measured at 295 K (Fig. 4.1.7a), cross-peaks between various proton groups of EOx or MOx units were detected, as well as weaker cross-peaks between side chain CH_3 or CH_2 protons of EOx units (signals at 1.05 ppm and 2.35 ppm, respectively) and CH_3 protons of MOx units (signal at 2.1 ppm). EOx and MOx units which are in close proximity (<0.5 nm) can be both from the same chain of the copolymer, assuming random-coil conformation of copolymer chains at room temperature, and from different copolymer chains. At 340 K the cross-peaks between EOx and MOx protons disappeared and cross-peaks between various proton groups of EOx or MOx units are weaker (Fig. 4.1.7b). In the NOESY spectrum measured at 360 K (Fig. 4.1.7c)

all cross-peaks disappeared (only the residual cross-peak between side chain CH_3 and CH_2 protons of EOx units remained) in spite of the fact that at this temperature 68% of copolymer segments (Fig. 4.1.3) are directly detected in NMR spectra.

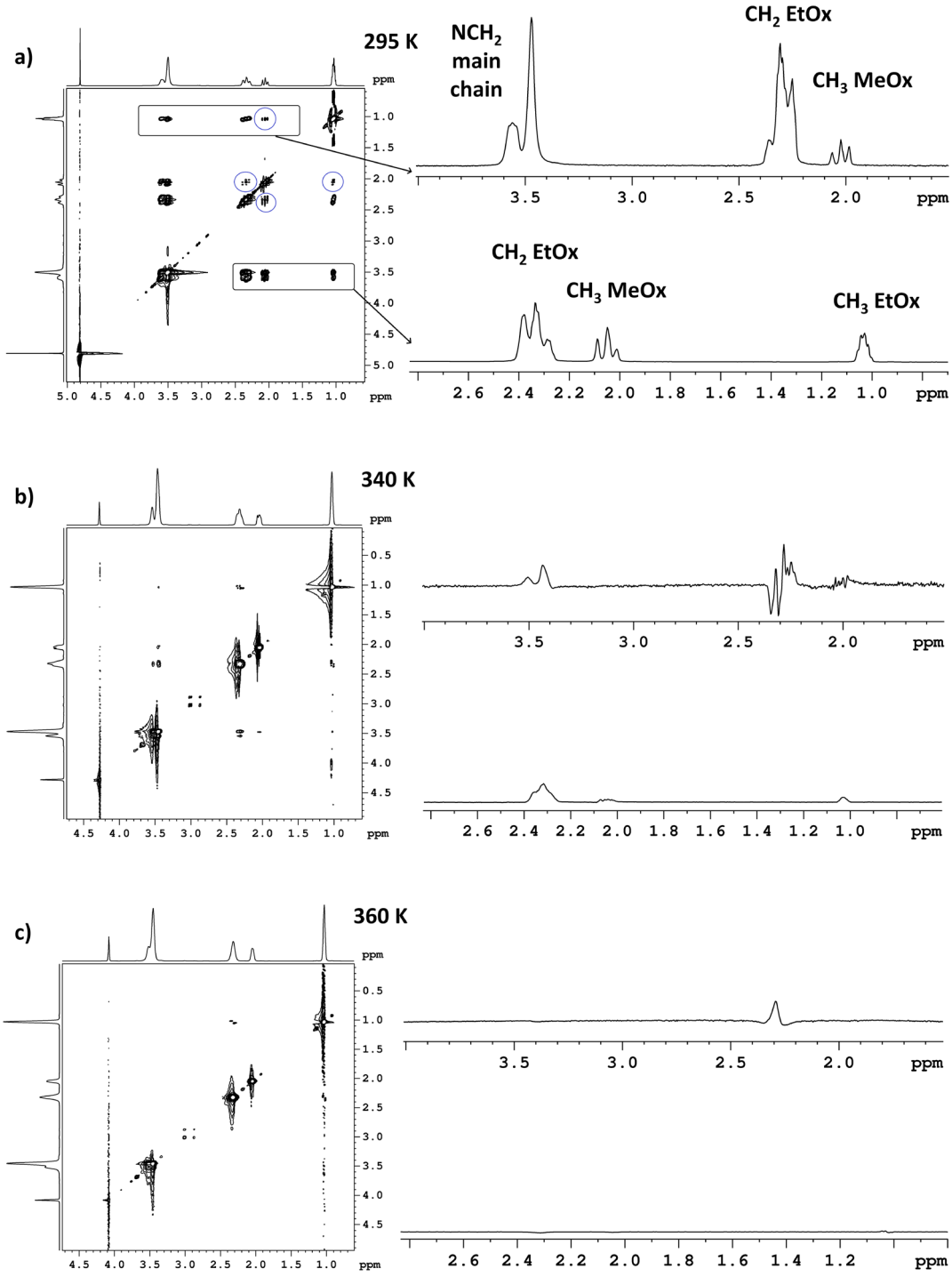

Fig. 4.1.7 2D NOESY spectra of P(EOx/MOx)(75/25)-L copolymer in D_2O solution measured at three temperatures with mixing time 600 ms. On the right there are 1D slice spectra extracted from the signal at 1.05 ppm of CH_3 protons of EOx units (in Figure 4.1.2 signal „c“) (at the top) and from the signal at 3.55 ppm of NCH_2 protons of both EOx and MOx units (in Figure 4.1.2 signal „a“).

For the quantitative characterization of the intensity changes of the cross-peaks, integrated intensities of signals of EOx and MOx proton groups in 1D slices extracted from the signal of CH_3 protons of EOx units at 1.05 ppm of the NOESY spectra (Fig. 4.1.7) were used. Temperature dependences of the absolute integrated intensities in slices were obtained from 2D NOESY for P(EOx/MOx)(75/25)-L copolymer D_2O solution (c = 5 wt%) measured with mixing times 100 ms, 200 ms and 600 ms, as well as for D_2O solution (c = 5 wt%) of the copolymer P(EOx/MOx)(53/47)-H measured with mixing time 200 ms. In all cases similar results were observed. Cross-peaks intensities decreases in the middle of the transition region (at 340 K) and drops to 0 at higher temperature (360 K). Additionally, cross-peak intensity between ethyl CH_3 and CH_2 protons of EOx units at 340 and 360 K is visibly reduced. Due to the fact that distance between protons of ethyl group cannot change with temperature it was assumed that there is other reason of this reduction and T_1 relaxation times of polymer were measured. From measurements of spin-lattice relaxation times T_1 it was found that in transition region with increasing temperature we move towards T_1 minimum where NOESY is ineffective. This is combined with the fact that in about one third of polymer segments their mobility is reduced to such an extent that they escape detection in high-resolution NMR spectra.

In summary, measurements of ^{1}H NMR spectra, 2D ^{1}H-^{1}H NOESY spectra and ^{1}H spin-spin relaxation time T_2 were used for the characterization of structural changes on molecular level and behavior of water molecules during the temperature-induced phase transition of thermoresponsive PEOx homopolymers and P(EOx-*grad*-MOx) copolymers in D_2O solutions. Temperature dependences of the p-fraction show that for D_2O solutions of PEOx homopolymers the phase transition is relatively sharp and transition temperatures substantially depend on molecular weight and concentration of the solution, as well as local structures formed during heating are preserved during cooling (irreversible phase transition on the molecular level). An anomalous dependence of the p-fraction observed for PEOx solution of higher concentration (c = 20 wt%) is presumably in connection with existence of physical network at room temperature; the network is disrupted around 350 K. For D_2O solutions of P(EOx-*grad*-MOx) gradient copolymers the temperature dependences of the p-fraction are the same for EOx and hydrophilic MOx units with very broad (~45 K) reversible (small hysteresis) phase transition. Temperature dependences of the p-fraction are for P(EOx-*grad*-MOx) copolymers virtually independent of the content of MOx units and molecular weight , and only slightly dependent on concentration of the solution. At the same time the maximum

values of the *p*-fraction are for copolymers very low (p_{max} = 0.32-0.44). From measurements of ^{1}H spin-spin relaxation times T_2 of HDO, a very similar behavior of the water molecules in homopolymer and copolymer solutions was observed. In all investigated solutions two types of water, „free“ and „bound“ with long and very short T_2 values, respectively, were detected at temperatures in the transition region and above the transition. 2D ^{1}H-^{1}H NOESY NMR spectra show that some EOx and MOx units are in close contact at room temperature. With increasing temperature the respective cross-peaks in NOESY spectra disappear though at 360 K there are still ~60-68% of copolymer segments that are directly detected in 1D ^{1}H NMR spectra. From the fact that at 340 and 360 K also intensity of the cross-peak between ethyl CH_3 and CH_2 protons of EOx units is markedly reduced it follows that reduced intensities of cross-peaks in NOESY spectra at elevated temperatures are mainly due to the reduced mobility of copolymer segments including those which remain hydrated and therefore are directly detected in NMR spectra.

4.2 PEOX block copolymers (publication 2)

Herein, NMR characterization of thermoresponsive behavior of terpolymers containing hydrophilic poly(ethylene oxide), thermoresponsive poly(2-ethyl-2-oxazoline) and hydrophobic poly(ε-caprolactone) blocks in aqueous solutions fully reported in **publication 2** (see Appendix) is briefly discussed. One linear poly(ethylene oxide)-*b*-poly(*2*-ethyl-2-oxazoline)-*b*-poly(ε-caprolactone) (PEO_{44}-*b*-$PEOx_{252}$-*b*-PCL_{35}) triblock and two Y-shaped [PEO_{44}-*b*-$PEOx_{252}$-*b*-$(PCL_{87})_2$], [PEO_{44}-*b*-$PEOx_{252}$-*b*-$(PCL_{131})_2$] terpolymers were synthesized by Svetlana Petrova using a combination of living cationic and anionic ring-openning polymerization. Structure and composition of copolymers was confirmed by ^{1}H NMR spectra recorded in deuterated chloroform (good solvent for all blocks). In all terpolymers length of PEO (44 units) and PEOx (252 units) was the same. Difference was in length of PCL blocks: 35 units for linear terpolymer and 2×87, 2×131 units for Y-shape. Due to hydrophobic PCL blocks nanoparticles (NPs) D_2O solutions (concentrations *c*=0.5 and 1.5 wt%) were prepared by Eliezer Jäger using nanoprecipitation method. For NMR characterization of temperature behavior of prepared NPs solution series of ^{1}H NMR and T_2 relaxation time experiments during gradual heating were performed.

^{1}H NMR spectra and fraction of units with significantly reduced mobility

Fig. 4.2.1 shows high-resolution ^{1}H NMR spectra of a D_2O solution (c=0.5 wt%) of the [PEO_{44}-*b*-$PEOx_{252}$-*b*-$(PCL_{87})_2$] NPs, measured under the same instrumental conditions at three temperatures. The chemical structure of terpolymer is on the right side of the figure and the assignment of resonances to various proton types is shown directly in the spectrum measured at 295 K. The weak and broad signals of hydrophobic PCL blocks and stronger signals of hydrophilic PEO and thermoresponsive PEOx blocks detected at 295 K demonstrate a moderately hydrated solid-like PCL core – PEOx, PEO liquid-like shell formation in the D_2O system. The remaining spectra presented in Fig. 4.2.1 were recorded at temperatures of 325 K (below LCST of PEOx) and 360 K (above LCST of PEOx). The most significant effect observed in the spectra obtained at higher temperatures is a visible change in the integrated intensity of all PEOx, PEO and PCL peaks; the PCL signals almost disappear and the intensity of PEOx and PEO signals is reduced. This reduction of intensity and signal broadening is related to the fact that with increasing temperature, the mobility of the part of polymer segments decreases to such an extent that they escape detection in high-resolution NMR spectra.

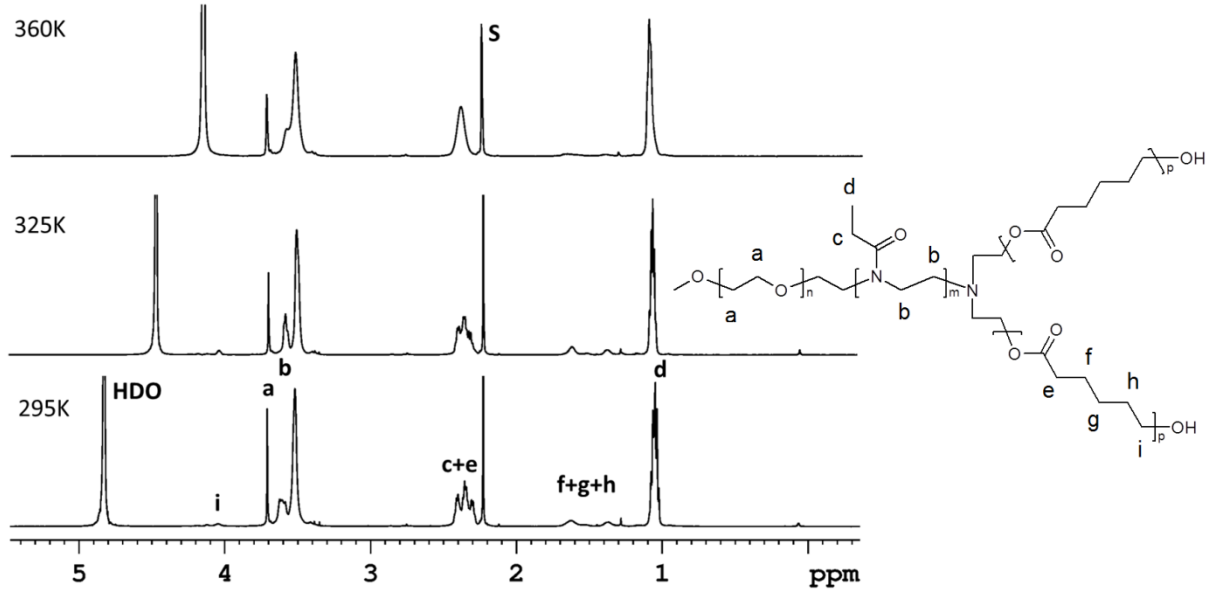

Fig. 4.2.1 600.2 MHz ^{1}H NMR spectra of [PEO_{44}-*b*-$PEOx_{252}$-*b*-$(PCL_{87})_2$] NPs in D_2O solution (c=0.5 wt%) measured at 295, 325 and 360 K under the same instrumental conditions.

High-resolution ^{1}H NMR spectra of the D_2O solution (c=0.5 wt%) of linear PEO_{44}-*b*-$PEOx_{252}$-*b*-PCL_{35} NPs recorded at three temperatures under the same instrumental conditions are presented in Fig. 4.2.2. Chemical structure of the linear terpolymer is shown above the spectrum recorded at 360 K. Peaks assignments of the various proton types are shown in the

in the same figure, above spectrum measured at 295 K. All signals are at the same positions as in the spectra of Y-shape terpolymer (Fig. 4.2.1). The major difference between these two types of copolymers is clearly visible in spectra measured at 325 K. In contrast to the non-linear terpolymer, in spectrum of linear copolymer integral intensities of PCL signals (f+g+h, i) are significantly increased. The spectrum at 360 K shows similar effects for both types of copolymers: decreasing integral intensity and broadening of all signals related to protons of PEO (a), PEOx (b,c,d), and PCL (e, f+g+h, i).

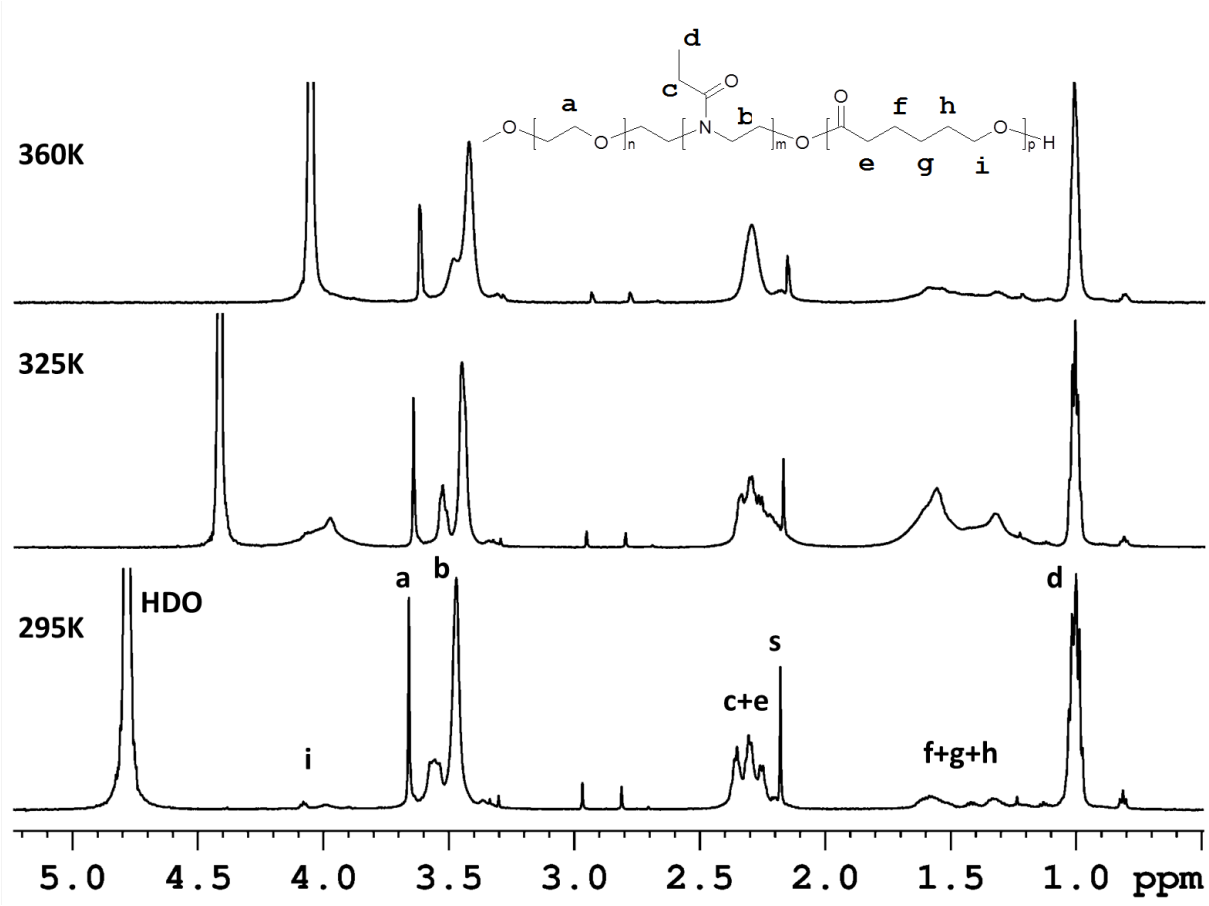

Fig. 4.2.2 600.2 MHz ^{1}H NMR spectra of PEO_{44}-*b*-$PEOx_{252}$-*b*-PCL_{35} NPs in D_2O solution (c=0.5 wt%) measured at 295, 325 and 360 K under the same instrumental conditions.

For quantitative characterization of changes appearing during the heating process, from integrated intensities in ^{1}H NMR spectra the *p*-fraction values of the units with significantly reduced mobility were calculated by using equation presented at Fig. 1.9c. Temperature dependences of the *p*-fraction of various proton types [PEO_{44}-*b*-$PEOx_{252}$-*b*-$(PCL_{87})_2$] NPs D_2O solution (c=0.5 wt%) are shown in Fig.4.2.3a. It is clearly visible that *p*-fraction values of all the blocks first slightly decrease and has a shallow minimum at ~315 K. Next, above 315 K the *p*-fraction values are increasing and copolymer chains become less

hydrated. Afterward, a strong jump of *p*-values related to the PCL block (f+g+h, i) occurs in the temperature range 330-340 K, additionally *p*-values corresponded to PEOx (b, d) and PEO (a) blocks increases. Final values p_{max} reached by the PCL blocks (≈0.65) at 360 K are higher than the p_{max} for the thermoresponsive PEOx blocks (≈0.42) and almost two times larger than values for hydrophilic PEO blocks (≈0.39). The rise of *p*-values is probably induced by thermoresponsive PEOx blocks which changed their hydrophilic properties to hydrophobic ones at the LCST. The main chain (b) and the side chain (d) of PEOx block exhibits the same phase transition behavior with a broad transition width (45 K) and LCST ≈338 K (temperature for $p_{max}/2$). The hydrophobicity of NPs increases and aggregation starts (increasing *p*-values of PEO blocks) above 320 K; the core of NPs becomes more solid-like (increasing *p*-values of PCL blocks) and they precipitate at high temperatures. Almost the same temperature behavior was observed for higher [PEO_{44}-*b*-$PEOx_{252}$-*b*-$(PCL_{87})_2$] NPs concentration (c=1.5 wt%), main difference between these two concentrations is larger p_{max} values obtained at the higher concentration: p_{max}= 0.85, 0.58 and 0.55 for PCL, PEOx and PEO blocks, respectively.

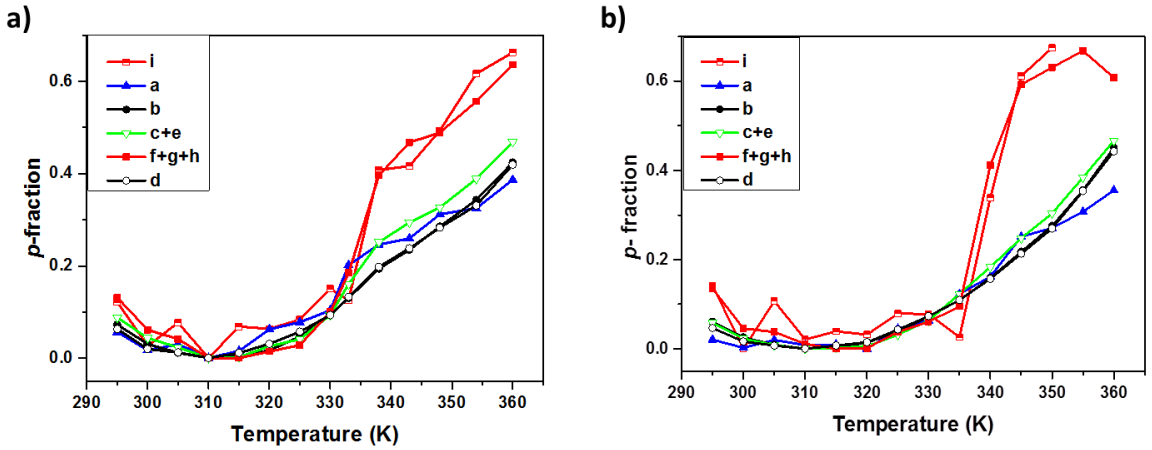

Fig. 4.2.3 Temperature dependences of *p*-fraction for various proton groups of NPs D_2O solutions (c=0.5 wt%): [PEO_{44}-*b*-$PEOx_{252}$-*b*-$(PCL_{87})_2$] (a) and [PEO_{44}-*b*-$PEOx_{252}$-*b*-$(PCL_{131})_2$] (b).

Similar effects are observed for the second Y-shape terpolymer with longer PCL blocks, its NPs water solution (c=0.5 wt%) temperature dependences of the *p*-fraction are presented in Fig. 4.2.3b. As was observed for [PEO_{44}-*b*-$PEOx_{252}$-*b*-$(PCL_{87})_2$] sample, also for [PEO_{44}-*b*-$PEtOx_{252}$-*b*-$(PCL_{131})_2$ the temperature dependences show a shallow minimum at ≈315 K and values of p_{max} are 0.67, 0.45 and 0.36 for PCL (f+g+h, i), PEtOx (b, d) and PEO (a) proton groups, respectively. Above 320 K the NPs start to collapse, aggregate (increasing *p*-values), and subsequently precipitate.

Temperature dependences of the *p*-fraction of the linear PEO_{44}-*b*-$PEOx_{252}$-*b*-PCL_{35} NPs D_2O solution (c=0.5 wt) is shown in Fig. 4.2.4a. In comparison to the Y-shape terpolymers in the linear copolymer similar behavior for the PEOx (b,d) and PEO (a) blocks is observed. The *p*-fraction values of these two blocks slightly decrease to minima at 315 K (PEO) and 325 K (PEOx). The *p*-values start to increase above these temperatures and reach final values $p_{max}\approx0.2$ at 360 K. Similarly to the systems with the Y-shape also here the transition for the PEOx main chain (b) and the side chain (d) is the same. In the linear system a significant difference in the behavior of the PCL block (signals f+g+h, i) during the heating process is observed in comparison with the non-linear terpolymes. Although the PCL units content (10.6 mol%) is in the linear terpolymer 3.5 times smaller than in [PEO_{44}-*b*-$PEOx_{252}$-*b*-$(PCL_{87})_2$] sample, value of the *p*-fraction for PCL segments at room temperature for this sample is five times larger (cf. Figs. 4.2.3a and 4.2.4a, signals i and f+g+h). This fact is evidence of important role of the terpolymer architecture on PCL behavior. High values of the *p*-fraction (≈0.8) for the PCL are virtually constant up to 315 K, next they steeply decrease to a minimum at 325 K, then return to their initial value at 340-345 K and remaining almost unchanged thereafter. These results show that PCL block plays a crucial role in the linear system studied. Similar behavior is observed for higher concentration c= 1.5 wt % presented in Fig. 4.2.4b.

The decrease of the *p*-fraction values related of the PCL blocks in the temperature range of 315-325 K can be caused by faster segmental motion in PCL blocks and/or in faster motion of NPs as a whole. Both of them are discussed in details in publication 2 and shortly described further. The first explanation is related to the melting point of the PCL homopolymer (332-337 K). In the NPs systems PCL blocks can melt at lower temperatures. From this point of view at 315-325 K decreasing of the *p*-values is caused by "melting" of the partially hydrated hydrophobic core and results in higher mobility of PCL blocks (i.e., the respective integrated intensity increases, cf. Fig. 4.2.2). Next, with increasing temperature the NPs reorganize, core collapses and returns back to a solid-like, partially hydrated state. Second possible explanation of decreasing of the *p*-fraction value of the PCL blocks at 325 K to the zero, can be related to the motion of the NPs as a whole. If the motion of the whole NPs is adequately fast, consequently spin-spin relaxation times T_2 of PCL protons can be long enough (and linewidths of PCL signals sufficiently narrow) for detection in high resolution spectra measured at liquid-state NMR spectrometer.

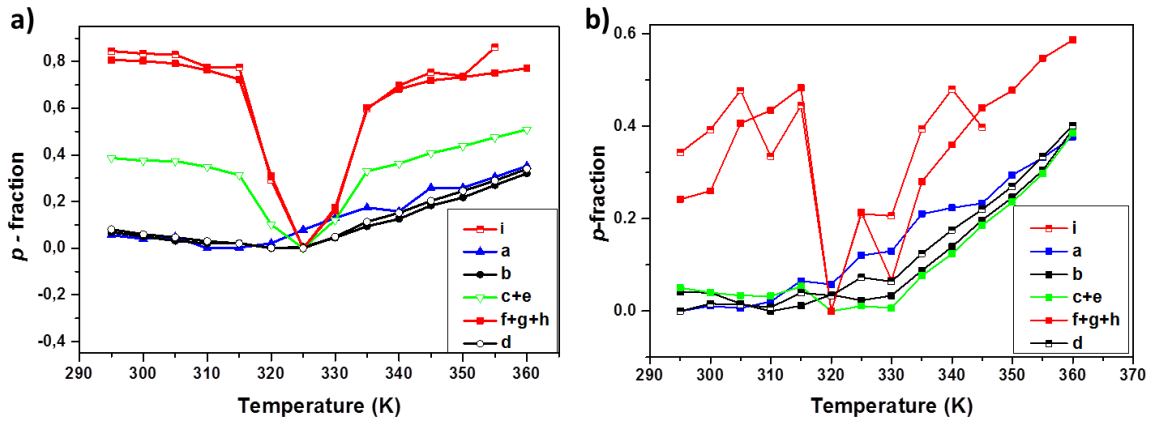

Fig. 4.2.4 Temperature dependences of *p*-fraction for various proton groups in PEO_{44}-*b*-$PEOx_{252}$-*b*-PCL_{35} NPs D_2O solutions: c=0.5 wt% (a) and c=1.5 wt% (b).

Spin-spin relaxation times T_2 of HDO molecules

To obtain information on behavior of water molecules and polymer-solvent interactions (hydration) during phase-transition in water solutions spin-spin relaxation times T_2 measurements were provided. T_2 experiments were run at the same temperatures and directly after ^{1}H NMR measurements used to *p*-fraction values calculation. In Fig. 4.2.5a temperature dependence of ^{1}H spin-spin relaxation time T_2 of HDO in [PEO_{44}-*b*-$PEOx_{252}$-*b*-$(PCL_{87})_2$] NPs D_2O solution (c=0.5 wt%) is presented. It is clearly visible that with increasing temperature (to 330 K) mobility (T_2 values) of the HDO molecules decreases. Hydration of the copolymer chains takes place and mobility of water molecules is reduced by creation of hydrogen bonds with carbonyl oxygen. Further heating (above 330 K) results in increasing T_2 values which is caused by aggregation of NPs; hydrophobic forces predominate, polymer-water hydrogen bonds break, water molecules are released and their mobility increases. Very similar dependence was obtained in [PEO_{44}-*b*-$PEOx_{252}$-*b*-$(PCL_{131})_2$] NPs D_2O solution (c=0.5 wt%). Different behavior was obtained for the PEO_{44}-*b*-$PEOx_{252}$-*b*-PCL_{35} linear terpolymer. Temperature dependence of ^{1}H spin-spin relaxation time T_2 of HDO of its NPs D_2O solution (c=0.5 wt%) is shown in Fig. 4.2.5b. In this case, T_2 values of HDO are constant up to 325 K, (PCL block *p*-fraction minimum, see Fig. 4.2.5a), but increasing of temperature results in splitting of the T_2 values into two components: one with higher, and one with much shorter values of relaxation times. This effect is related to the reorganization of NPs at 325 K, one part of water molecules (high values of T_2) is in solution and further increasing of those T_2 values with temperature signifies that some of them are released from interactions with the polymer segments. The presence of the second component with very short T_2 values

(T_2≈10ms) demonstrates that part of water molecules is bound inside the NPs, and constant values for the short component indicates that these molecules are not released up to 360 K.

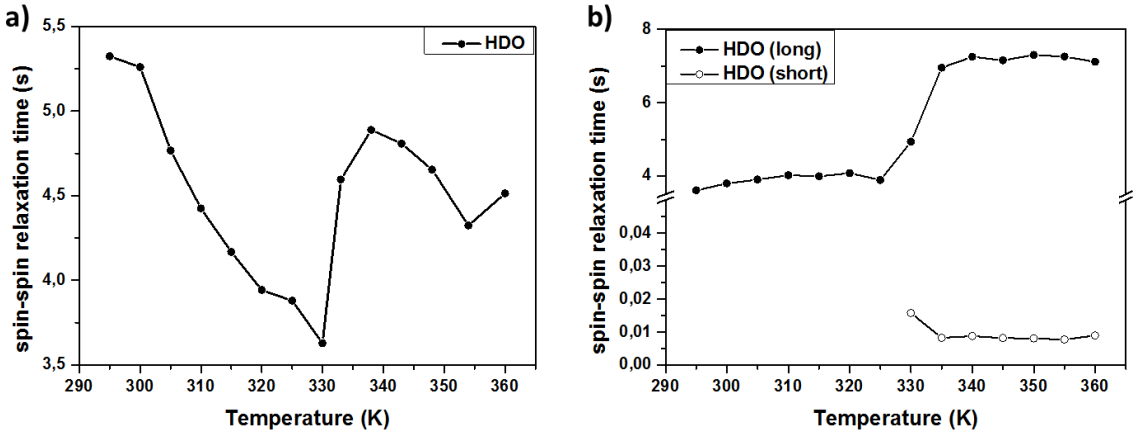

Fig. 4.2.5 Temperature dependence of ^{1}H spin-spin relaxation time T_2 of HDO in [PEO_{44}-*b*-$PEOx_{252}$-*b*-$(PCL_{87})_2$] (a), and PEO_{44}-*b*-$PEOx_{252}$-*b*-PCL_{35} (b) NPs D_2O solutions with c=0.5 wt%.

In contrast to the lower concentration of Y-shape terpolymer, smaller (around 3.0 s) starting T_2 value at 295 K is observed. This effect is caused by higher polymer concentration, because in the hydration process more water molecules are involved. During gradual heating T_2 values are roughly constant up to 320 K. At this temperature NPs start aggregate, and at higher temperatures, similarly to linear PEO_{44}-*b*-$PEOx_{252}$-*b*-PCL_{35} (c=0.5 wt%) division for two T_2 components is required to fit the experimental relaxation curves. As in the linear terpolymer samples, results show the existence of two types of water molecules at temperatures above 320 K. First type is "free" water with longer relaxation times (>3 s); HDO molecules in solution. Second type is "bound" water with very short T_2 relaxation times (≈10ms); HDO molecules bound (confined, entrapped) inside the NPs aggregates. Similar behavior is observed for PEO_{44}-*b*-$PEtOx_{252}$-*b*-PCL_{35} NPs D_2O solution (c=1.5 wt%).

In summary ^{1}H NMR methods were used to study temperature behavior of NPs water solutions of terpolymers containing PEO, PEOx and PCL blocks with linear (PEO_{44}-*b*-$PEOx_{252}$-*b*-PCL_{35}, c= 0.5 and 1.5 wt%) and non-linear (Y-shape) ([PEO_{44}-*b*-$PEOx_{252}$-*b*-$(PCL_{87})_2$], c=0.5 and 1.5 wt%) and [PEO_{44}-*b*-$PEOx_{252}$-*b*-$(PCL_{131})_2$], c=0.5 wt%), architectures for the first time. As a result of ^{1}H NMR measurements in all investigated samples a broad transition of PEOx blocks was observed in a temperature range ~320-360 K. Maximum values of the *p*-fraction (fraction of units with significantly reduced mobility) for PEOx blocks was obtained around $p_{max} \approx 0.4$. Additionally similar behavior for the PEO blocks was detected. Furthermore, it was found that architecture of terpolymers affects temperature

behavior and differences between linear and non-linear systems were found. Specifically, the PCL blocks play important role in the different temperature behavior of the linear and non-linear based NPs solutions. Spin-spin relaxation times T_2 measurements of HDO, shows different behavior of the water molecules in NPs solutions based on linear and Y-shape terpolymers. Especially, two types of water ("free" and "bound") were detected at higher temperatures in NPs solutions of the linear copolymer (c=0.5 wt%). For Y-shape terpolymers NPs solutions such effect was observed only for the higher (1.5 wt%) polymer concentration.

4.3 PNIPAm block copolymers (publications 3-5)

In this part NMR study of temperature behavior of diblock PEO-*b*-PNIPAm, and triblock PEO-*b*-(PNIPAm)$_2$ copolymers aqueous solutions will be briefly discussed. Full study, which contains also FTIR, DSC and quantum-chemical calculations, was published in **publications 3-5** (see Appendix). By modification of PEG 5000 monomethyl ether, macroiniciator was prepared. In next steps three PEO-*b*-PNIPAm copolymers with PNIPAm 109, 154 and 249 units, and two Y-shape PEO-*b*-(PNIPAm)$_2$ copolymers with 47 and 165 PNIPAm units were synthesized by Eva Čadová using single-electron transfer living radical polymerization method. For NMR measurements D_2O solutions of PEO-*b*-PNIPAm and PEO-*b*-(PNIPAm)$_2$ copolymers with polymer concentrations c = 0.2, 5 and 20 wt% were prepared. Moreover, D_2O solutions (c = 5 and 20 wt%) of the PNIPAm homopolymer were also studied.

^{1}H NMR spectra and fraction of units with significantly reduced mobility

Figure 4.3.1 shows ^{1}H NMR spectra of the linear PEO-*b*-PNIPAm$_{109}$ diblock copolymer in D_2O solution (c = 5 wt%) recorded under the same instrumental conditions at two temperatures. The assignment of the signals of various proton types is shown in the spectrum recorded at 300.5 K, temperature below the LCST of PNIPAm homopolymer. Chemical structure is presented at the same figure above the second spectrum which was recorded at 313.9 K (above the LCST of PNIPAm). Peaks **a** and **b** corresponds to PEO protons CH_3 end group and OCH_2 main chain respectively, while signals **e**, **d**, **c** and **f** with integrated intensities in the ratio 1:1:2:6 are related to isopropyl CH, main chain CH, CH_2 and CH_3 groups of PNIPAm units. The main difference observed between these two spectra is a

marked reduction of integrated intensities of all PNIPAm peaks which, with exception of signal of CH_3 protons, almost completely disappeared from the spectrum. This is caused by the fact that at temperature above LCST mobility of PNIPAm units in polymer chains is reduced to such an extent that the corresponding signals become too broad to be detected in high-resolution NMR spectra and forms compact micellar core. Additionally, the intensity of the signal of PEO segments remains almost unchanged; this provides information that mobile PEO is forming a shell of micelles.

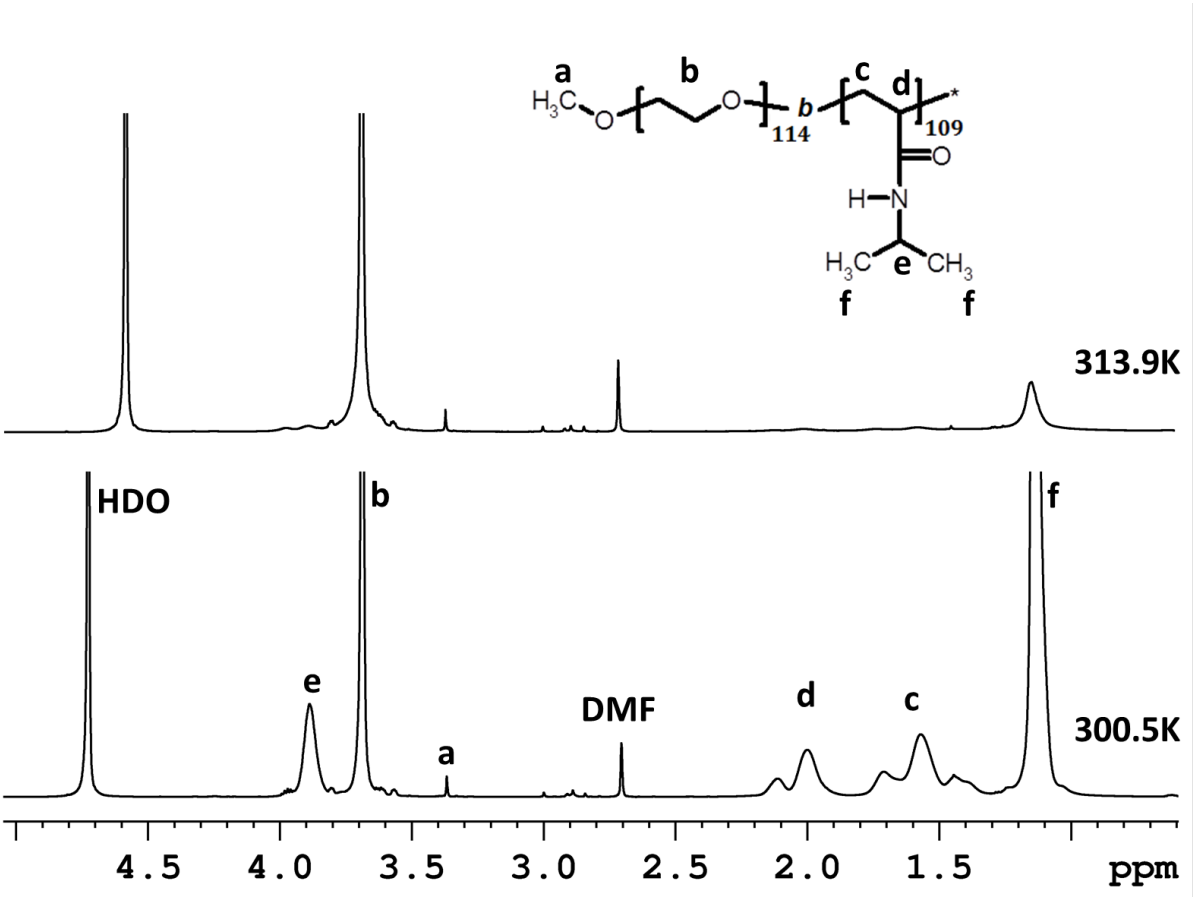

Fig. 4.3.1 600.2 MHz ^{1}H NMR spectra of PEO_{114}-*b*-$PNIPAm_{109}$ in D_2O solution (c = 5 wt%) measured at 300.5 and 313.9 K under the same instrumental conditions.

Similarly to previous chapters for quantitative characterization of changes appearing during the heating and cooling processes, fractions p of the units with significantly reduced mobility (i.e. units in the micellar core) were calculated from integrated intensities in ^{1}H NMR spectra by using equation presented at Fig. 1.9c. In Figure 4.3.2 there are presented temperature dependences of the fraction p for D_2O solutions (c = 5 wt%) of the investigated PEO - PNIPAm block copolymers and neat PNIPAm. Due to the fact that all proton groups of PNIPAm units show the same way of phase transition during gradual heating and cooling,

signal of isopropyl CH protons (signal *e* in Fig. 4.3.1) was chosen as the example and represents PNIPAm units as a whole. From these dependences it follows that the LCST temperatures of the block copolymers are higher than for neat PNIPAm. For the almost all copolymers small difference up to ~ 1 K (temperatures at $p_{max}/2$) is observed. The exception of this effect is detected in the Y-shape PEO_{114}-*b*-$(PNIPAm_{47})_2$ copolymer solution where the transition is shifted 3 K towards higher temperatures. Second difference observed between neat PNIPAm and copolymers are broader transition widths for copolymers (e.g., for PEO_{114}-*b*-$PNIPAm_{109}$ diblock the transition is approx. 7 K broad), and the largest transition width 12 K is again shown by PEO_{114}-*b*-$(PNIPAm_{47})_2$ copolymer, in comparison to rather sharp (transition width 2 K) of the PNIPAm. Furthermore, maximum values of the *p*-fraction for copolymers are slightly lower than for neat PNIPAm, especially in samples with lowest PNIPAm block length is reduced to $p_{max} = 0.9$; probably 10% of PNIPAm units which retain high mobility correspond to PNIPAm blocks which are too short to participate in the phase transition. At this point it is worth to mention that for all investigated block copolymers, we did not observe any hysteresis during cooling.

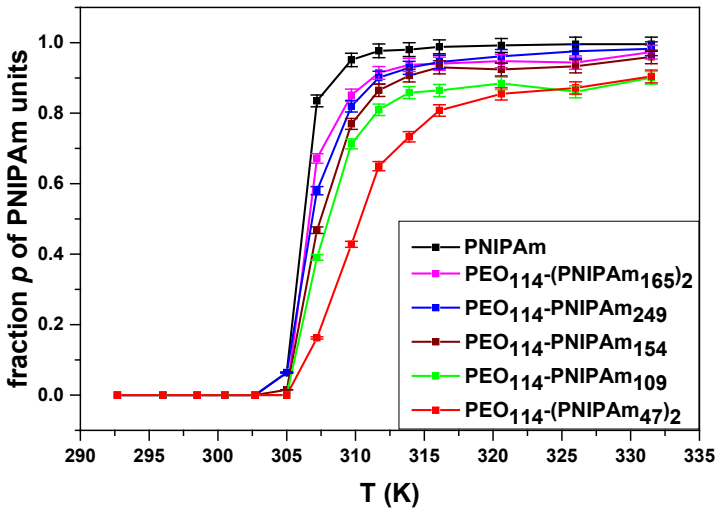

Fig. 4.3.2 Temperature dependences of the fraction *p* of PNIPAm units with significantly reduced mobility (units in micellar core) for of PEO and PNIPAm block copolymers, and for neat PNIPAm, in D_2O solutions (*c* = 5 wt%) during gradual heating.

In next step of the study, effect of copolymer concentration on transition temperatures was investigated. Results are shown in Figure 4.3.3. It follows that for linear diblock copolymer (Fig. 4.3.3a) the transition shifts about 3.5 K to lower temperatures with increasing of the concentration to 20 wt%. In comparison to diblock, for Y-shape triblock copolymer PEO-*b*-$(PNIPAm_{165})_2$ about twice smaller (1.5 K shift towards lower temperature for *c* = 20

wt%) change of the transition temperature is detected (Fig. 4.3.3b). Similar to this copolymer is behavior of the PNIPAm homopolymer, where increasing of polymer concentration to 20 wt% results in 1.3 K lower LCST (Fig. 4.3.3c).

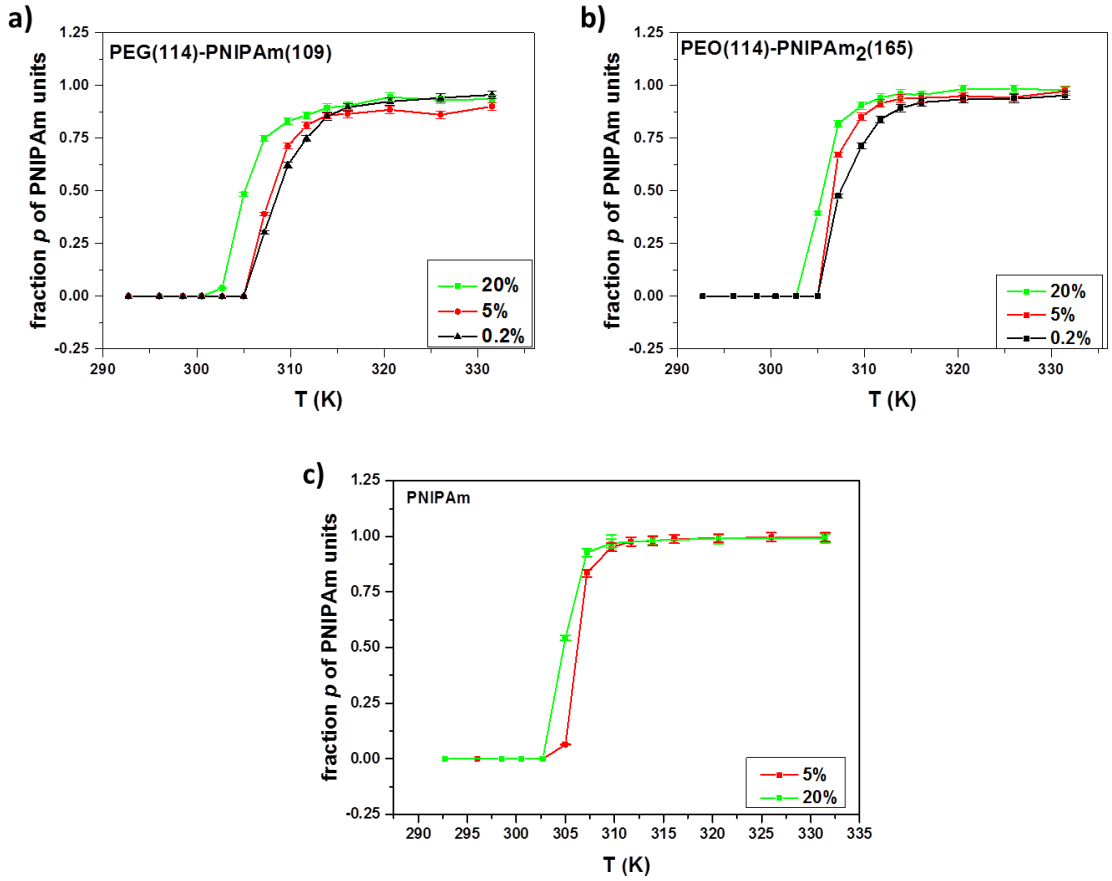

Fig. 4.3.3 Temperature dependences of the *p*-fraction of PNIPAm units of the block copolymers PEO_{114}-*b*-$PNIPAm_{109}$ (a), PEO_{114}-*b*-$(PNIPAm_{165})_2$ (b) and PNIPAm homopolymer (c) D_2O solutions obtained for various polymer concentration during gradual heating.

Temperature behavior of hydrophilic PEO block was also investigated. However, both the intensity and shape of PEO signal is virtually not changing at temperatures below 320 K, but it was discovered that at higher temperatures its integrated intensity is reducing. Similarly to thermoresponsive PNIPAm block, the *p*-fraction of PEO units with significantly reduced mobility was calculated. Temperature dependences of the all investigated block copolymers D_2O solutions (c = 5 wt%) are presented in Fig. 4.3.4a. The values of the *p*-fraction of PEO, depends on the sample, detected at highest temperature (332 K) are in the range 0.02-0.09. For diblock copolymers it is observed relation between these values and length of the PNIPAm block: with increasing number of PNIPAm repeating monomer units, *p*-fraction of PEO also increases. On the other hand, *p*-fraction values for both Y-shape block copolymers

are very similar. Additionally, *p*-fraction of PEO units significantly increases with increasing copolymer concentration. This effect is illustrated in Fig. 4.3.4b, and this is a result of aggregation of micelles, which is promoted at higher concentrations.

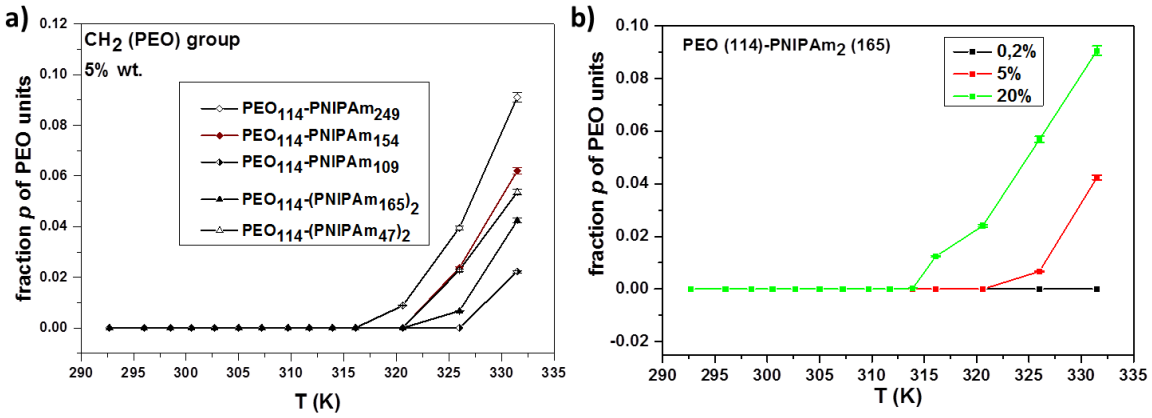

Fig. 4.3.4 Temperature dependences of the *p*-fraction of PEO units for various investigated block copolymers in D_2O solutions (c = 5 wt%) (a), and for the PEO_{114}-*b*-$(PNIPAm_{165})_2$ block copolymer in D_2O solutions with various polymer concentration (b).

Spin-spin relaxation times T_2 of HDO molecules

Similarly to previous systems, information on behavior of water during the phase transition in D_2O solutions was obtained from measurements of ^1H spin-spin relaxation times T_2 of HDO molecules. Figure 4.3.5 shows T_2 values of HDO in D_2O solutions recorded for diblock PEO_{114}-*b*-$PNIPAm_{249}$ copolymer and Y-shape PEO_{114}-*b*-$(PNIPAm_{165})_2$ triblock copolymer at temperatures 295 K (below the transition) and 325 K (above the phase transition). In both cases T_2 values are significantly shorter at higher temperature (full symbols) than values obtained at temperature below LCST (open symbols). This result is related to fact that in these systems at temperatures above the LCST, there exists a fraction of HDO molecules bound in compact micellar core formed by PNIPAm segments. In all cases single line of HDO in ^1H NMR spectrum was observed, moreover T_2 relaxation curves were monoexponential. This indicates a fast exchange between bound and free sites. At the same figure there are also shown time dependences of the T_2 values of HDO at 325 K. From comparison between the diblock copolymer and triblock copolymer solutions, a very different behavior follows. For Y-shape triblock copolymer solution a continuous increase of T_2 values with time was observed. This increase shows that water originally bound, is slowly released with time from the micellar core. In contrast to Y-shape triblock copolymer, no release of water (for 18 h) from micellar cores was detected in D_2O solution of diblock copolymer.

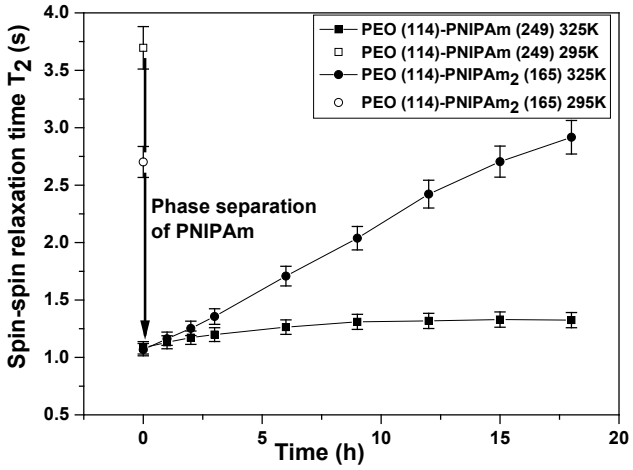

Fig. 4.3.5 Time dependences of ^{1}H spin-spin relaxation time T_2 of HDO in D_2O solutions (c = 5 wt%) of the PEO_{114}-*b*-$PNIPAm_{249}$ and PEO_{114}-*b*-$(PNIPAm_{165})_2$ block copolymers measured at 325 K. Open symbols show the respective T_2 values at 295 K.

2D ^{1}H-^{1}H NOESY spectra

To obtain information on the spatial proximity between protons of PEO block and various proton types of PNIPAm block, were measured temperature dependences of 2D ^{1}H-^{1}H NOESY spectra for 20 wt% D_2O solutions of diblock PEO_{114}-*b*-$PNIPAm_{109}$ and Y-shape PEO_{114}-*b*-$(PNIPAm_{165})_2$ triblock copolymers. As an example in Figure 4.3.6 it is shown 2D NOESY spectrum of PEO_{114}-b-$(PNIPAm_{165})_2$ Y-shape triblock copolymer in D_2O solution (c= 20 wt%) measured at 292.7 K (the same effect was obtained for diblock copolymer). In the spectrum besides strong cross-peaks between various proton groups of PNIPAm units, weaker cross-peaks between PEO protons (signal at 3.7 ppm) and isopropyl CH (3.9 ppm), main chain CH (2.0 ppm), main chain CH_2 (1.6 ppm) and CH_3 (1.15 ppm) protons of PNIPAm units are also visible. As it was mentioned in the Introduction, these cross-peaks shows that distances between respective protons are smaller than 0.5 nm. In next step, for the quantitative characterization of the intensities of the crosspeaks between PEO and PNIPAm protons we used integrated intensities of signals of PNIPAm proton groups (isopropyl CH, main chain CH, main chain CH_2, CH_3) in 1D slices extracted from the PEO signal of the 2D NOESY spectra (as illustrated in the right side of the Fig. 4.3.6).

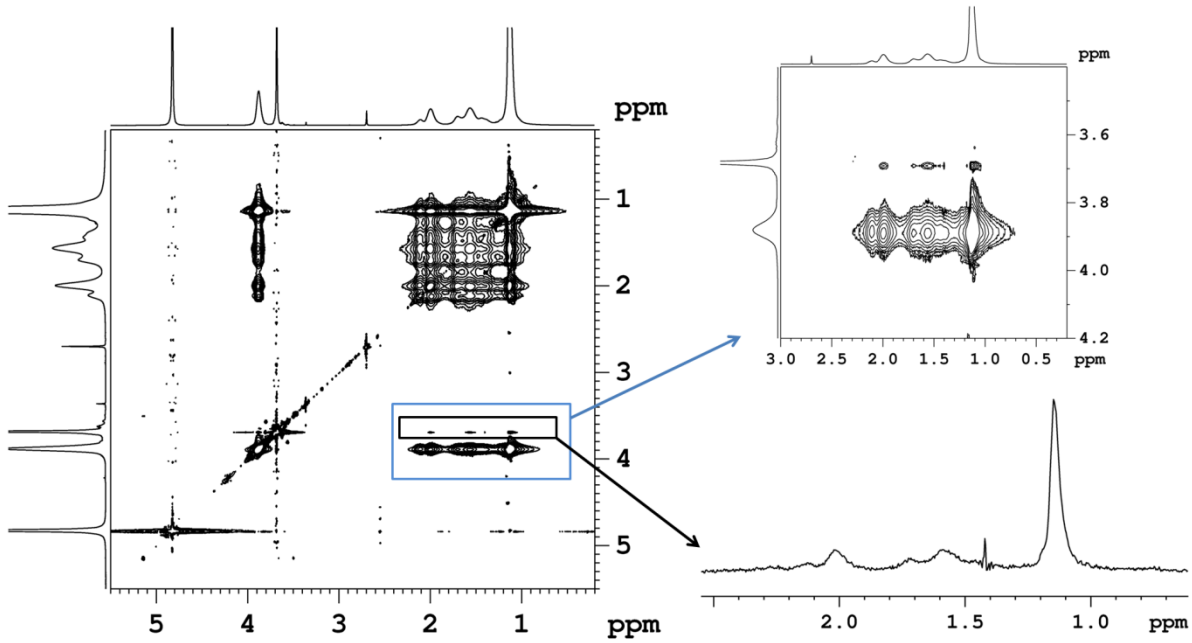

Fig. 4.3.6 2D NOESY spectrum of PEO_{114}-b-$(PNIPAm_{165})_2$ Y-shape triblock copolymer in D_2O solution (c= 20 wt%) measured at 292.7 K with mixing time 400 ms. On the right up there are in detail crosspeaks between PEO protons and PNIPAm protons (main chain CH, CH_2 and isopropyl CH_3), on the right down there is 1D slice spectrum extracted from the PEO signal of the NOESY spectrum.

In Fig. 4.3.7 are shown temperature dependences of the absolute integrated intensities of PNIPAm signals in 1D slices, extracted from 2D NOESY spectra measured with mixing time 400 ms for D_2O solutions of both diblock (Fig. 4.3.7a) and Y-shape triblock copolymers (Fig. 4.3.7b). Similar dependences of the respective integrated intensities were obtained for NOESY spectra measured with mixing time 100 ms. Additionally, similar dependences was obtained by using the volume integrals of the respective cross-peaks between PEO and PNIPAm protons directly in 2D NOESY spectra. In both systems, intensity of these cross-peaks is decreasing in the transition region (temperatures > 302.5 K), and at higher temperatures (above the transition) are not detectable. This is evidently related to significant reduction in mobility of PNIPAm segments. Differences in behavior between these two systems are observed at lower temperatures (292.7 K to 301.6 K). While for Y-shape triblock copolymer (Fig. 4.3.7b) intensities of cross-peaks continuously decrease with temperature, for diblock copolymer (Fig. 4.3.7a) an atypical increasing of intensity of cross-peaks between PEO protons and main chain CH and CH_2 protons, and isopropyl CH protons of PNIPAm units was discovered. This effect shows that either average distance between PEO protons and respective PNIPAm protons decreases at 301.6 K than at 292.7 K, and/or that number of close contacts (< 0.5 nm) between PEO protons and respective PNIPAm protons is significantly

increased at 301.6 K. In both cases this is caused by a change in conformation of the block copolymer, and this change occurs at temperature which is still below the LCST transition of PNIPAm component. In contrast to diblock copolymer, Y-shape triblock copolymer cannot form similar conformation as observed for diblock copolymer at 301.6 K, probably from steric reasons.

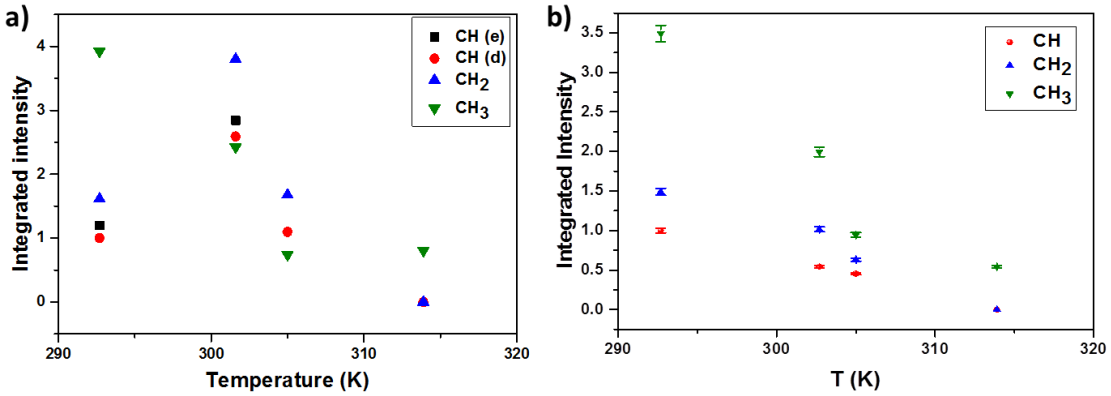

Fig. 4.3.7 Temperature dependences of integrated intensities of various PNIPAm signals in 1D slices extracted from the PEO signal of the NOESY NMR spectra of D_2O solutions (c = 20 wt%) of PEO_{114}-*b*-$PNIPAm_{109}$ (a) and PEO_{114}-*b*-$(PNIPAm_{165})_2$ (b) block copolymers. In figure (a) CH(e) is isopropyl CH and CH(d) is main chain CH; in figure (b) is main chain CH signal.

In summary, the changes observed at ^{1}H NMR spectra proved that above LCST temperature the block copolymers form micelles with compact core created from immobilized PNIPAm blocks, and shell consisting mobile PEO blocks. LCST depends on length of PNIPAm block, copolymer architecture and polymer concentration. Increasing of the values of the fraction of PEO units with significantly reduced mobility with increasing polymer concentration at temperatures above 320 K is caused by aggregation of micelles. From T_2 measurements the existence of water bound in micellar cores at temperatures above LCST was revealed. Further behavior of water at this temperature depends on copolymer architecture: for Y-shape triblock copolymer water is slowly released with time, and there is no release of water for diblock copolymer. 2D NOESY NMR spectra also showed difference in behavior of both types of the block copolymers: PEO-*b*-PNIPAm block copolymer shows certain conformation changes already in the pretransition region, while no similar conformation change was detected for PEO-*b* -$(PNIPAm)_2$ triblock copolymer.

4.4 PNIPAm/CLAY hydrogels (publications 6 and 7)

Herein, results obtained by NMR spectroscopy experiments and published in **publications 6 and 7** will be shortly presented. For PNIPAm/clay hydrogels systems ^{1}H NMR spectroscopy methods were used to study interactions between the reaction mixture components in the *N*- isopropylacrylamide (NIPAm), *N,N,N',N'*-tetramethylethylenediamine (TEMED), PNIPAm (polymer) and clay (Laponite XLS) (publication 6 and 7), as well as for behavior of reaction mixture during the cooling processes (to freezing), and to follow the course of polymerization reaction *in situ* (publication 7).

Interactions of clay with reaction components

Figure 4.4.1 shows ^{1}H NMR spectra of D_2O solutions of TEMED (a), NIPAm-TEMED (b), PNIPAm-TEMED (c), reaction mixture 30X, clay-NIPAm–TEMED/APS (3:1), t(reaction)=0, (d), reaction mixture t=20 min (e), gel 30X (f). From the spectra is follows that TEMED signals related to CH_2 and CH_3 groups (Fig. 4.4.1a) remain quite sharp in the mixture with NIPAm monomer (Fig. 4.4.1b), and are slightly shifted in the polymer solution (Fig. 4.1.1c). This is an effect of the interactions of TEMED molecules with NIPAm monomer and polymer. In the reaction suspension containing clay, NIPAm, TEMED and APS with reaction time t=0 (Fig. 4.4.1d) signals of monomer are broader then in mixture without clay (Fig. 4.4.1b), and TEMED peaks appear as one very broad signal. This effect on TEMED signal is the same during the polymerization (Fig. 4.4.1e), as well as in final gel in which it was almost undetectable (Fig. 4.4.1e). The disappearance and shape changes of TEMED signal in presence of clay is caused by strong adsorption and immobilization of TEMED molecules at the clay surface. In contrast, the fact that all signals of NIPAm and PNIPAm were broader and still present in the spectra indicates that monomer and polymer were also adsorbed on clay, but interactions with clay were weaker than in case of TEMED.

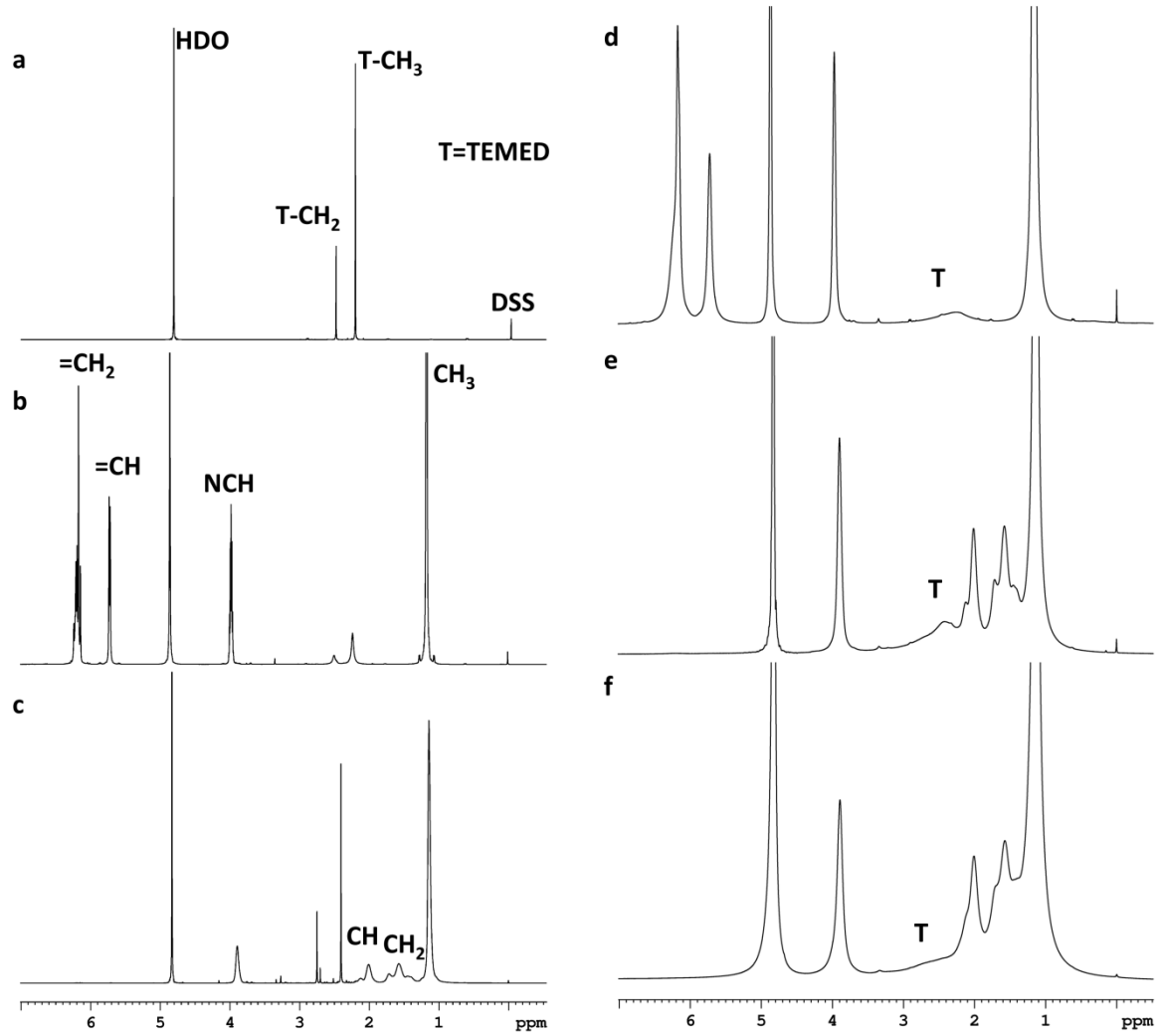

Fig. 4.4.1 ^{1}H NMR spectra of TEMED (a), NIPAm-TEMED (b), PNIPAm-TEMED (c), reaction mixture 30X, clay-NIPAm–TEMED/APS (3:1), t(reaction)=0, (d), reaction mixture t=20 min (e), gel 30X (f). All spectra were measured in D_2O at room temperature.

For a quantitative evaluation of aforementioned interactions, the T_2 relaxation times characterizing the mobility of corresponding protons were determined. Obtained results are present in Table 4.4.1. T_2 values of TEMED are drastically reduced in the clay suspension (from 945ms to 1.1ms), and even more in reaction mixture (0.9ms), and in gel (0.5ms). Additionally, around 10 times longer T_2 relaxation times of NIPAm or PNIPAm than those obtained for TEMED in presence of clay were detected. This result is an effect of weaker interactions (higher mobility) of monomer and polymer with clay than TEMED molecules.

Table 4.4.1 ^{1}H spin-spin relaxation times T_2 of: TEMED, DMEA, NIPAm and PNIPAm molecules.

Sample	T_2[ms]					
	TEMED (or DMEA)		NIPAm (or PNIPAm)			
	NCH_2	NCH_3	CH2=	CH=	NCH	CH3
TEMED	945	868				
NIPAm			805	648	1343	722
TEMED-NIPAm	26	24	111	104	287	71
TEMED- clay	1.1[a]	2.2[a]				
DMEA-clay	3.0[a]	3.8[a]				
Reaction mixture, t=0 TEMED-NIPAm-clay	0.9[a,b]		10	9	24	15
Polymerization, t=20 min TEMED-NIPAm-PNIPAm-clay	0.8[a,b]				7[c]	
Final gel	0.5[a,b]				7[c]	7[c]

[a]Determined after deconvolution from the linewidth Δν using the relation $T_2 = (\pi\ \Delta\nu)^{-1}$.
[b]One broad band for both NCH_3 and NCH_2 protons.
[c] PNIPAm

Temperature behavior of NIPAm and water

^{1}H NMR spectroscopy was used to study temperature behavior of NIPAm aqueous solution during gradual cooling. This process results in a separation of the system into two phases: liquid phase containing monomer, initiators, clay and/or polymer and solid ice phase. Figure 4.4.2 shows ^{1}H NMR spectra of NIPAm aqueous solution at three temperatures: 15, -8 and -13.5°C. From the Figure it follows that decreasing temperature to T = -8°C, was not affecting the mobility of components in the supercooled solution, but after freezing signal of water is significantly reduced, and all signals becomes broader. The fact that the water and monomer signals are still observed indicates the presence of a liquid phase composed of water and NIPAm. Signal broadening is caused by significant reduction in mobility of components in semi-frozen state. ^{1}H spin-spin relaxation times T_2 were determined for quantifying the effect. As a result it was obtained shortening of the relaxation time in supercooled solution by 45%, and decreasing by almost two orders of magnitude after freezing. Additionally, the mobile fraction of NIPAm and water was determined from ^{1}H NMR spectra using absolute integrated intensities of respective signals. Results are shown in Fig. 4.4.3 and display a sharp drop in mobile fraction of water and gradual decreasing of values related to NIPAm liquid

monomer during cooling. This partial immobilization of NIPAm is a result of its crystallization.

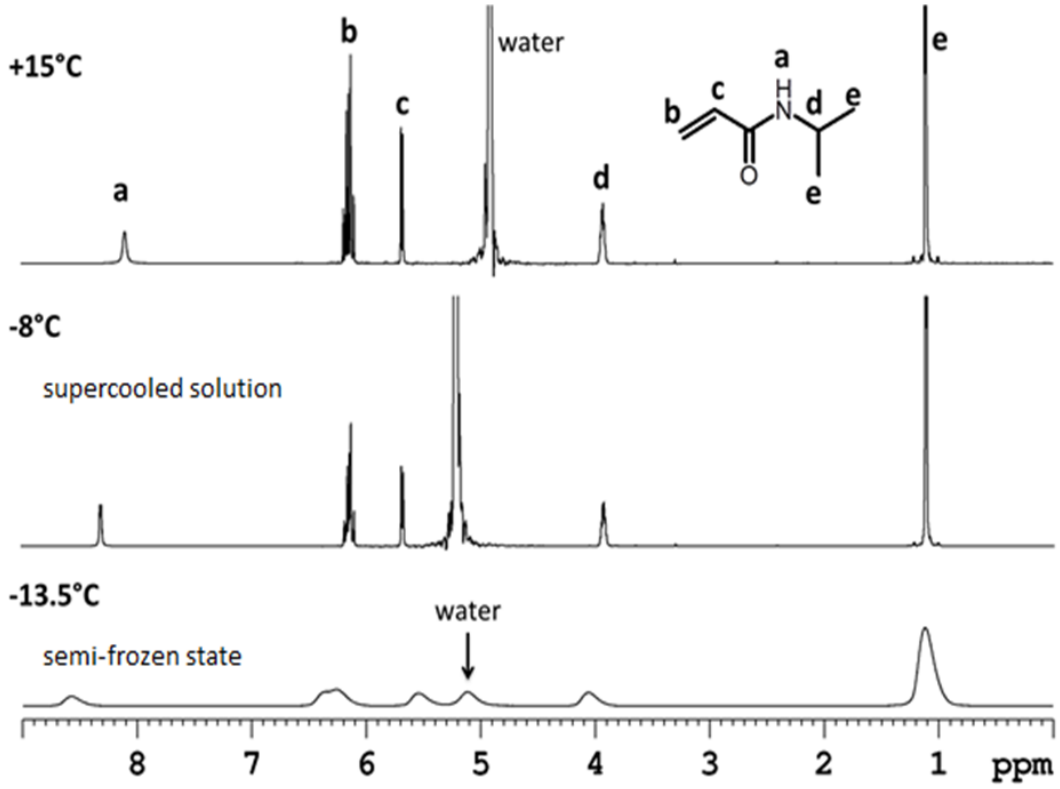

Fig. 4.4.2 ^{1}H NMR spectrum of the 8.5 wt.% NIPAm solution in H_2O/D_2O (80/20) mixture at cooling (a) T= 15 °C, (b) T= -8 °C, prior to crystallization, (c) T= -13.5 °C, after crystallization. Mixture H_2O/D_2O (80/20) was used as the solvent in this case in order to detect better the signal of residual water also after freezing. The peaks assignment of NIPAm and water is described in the figure.

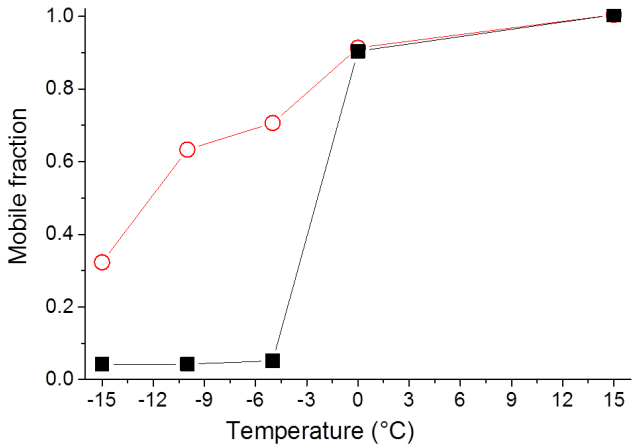

Fig. 4.4.3 Mobile fraction of water (■) and NIPAm (○) as a function of temperature in NIPAm/D_2O solution (8.5 wt. % of NIPAm). Virtually the same dependence was obtained for various proton groups of NIPAm.

Kinetics of cryopolymerization

Kinetics of the cryopolymerization (initiated with the redox system APS/TEMED) was characterized as conversion of the monomer NIPAm, and monitored in situ by NMR spectroscopy. CH_2= and/or CH= NIPAm monomer groups signals were used to this purpose. Additionally, three effects which can influence the cryopolymerization rate were investigated: (I) low temperature slowing down the polymerization, (II) cryoconcentration (freezing is resulting in acceleration of the reaction in the concentrated liquid phase of the semi-frozen system), (III) steric confinement and reduction of mobility of reactive species (densification of a solution and a clay aggregation after freezing). To exclude the effect of cryoconcentration and to determine only the effect of decreasing temperature, polymerization at a low temperature was followed in the metastable supercooled state in the absence of crystallization. Fig. 4.4.4 shows the kinetics of polymerization of NIPAm (Fig. 4.4.4a) and the NIPAm/clay system (Fig. 4.4.4b) at different temperatures T_c = 15 °C, 0 °C and –10 °C (curves 1, 2 and 3). The decrease in polymerization temperature results in slowing down the polymerization and an appearance of the pronounced induction period. Moreover, the polymerization is slower and the induction period is longer in the PNIPAm/clay gel forming mixture compared to the linear NIPAm polymerization.

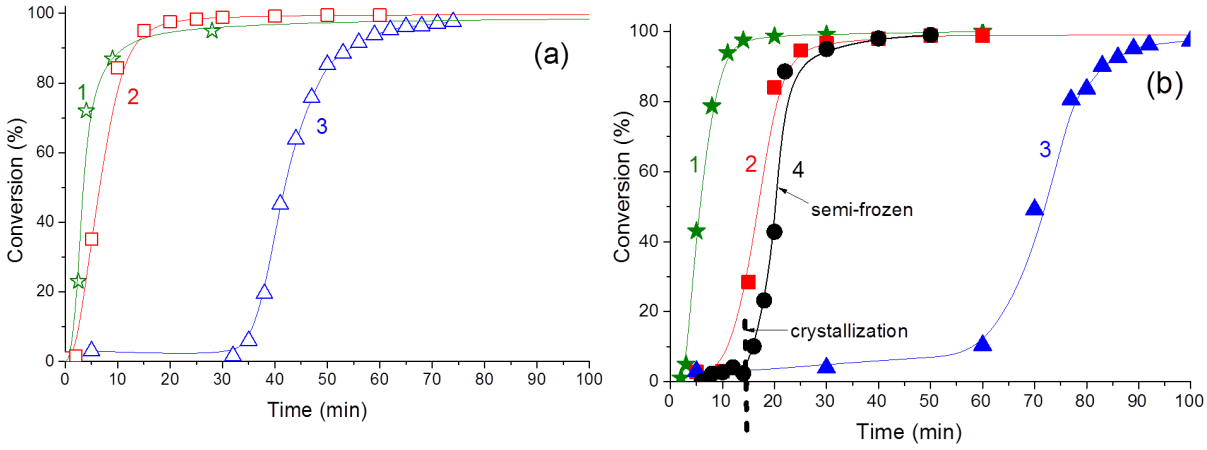

Fig. 4.4.4 Kinetics of polymerization of (a) NIPAm and (b) NIPAm/clay system at different temperatures. Curves: 1- 15 °C, 2- 0 °C, 3- (-10) °C, unfrozen state, 4- (-10) °C semi-frozen state, dashed line indicates crystallization.

Second effect abovementioned is an increasing concentration of the non-frozen solution which occurs after the water crystallization. The effect of freezing on polymerization is shown in Fig. 4.4.4b. In comparison between the polymerization kinetics of NIPAm/clay system at T = -10 °C in the semi-frozen (curve 4) and the unfrozen supercooled (curve 3) states is

observed much faster polymerization in the semi-frozen state. The fast propagation starts just after crystallization point by the dash line. The freezing was detected by a marked decrease in intensity of the water signal. The shortening of the induction period as well as the higher propagation rate are the results of the increased cryoconcentration in the non-frozen liquid phase including both initiators and monomer NIPAm. By crystallization of water concentration of the liquid phase is increased about 4-5 times, from 8.5 wt. % up to 39 wt. %. The concentration of initiators increases, polymerization starts and it is accelerated just after water crystallization when this cryoconcentrated phase is formed. Third factor appears after freezing of water. Polymerization proceeds in the cryo-concentrated liquid phase between ice crystallites and the aggregation of clay under confined conditions. Figure 4.4.5 shows ^{1}H NMR spectra of NIPAm and NIPAm/clay polymerization mixtures in D_2O at *T*= -10 °C in PNIPAm unfrozen solution (a), PNIPAm semi-frozen solution (b), PNIPAm/clay unfrozen solution (c) and PNIPAm/clay semi-frozen solution (d). From the spectra is follows that mobility of both monomer and polymer chains significantly decreases after water crystallization. In the system without clay, during polymerization at *T*= -10 °C in the supercooled system (Fig. 4.4.5a) narrow peaks of water, monomer NIPAm and catalyst TEMED are observed in the NMR spectrum, as well as broader peaks corresponding to the PNIPAm polymer. Therefore, all substances of the polymerization mixture exhibit a quite high mobility. The freezing of the water is shown by notable reduction of its signal (Fig. 4.4.5b). After freezing, all signals significantly broaden and by this demonstrate a reduction of mobility of all substances due to a steric confinement and a viscosity rise. Moreover, signals of the polymer completely disappear indicating that the confined conditions affect more the mobility of polymer chains.

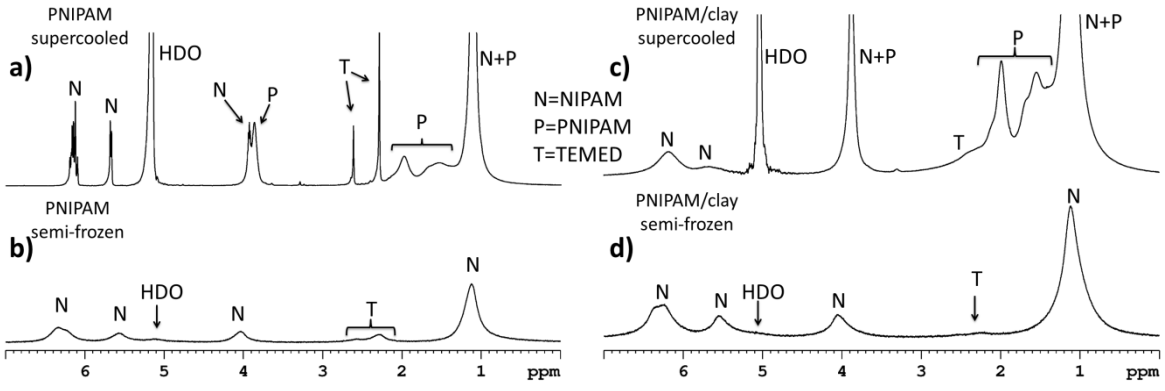

Fig. 4.4.5 ^{1}H NMR spectra of NIPAm and NIPAm/clay polymerization mixtures in D_2O at *T*= -10 °C. a) PNIPAm unfrozen solution, b) PNIPAm semi-frozen solution, c) PNIPAm/clay unfrozen solution, d) PNIPAm/clay semi-frozen solution. P–polymer, N–NIPAm, T-TEMED.

In the system NIPAm/clay, NIPAm, polymer as well as the initiator TEMED are strongly adsorbed on the clay surface resulting in reduction of their mobility. In the spectrum of the supercooled solution (Fig. 4.4.5c), monomer and polymer peaks are broad, and the TEMED peaks almost disappeared. Similarly to system without clay, after freezing, the signals of NIPAm become broader (Fig. 4.4.5d) and polymer peaks disappear. The results show that both cryoconcentration after freezing and the presence of clay significantly reduce mobility of NIPAm monomer and polymer chains. Nevertheless, Fig. 4.4.4b (curve 4) shows that the decrease of the reagents mobility in the confined space after freezing and clay aggregation does not affect significantly the polymerization kinetics.

In summary NMR spectroscopy methods were successfully used in characterization of the interactions between components in the reaction mixture composed from the NIPAm, TEMED, PNIPAm and clay, as well as for behavior of reaction mixture during the cooling processes (to freezing). Moreover it was proved that NMR spectroscopy is good method to study effects which have an impact on cryopolymerization kinetics.

4.5 PVME/additives (publication 8)

In this part of the thesis effects of additives on phase transition of poly(vinyl methyl ether) aqueous solutions will be discussed. In my work I was analyzing influence of ketones on PVME water solutions phase transition. Some my results (*t*-butyl methyl ketone, TBMK) are presented in **publication 8**, and will be discussed here together with unpublished data obtained with isopropyl methyl ketone (IMK) and methyl ethyl ketone (MEK).

^{1}H NMR spectra and fraction of units with significantly reduced mobility

Figure 4.5.1 shows high-resolution ^{1}H NMR spectra of a D_2O solution of the PVME with TBMK additive (c_p = 5 and c_{ad} = 5 wt%) measured under the same instrumental conditions at temperatures below (a) and above (b) LCST. The assignment of resonances to various proton types is shown directly in the spectrum measured below the LCST and chemical structures of polymer and additive are shown at the figure. The signals “A” and “B” are related to CH_2 and CH protons from the main chain of PVME, while PVME side chain OCH_3 group correspond to peak “C”. Signals “D” and “E” are related to additive methyl and *tert*-butyl groups respectively. The most significant effect observed in the spectra is a visible

reduction in integral intensities of all signals of PVME units, as well as changes in shape of signals of TBMK. This result is evidently related to the fact that with increasing temperature, the mobility of the part of polymer segments which form globular-like structures decreases to such an extent that they escape detection in high-resolution NMR spectra.

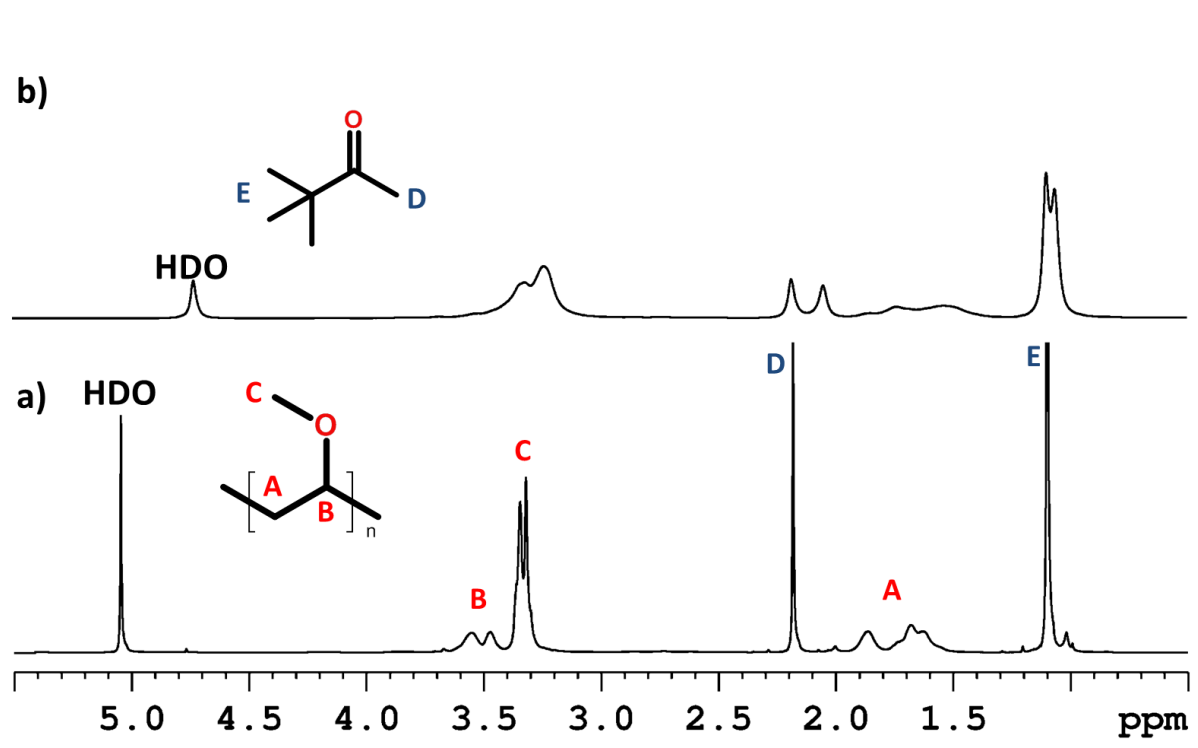

Fig. 4.5.1 ^{1}H NMR spectra of PVME D_2O solution with TBMK (c_p = 5 and c_{ad} = 5 wt%) measured below (a) and above (b) LCST under the same instrumental conditions.

Similarly to previous temperature responsive polymer systems, for quantitative characterization of changes appearing during the heating processes, fractions p of the units with significantly reduced mobility were calculated from integrated intensities in ^{1}H NMR spectra by using equation presented at Fig. 1.9c. In Figure 4.5.2a temperature dependences of the fraction p (of $CHOCH_3$ of PVME signal) are presented for D_2O solutions of neat PVME (c_p = 5 wt%) and PVME/additives (c_p = 5 and c_{ad} = 5 wt%) obtained during gradual heating. From this figure it follows that all solutions with additives exhibits broader transition region than the neat PVME solution. It is clearly visible that broadness of transition depends on hydrophobicity of additive and this effect is most significant for PVME/TBMK solution where transition is ~12 K broad. Similar dependence is observed also for LCST; more hydrophobic additive provides shifting in transition temperature (0.5 of p_{max}) to lower values. Moreover, effect of additive concentration on phase transition of PVME (c_p = 5 wt%) was studied and obtained results are presented in Figure 4.5.2b. Increasing concentration of the

additives results in decreasing of transition temperature. This behavior is most visible for TBMK in which increasing of additive concentration (to c_{ad} = 5 wt%) results in 10 K shift of LCST values.

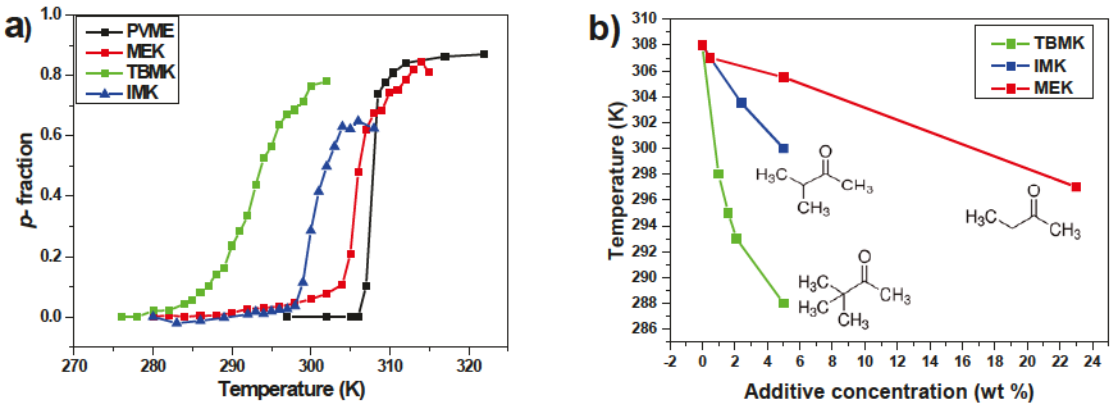

Fig. 4.5.2 Temperature dependences of the fraction p of PVME ($CHOCH_3$ protons) units with significantly reduced mobility for D_2O solutions of neat PVME (c_p = 5 wt%), PVME/additives (c_p = 5 and c_{ad} = 5 wt%) during gradual heating (a), and concentration dependence on transition temperature for PVME/additives D_2O solutions (c_p = 5 wt%) (b).

Mobility of water and additive molecules during phase transition

The mobility of the water and TBMK molecules were studied by measurements of ^1H spin-spin relaxation times T_2. Comparative analysis of T_2 was performed at temperatures below and above transition to characterize changes in behavior of the TBMK and water. For this purpose T_{2im} was calculated as the ratio of the measured T_2 values in the polymer-TBMK system ($T_{2(pvme+TBMK)}$) and in corresponding TBMK/D_2O solution ($T_{2(TBMK)}$) at the same temperature; T_{2im}= $T_{2(pvme+TBMK)}/T_{2(TBMK)}$. The value of T_{2im} gives temperature independent information about the extent of the immobilization of the water and TBMK molecules caused by the presence of the polymer. If there is no interaction with the polymer T_{2im} value should be equal to 1 (if the viscosity effects can be neglected), lower value – higher immobilization effect caused by polymer - water or polymer additive interaction. T_{2im} values were calculated for HDO molecules and $(CH_3)_3$ group of TBMK in PVME/TBMK solution (c_p = 5 and c_{TBMK} = 5 wt%) and were $T_{2im(HDO)}$= 0.16; $T_{2im(TBMK)}$=0.42 below and $T_{2im(HDO)}$= 0.14; $T_{2im(TBMK)}$=0.32 above LCST. From this result is follows that that water and TBMK molecules are strongly involved in the interactions with PVME at temperatures below and above LCST. Moreover, to follow possible time changes in the mobility of water and TBMK above LCST, time dependences of ^1H spin-spin relaxation time T_2 of HDO and $(CH_3)_3$ protons of additive in PVME/TBMK aqueous solution (c_p = 5 and c_{ad} = 5 wt%) above the phase transition were

measured. Results are shown in Figure 4.5.3. The T_2 values of HDO and TBMK increase with a time, so providing evidence that water and additive molecules originally bound in polymer globules are with a time released from them.

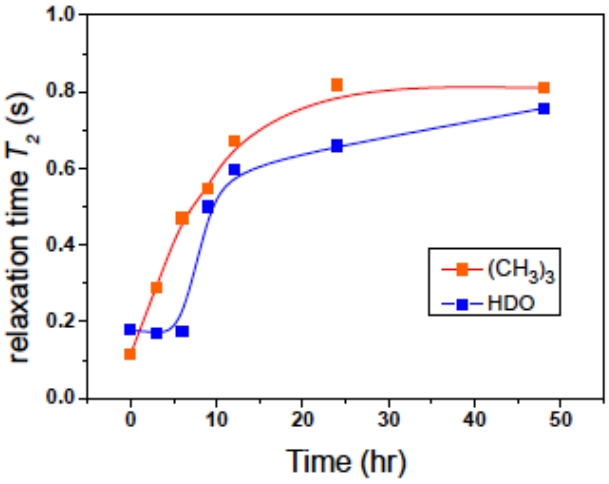

Fig. 4.5.3 Time dependences of ^{1}H spin-spin relaxation time T_2 of HDO and $(CH_3)_3$ protons of additive in PVME/TBMK aqueous solution (c_p = 5 and c_{ad} = 5 wt%) measured above the phase transition.

In summary, an effect of additives on phase transition of PVME aqueous solutions was studied by NMR spectroscopy. For this purpose PVME aqueous solutions (c_p = 5 wt%) with three ketones (MEK, IMK, TBMK with different concentrations) were prepared. LSCT and phase transition of PVME depend on hydrophobicity and concentration of additive in the relation: more hydrophobic additive – broader transition width and lower LCST of polymer. Measurements of the T_2 values of HDO and TBMK provide evidence that water and additive molecules originally bound in polymer globules are with a time released from them.

4.6 pH and ROS responsive polymers (publications 9-11)

Determination of the chemical structure during and/or after chemical synthesis is essential for further characterization of physical, chemical and biological properties of novel compounds. NMR spectroscopy (1D and 2D NMR) is the most common analytical method used for this purpose. In macromolecular chemistry NMR spectroscopy is used for structure determination of polymers, as well as for characterization of composition, tacticity, molecular weight, etc. of polymer chains. Herein, NMR characterization of novel pH and ROS responsive polymers published in **publications 9-11** will be presented.

➢ pH responsive

The MPEO-PCL diblock copolymers (Table 4.6.1) with acid labile ketal group as a block linkage that is highly sensitive to pH at physiological conditions were synthesized by Svetlana Petrova. A new synthetic pathway was developed using for the first time the combination of "click" reaction with carbodimide chemistry (DCC method) and ring-opening polymerization (ROP) (Scheme 4.6.1). The final block copolymer (Scheme 4.6.1, compound 7) was obtained by using previously synthesised *α*-methoxy-*ω*-hydroxy-poly(ethylene oxide) containing a ketal group (Scheme 4.6.1, compound 6) as a macroinitiator in the presence of $Sn(Oct)_2$ as a catalyst. The lengths of the PCL blocks were controlled by regulating the ε-CL/macroinitiator molar ratio. The newly obtained compounds (precursors, macromer, macroinitiator and final diblock copolymers) were assessed by ^{1}H NMR, ^{13}C NMR, FT-IR spectroscopy and SEC analysis, which are described in detail, together with the full synthetic routes in the **publication 9.**

Table 4.6.1 Macromolecular characteristics of MPEO-*b*-PCL diblock copolymers.

Sample	M_n[a],(NMR)	M_n[b],(NMR)	M_n[c],(SEC)	M_w/M_n,[d](SEC)
$MPEO_{44}$-*b*-PCL_{17}	4000	5400	3130	1.79
$MPEO_{44}$-*b*-PCL_{44}	7000	6830	7570	1.79

[a] $M_n = [M]_o/[I]_o$ x 114.14 + M_n α-methoxy-ω-hydroxy-MPEO containing ketal group **(6)**.

[b] M_n was calculated by ^{1}H NMR spectroscopy using eq. 3 in publication 9 (see Appendix).

[c] M_n and [d]M_w/M_n values relative to PS standards.

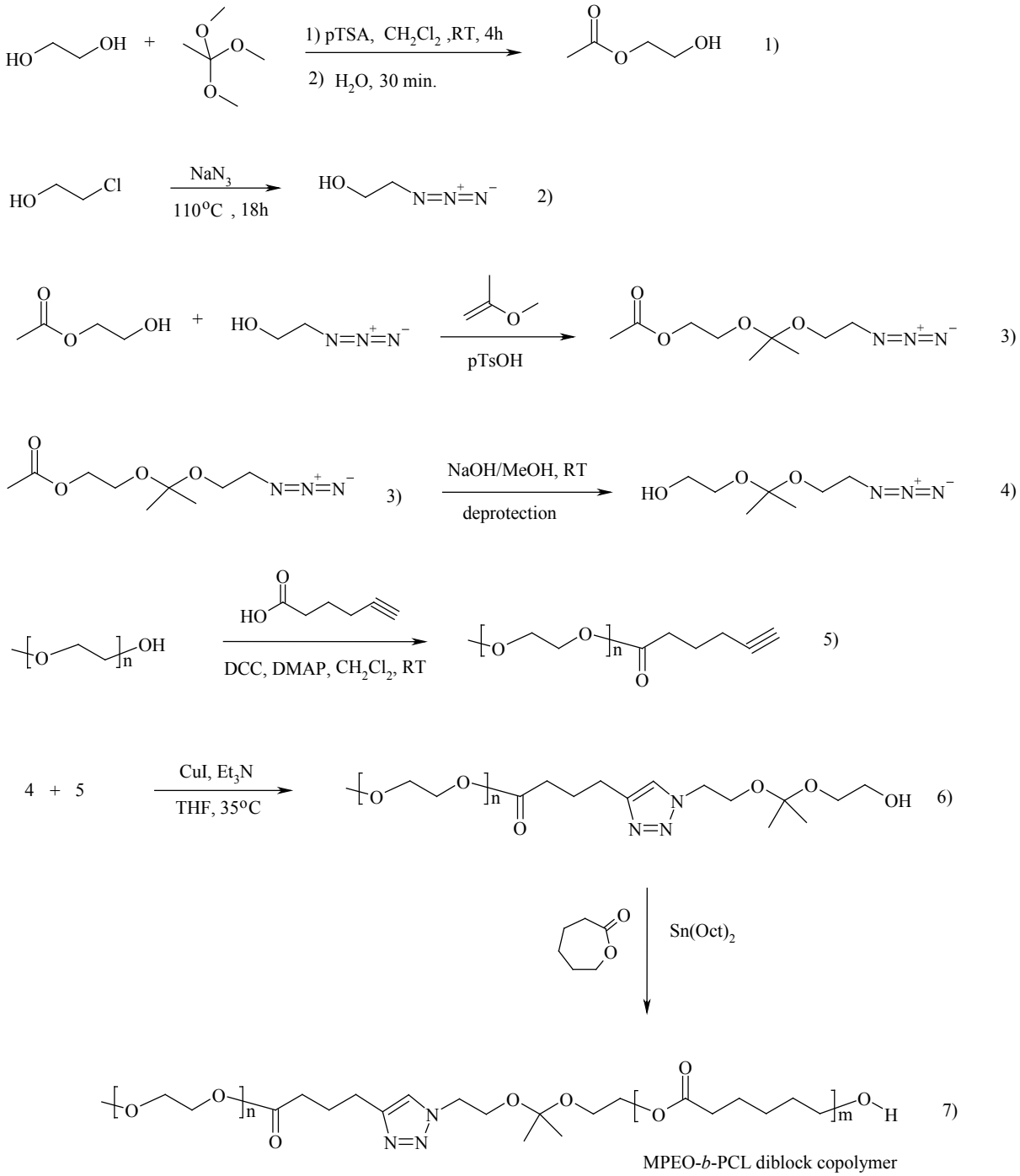

Scheme 4.6.1 Synthetic route for the preparation of MPEO-*b*-PCL diblock copolymers.

Figure 4.6.1 shows ^{1}H NMR (left) and ^{13}C NMR (right) spectra of the MPEO-b-PCL diblock copolymer with the structure and signal assignment, measured in $CDCl_3$ at 295K. The ^{1}H NMR spectrum of the diblock copolymer shows the characteristic signals for the protons belonging to ε-CL and EO repeated units. The signals for the methylene protons of the ε-CL units were detected at 4.06 ppm (**r**) –C***H***$_2$-OC(O)-, 2.29 ppm (**m**) –C(O)C***H***$_2$-, 1.58 ppm (**n** + **p**) -C(O)-CH$_2$-C***H***$_2$-CH$_2$-C***H***$_2$- and 1.34 ppm (**o**) –C(O)-CH$_2$-CH$_2$-C***H***$_2$-. The methylene

protons of EO repeating units were observed at 3.63 ppm (**b**) whereas the singlet signal attributed to the C***H***$_3$-O appears at 3.39 ppm (**a**)-. However, the signals from the methylene protons next to the PEO repeating units –O-C***H***2–CH_2-OC(O) (**c**) as well as the methylene protons next to ketal group (**k)** were not detectable since they appear hidden under the peak of EO units (3.63 ppm) in the spectra. The signal observed at 1.31 ppm (**j + j'**) attributed to the six protons of the dimethyl ketal group –OC(C***H***$_3$)$_2$-O– and the resonance signal at 7.37 ppm (**h**) assigned to triazole ring demonstrates that after ROP the ketal group and the triazole ring remain unaffected. Furthermore, in the spectrum there were signals at 4.57 ppm (**l**) attributed to methylene protons from the -C***H***$_2$-O-C(O)- fragment, 4.45 ppm (**d**) assigned to the last monomer unit of PEO, 4.21 ppm (**i + i')** ascribed to the methylene protons from the fragment between the triazole ring and the ketal group N-C***H***$_2$-C***H***$_2$-O-C(CH$_3$)$_2$-O-. Low intensity signals at 2.76 (**g**), 2.31 (**e**) and 1.68 ppm (**f**) for the protons from the OC(O)-C***H***$_2$-C***H***$_2$-C***H***$_2$-triazole ring also are present. The ^{13}C NMR spectrum of the diblock copolymers shows carbon signals consistent with the desired structure. The more important carbon signals are highlighted, *i.e.*, those which correspond to carbons from dimetyl ketal group at 24.39 ppm (**13)** and the quaternary carbon from the same group –O***C***(CH$_3$)$_2$-O– at 121.50 ppm (**12**). Other significant signals appear at 147.44 (**9**) and 161.1 ppm (**8**) for the triazole ring –CH_2-***C***H=***C***H-N-, at 173.58 ppm (**4 + 16**) for the carbon from carbonyl group –CH_2-O-***C***(O)-(CH_2)$_3$- next to PEO and for the carbon from carbonyl group in PCL. All other remaining signals are attributed to the carbon atoms from the diblock copolymer structure.

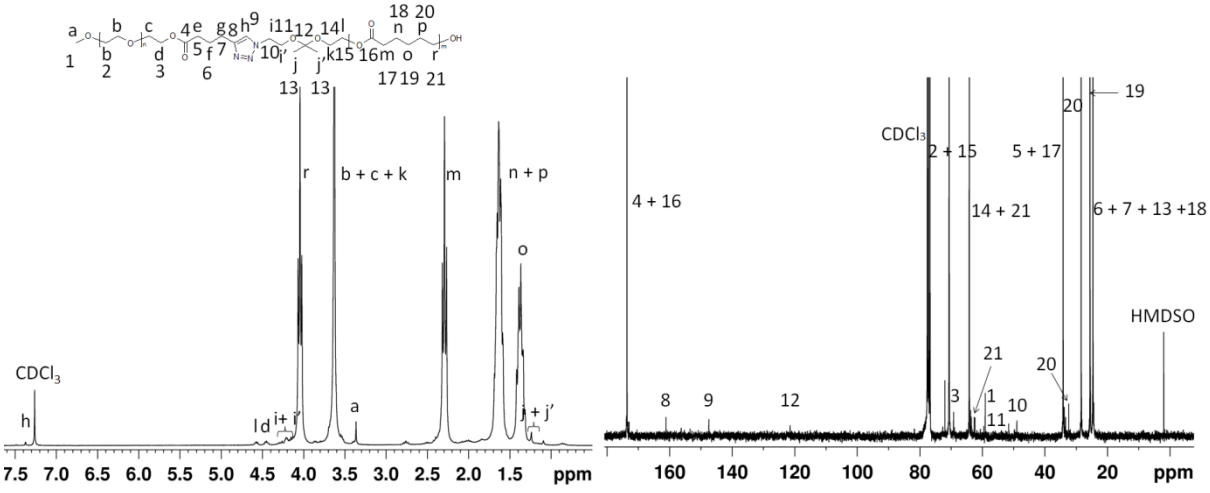

Fig. 4.6.1 ^{1}H (left) and ^{13}C (right) NMR spectra of the MPEO-b-PCL diblock copolymer in $CDCl_3$.

The sensibility of the PEO_{44}-*b*-PCL_{17} copolymer containing the acid-labile ketal group in acid media (pH ~ 5) under physiological conditions (37 °C) was investigated by ^{13}C NMR spectroscopy. For the NMR study 40-50 mg of the $MPEO_{44}$-*b*-PCL_{17} diblock copolymer was dissolved in 0.6 mL of deuterated chloroform followed by the addition of 25 µl of hydrochloric acid-d (DCl). The degradation was determined based on the disappearance of the signal from the ketal linkage between the PEO and PCL blocks. Figure 4.6.2 shows the ^{13}C NMR spectra of $MPEO_{44}$-*b*-PCL_{17} copolymer (A) before and (B) after DCl addition. The ^{13}C NMR spectra reveals the complete disappearance of the carbon signal from ketal group linker $–OC(CH_3)_2-O–$ at 121.50 ppm after the DCl addition. This is strong evidence that hydrolytic degradation takes place in the ketal linkage of $MPEO_{44}$-*b*-PCL_{17} diblock. Unfortunately, the usual degradation products resulted from the acid hydrolysis of a ketal group, appears hidden under ε-CL repeating units in the ^{13}C NMR. However, the presence of the signals at 161.1 (8) and 146.97 ppm (9) related to the carbons from the triazole ring $–CH_2-CH=CH-N-$ and at 173.29 ppm (4) attributed to the carbonyl carbon from the group $–CH_2-OC(O)-(CH_2)_3-$ indicated that the triazole ring and the ester bonds were not affected by the acid addition.

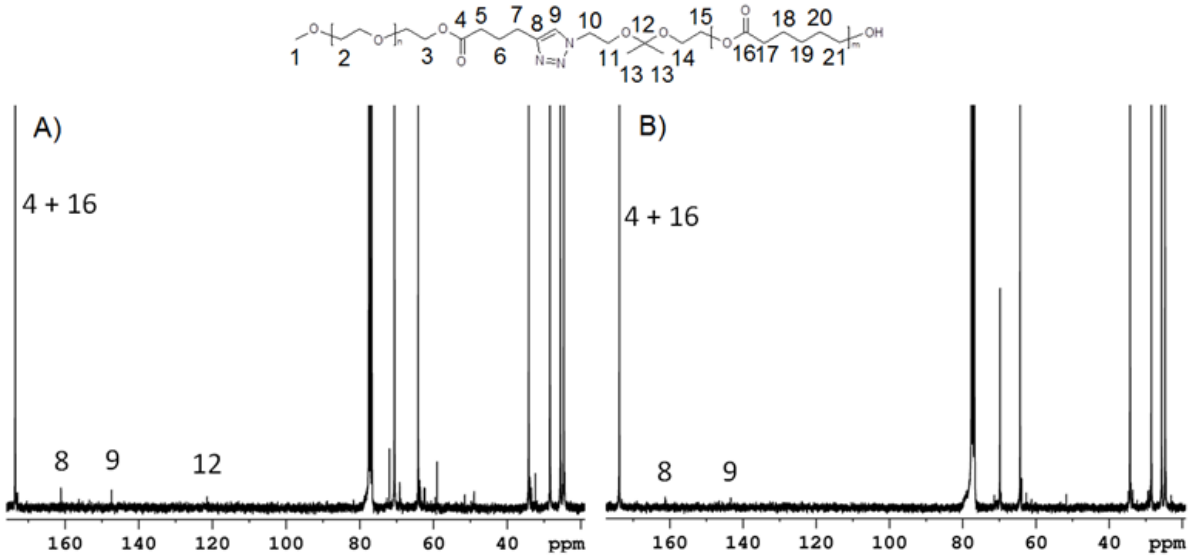

Fig. 4.6.2 ^{13}C NMR spectra of $MPEO_{44}$-*b*-PCL_{17} diblock copolymer (A) before degradation and (B) after degradation.

In summary, ^{1}H and ^{13}C NMR was used for structure characterization of seven step synthesis products of novel MPEO-PCL diblock copolymers with acid labile ketal group as a block linkage. Moreover, ^{13}C NMR measurements prove ketal group degradation under physiological conditions.

➢ ROS - responsive

Two types of ROS – responsive polymers discussed in detail in **publications 10 and 11** were prepared by Eliézer Jäger. First one (publication 10), contains a biocompatible and biodegradable ROS-sensitive polymer backbone with the capability of cellular imaging in a ROS-rich environment was synthesized by step-growth polymerization from monomers bearing a ROS-degradable pinacol-type boronic ester and an alkyne moiety suitable for click chemistry-based attachment of the active cargo. All monomers and final polymer structures were confirmed by ^{1}H and/or ^{13}C NMR spectra. Figure 4.6.3 shows ^{1}H NMR spectrum of ROS-responsive polymer, structure and signal assigment are also presented in the same figure. Polymer was also characterized by size exclusion chromatography (SEC) analysis. The ^{1}H NMR spectrum shows characteristic signals for protons belonging to the repeating units of the monomers. The signals from the protons of aromatic rings were detected at δ = 7.68 ppm (1), δ = 7.41 ppm (2), and δ = 7.16 ppm (3). The methylene protons (4) of aromatic monomers from the main chain of polymer were observed in the same position at δ = 5.08 ppm, whereas the signals attributed to the methylene groups of side chains of these monomers (5) and (6) appear at δ = 4.88 and 4.57 ppm, respectively. The signal of the proton of the terminal alkyne group (7) is at δ = 2.51 ppm. Furthermore, the spectrum displayed signals of methylene groups (10) from the pimeloyl chloride monomeric repeating unit at δ = 1.48 ppm, and the peaks of the methyl with methylene groups (8 + 9, 12 + 11) with chemical shifts at δ = 2.25 and 1.26 ppm, respectively.

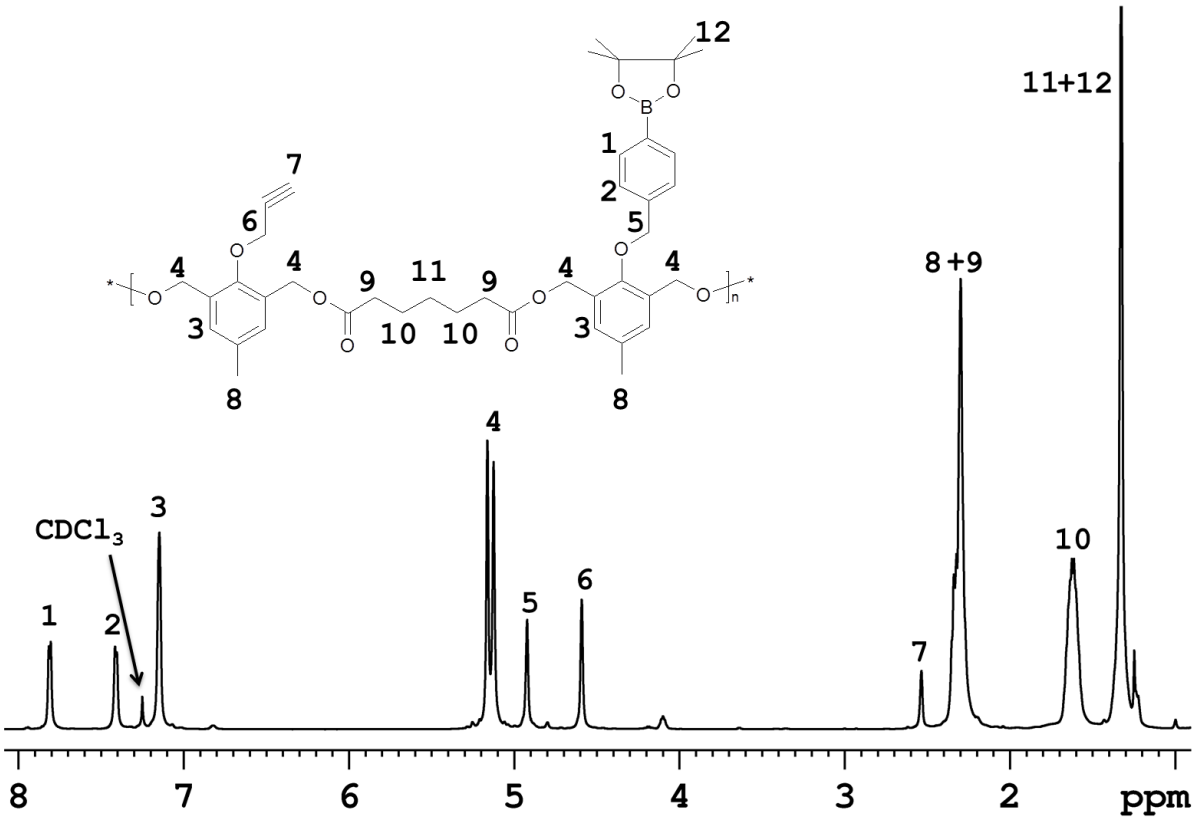

Fig. 4.6.3 ^{1}H NMR spectrum of ROS-responsive polymer measured in $CDCl_3$ at 295 K.

The degradation of responsive polymer was also evaluated by ^{1}H NMR (Fig. 4.6.4) and was complete after 5 days of incubation with 50 mM H_2O_2 after 5 days at 310 K. Broad peaks of polymer NPs observed in ^{1}H NMR (Fig. 4.6.4a) were replaced by sharp peaks of the low-molecular-weight degradation products (Fig. 4.6.4b) confirming the depolymerisation of responsive polymer triggered by H_2O_2.

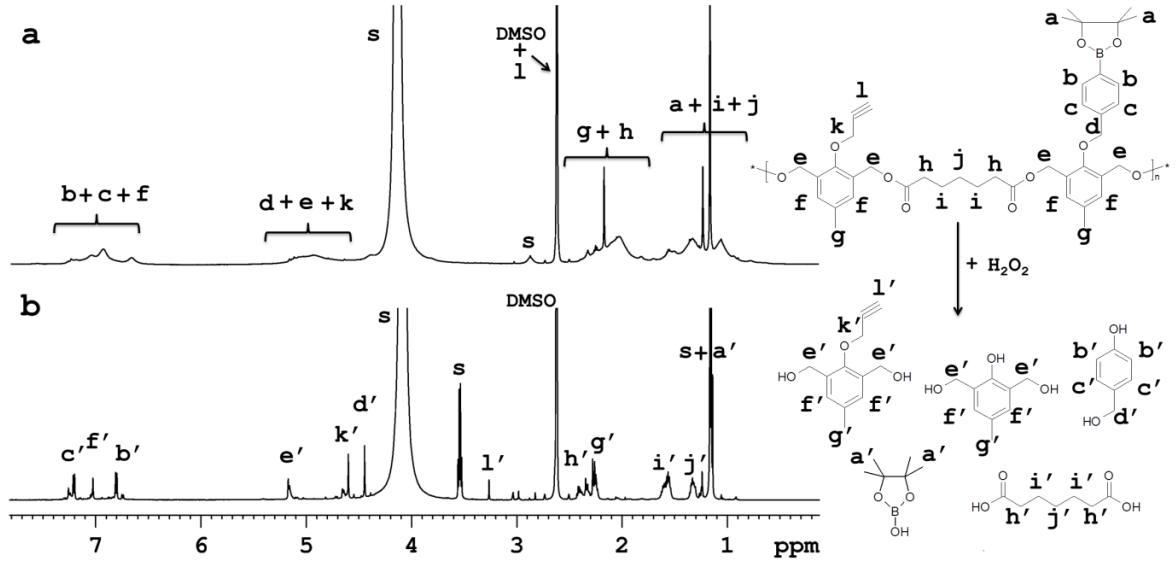

Fig. 4.6.4 ^{1}H NMR spectra of responsive polymer in d_6-DMSO, deuterium PBS (a) without H_2O_2 and (b) incubated with 50 mM H_2O_2 after 5 days at 310 K. "s" refers to solvent peaks.

Second system, self-immolative biodegradable polyoxalate prodrug based on the anticancer chemotherapeutic hormone analog diethylstilbestrol was synthesized via one-pot step-growth polymerization. The resulting polyprodrugs with varied amounts of DEB (PDEB1 ∼2.3 wt%; PDEB2 ∼7.5 wt% and PDEB3 ∼13.0 wt% of DEB) were obtained by varying the DEB, oxalyl chloride and CHD ratio (see Fig. 4.6.5). Successful polymer synthesis was confirmed by ^{1}H NMR (Fig. 4.6.5) and by size exclusion chromatography (SEC) analysis. The spectra depict the observed characteristic signals for protons belonging to the repeating units of monomers. Peaks assignments of the various proton types are shown in the spectrum and chemical structure of the polymer is shown in the same figure. The signals from protons of the DEB aromatic rings were detected at δ = 7.02 ppm (a) and δ = 6.87 ppm (b). The methylene (c) and methyl (d) protons of DEB where observed at δ = 2.09 and δ= 0.72 ppm respectively, whereas the signals attributed to the methylene group (e) of 1,4-Cyclohexanedimethanol monomer units are at δ = 4.00-4.30 ppm. The signals of the protons of the aliphatic cycle (f, g) are in the range between δ = 0.88-1.91 ppm. Similarly to the previous system, the degradation of PDEB1 upon incubation with of H_2O_2 was evaluated by ^{1}H NMR spectroscopy and was complete after 3 days of incubation (Fig. 4.6.6 top before H_2O_2 addition, middle after 24 h and bottom after 72 h). It is clearly visible that the broad peaks in ^{1}H NMR related to the polyprodrug are replaced by sharp peaks of the low-molecular-weight degradation products, confirming the self-immolative depolymerization triggered by H_2O_2.

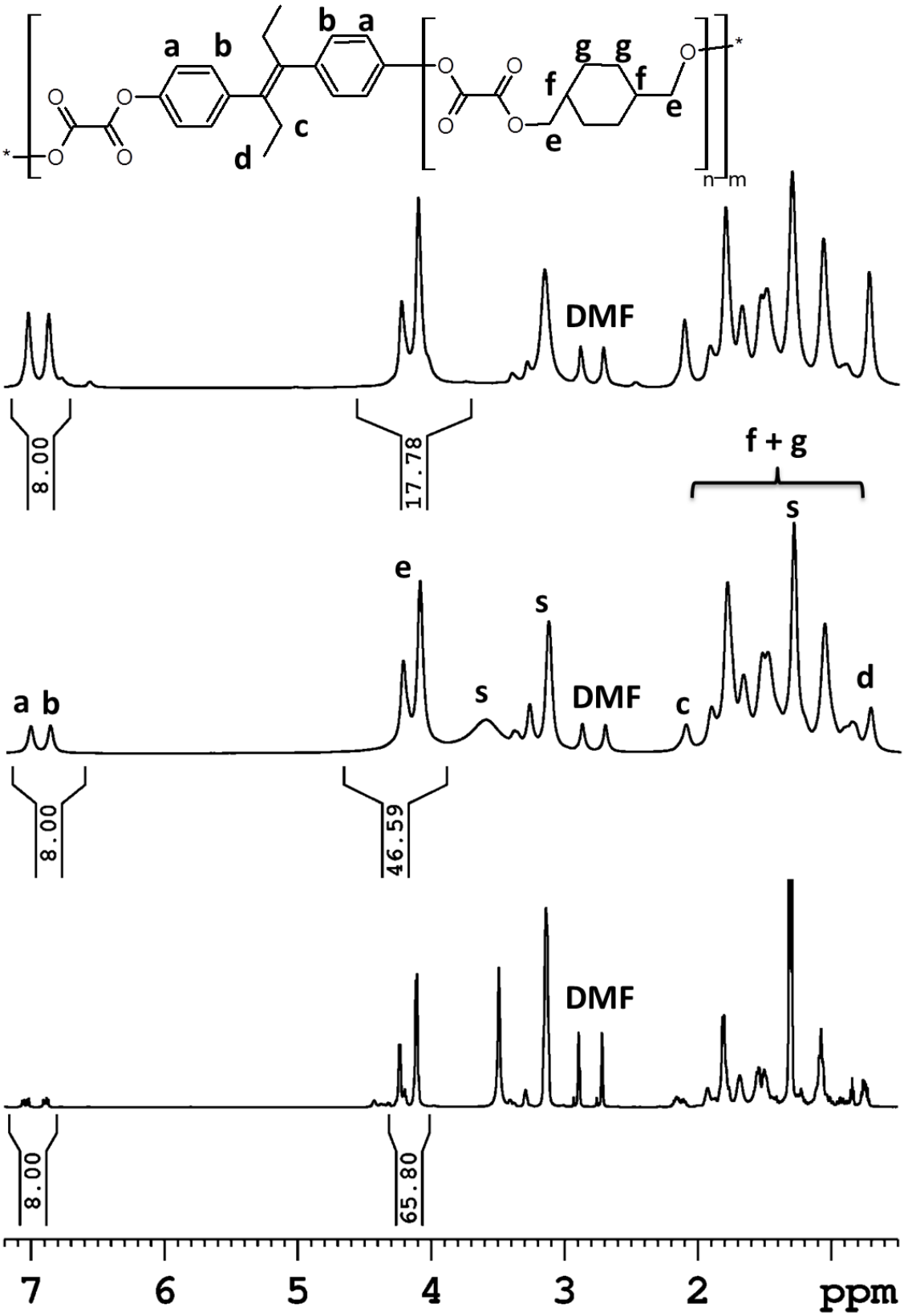

Fig. 4.6.5 ^{1}H NMR spectra of the synthesized polyprodrugs with different DEB moles ratio PDEB3 1~4 (top), PDEB2 1~12 (middle) and PDEB1 1~16 (bottom) in deuterated DMF, „s“ is related to solvents impurities.

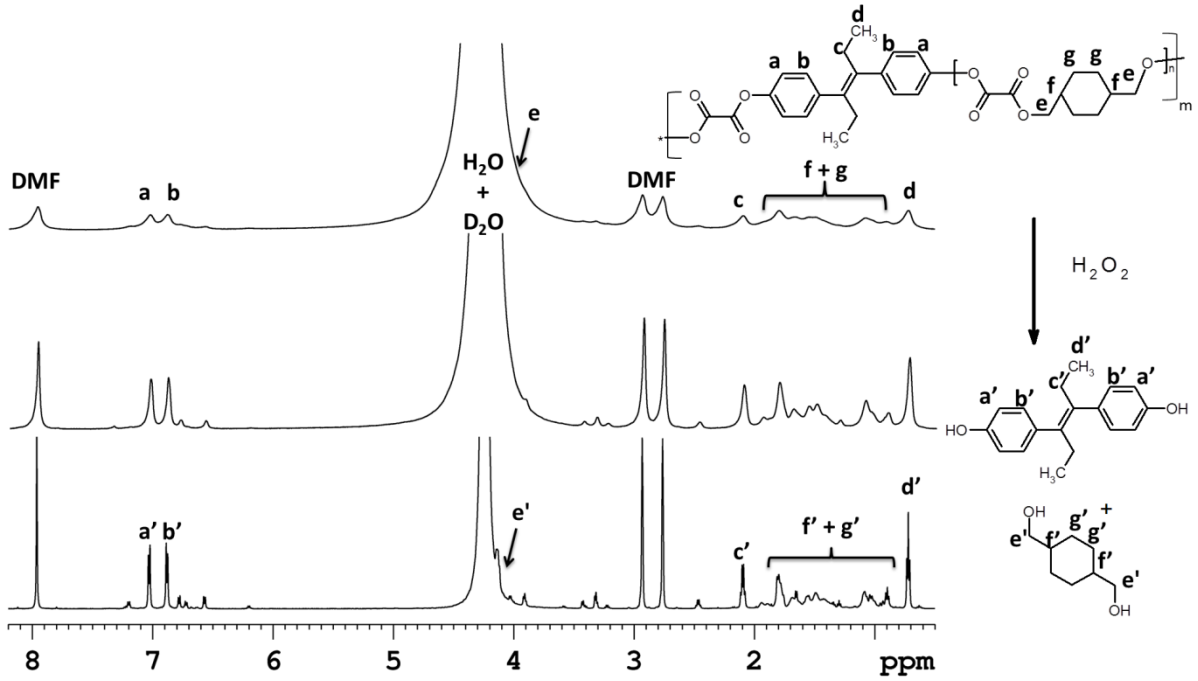

Fig. 4.6.6 ^{1}H NMR spectra of the synthesized ROS self-immolative PDEB1 polyprodrug (before H_2O_2 addition in PBS/DMF-d_7) (top) and the degradation upon incubation with 1 mM of H_2O_2 after 24 h (middle) and 72 h (bottom).

In summary of this part, ^{1}H and/or ^{13}C NMR spectroscopy were succesfully used for structrure determination, as well as degradation of novel pH and ROS responsive polymers for drug delivery systems.

5 Summary

In this work NMR spectroscopy methods were successfully used for structure characterization and study of behavior of temperature (chapters 4.1-4.5), pH and ROS (chapter 4.6) responsive polymer systems.

In chapter 4.1 ^{1}H NMR, 2D ^{1}H-^{1}H NOESY and ^{1}H spin-spin relaxation time T_2 measurements were used for the characterization of structural changes on molecular level and behavior of water molecules during the temperature-induced phase transition of thermoresponsive PEOx homopolymers and P(EOx-*grad*-MOx) copolymers in D_2O solutions. For D_2O solutions of PEOx homopolymers the phase transition is relatively sharp, irreversible, depends on molecular weight and concentration of the solution. An anomalous temperature was observed for PEOx solution of higher concentration (c = 20 wt%). For D_2O solutions of P(EOx-*grad*-MOx) gradient copolymers the same behavior for EOx and hydrophilic MOx units with very broad (~45 K) reversible transition (small hysteresis) which is virtually independent of the content of MOx units and molecular weight , and only slightly dependent on concentration of the solution phase transition was observed. ^{1}H spin-spin relaxation times T_2 of HDO measurements show a very similar behavior of the water molecules in homopolymer and copolymer solutions with two types of water; „free“ and „bound“ with long and very short T_2 values, detected at temperatures in the transition region and above the transition. 2D ^{1}H-^{1}H NOESY NMR spectra show that some EOx and MOx units are in close contact at room temperature. With increasing temperature the respective cross-peaks in NOESY spectra disappear though at 360 K there are still ~60-68% of copolymer segments that are directly detected in 1D ^{1}H NMR spectra.

In chapter 4.2 ^{1}H NMR spectra and ^{1}H spin-spin relaxation time T_2 NMR methods were used to study temperature behavior of NPs water solutions of terpolymers containing PEO, PEOx and PCL blocks with linear and non-linear architectures. As a result of ^{1}H NMR measurements in all investigated samples a broad transition with low p_{max} values (≈ 0.4) of PEOx blocks was observed. Similar behavior for the PEO blocks was detected. Furthermore, temperature behavior is affected by architecture of terpolymers and the PCL blocks play key role in this process. Spin-spin relaxation times T_2 measurements of HDO show different behavior of the water molecules in NPs solutions based on linear and Y-shape terpolymers.

In chapter 4.3 ^{1}H NMR, 2D ^{1}H-^{1}H NOESY and ^{1}H spin-spin relaxation time T_2 measurements were used for the characterization temperature behavior of D_2O solutions of thermoresponsive diblock PEO-*b*-PNIPAm copolymers and Y-shape triblock PEO-*b*-

$(PNIPAm)_2$ copolymers. Above the LCST the block copolymers form micelles with compact core created by immobilized PNIPAm blocks, and shell consisting mobile PEO blocks. LCST depends on the length of PNIPAm block, copolymer architecture and polymer concentration. T_2 measurements revealed the existence of water bound in micellar cores at temperatures above the LCST and behavior of water at this temperature with time depends on copolymer architecture. 2D NOESY NMR spectra also have shown difference in behavior of both types of the block copolymers.

In chapter 4.4 ^{1}H NMR spectra and ^{1}H spin-spin relaxation time T_2 NMR measurements were successfully used in characterization of interactions between components in the reaction mixture composed from the NIPAm, TEMED, PNIPAm and clay, as well as in the characterization of the behavior of reaction mixture during the cooling processes (to freezing). Moreover it was proved that NMR spectroscopy is a good method to study effects which have an impact on cryopolymerization kinetics.

In chapter 4.5, an effect of additives (three ketones, MEK, IMK, TBMK, with different concentrations) on phase transition of PVME aqueous solutions was studied by ^{1}H NMR and ^{1}H spin-spin relaxation time. LSCT and phase transition of PVME depend on hydrophobicity and concentration of the additive in the relation; more hydrophobic additive – broader transition width and lower LCST of polymer. Measurements of the T_2 values of HDO and TBMK provide evidence that water and additive molecules originally bound in polymer globules are with a time released from them.

Successful structure determination and degradation behavior of novel pH and ROS responsive polymer systems studied by ^{1}H and/or ^{13}C NMR spectroscopy is described in chapter 4.6.

6 References

1. Bloch, F., Hansen, W. W. & Packard, M. Nuclear Induction. *Phys. Rev.* **69,** 127 (1946).
2. Purcell, E. M., Torrey, H. C. & Pound, R. V. Resonance Absorption by Nuclear Magnetic Moments in a Solid. *Phys. Rev.* **69,** 37–38 (1946).
3. Spěváček, J. NMR investigations of phase transition in aqueous polymer solutions and gels. *Curr. Opin. Colloid Interface Sci.* **14,** 184–191 (2009).
4. Jacobsen, N. E. *NMR Spectroscopy Explained: Simplified Theory, Applications and Examples for Organic Chemistry and Structural Biology*. (John Wiley & Sons, Inc., Hoboken, New Jersey, 2007).
5. CLARIDGE, T. D. W. *High-Resolution NMR Techniques in Organic Chemistry*. (Elsevier Linacre House, Jordan Hill, Oxford OX2 8DP, UK Radarweg 29, PO Box 211, 1000 AE Amsterdam, The Netherlands, 2009).
6. Gil, E. S. & Hudson, S. M. Stimuli-reponsive polymers and their bioconjugates. *Progress in Polymer Science (Oxford)* **29,** 1173–1222 (2004).
7. Jeong, B. & Gutowska, A. Lessons from nature: Stimuli-responsive polymers and their biomedical applications. *Trends Biotechnol.* **20,** 305–311 (2002).
8. Kikuchi, A. & Okano, T. Intelligent thermoresponsive polymeric stationary phases for aqueous chromatography of biological compounds. *Prog. Polym. Sci.* **27,** 1165–1193 (2002).
9. Priya James, H., John, R., Alex, A. & Anoop, K. R. Smart polymers for the controlled delivery of drugs – a concise overview. *Acta Pharm. Sin. B* **4,** 120–127 (2014).
10. Kotsuchibashi, Y., Ebara, M., Aoyagi, T. & Narain, R. Recent advances in dual temperature responsive block copolymers and their potential as biomedical applications. *Polymers* **8,** (2016).
11. Osada, Y. & Gong, J. Stimuli-responsive polymer gels and their application to chemomechanical systems. *Progress in Polymer Science* **18,** 187–226 (1993).
12. Mendes, P. M. Stimuli-responsive surfaces for bio-applications. *Chem. Soc. Rev.* **37,** 2512 (2008).
13. Urban, M. W. Stratification, stimuli-responsiveness, self-healing, and signaling in polymer networks. *Prog. Polym. Sci.* **34,** 679–687 (2009).
14. Meng, H. & Li, G. A review of stimuli-responsive shape memory polymer composites. *Polymer (Guildf).* **54,** 2199–2221 (2013).
15. Colfen, H. Double-hydrophilic block copolymers: Synthesis and application as novel

surfactants and crystal growth modifiers. *Macromol. Rapid Commun.* **22,** 219–252 (2001).

16. Liu, F. & Urban, M. W. Recent advances and challenges in designing stimuli-responsive polymers. *Prog. Polym. Sci.* **35,** 3–23 (2010).
17. Manouras, T. & Vamvakaki, M. Field responsive materials: photo-, electro-, magnetic- and ultrasound-sensitive polymers. *Polym. Chem.* **8,** 74–96 (2017).
18. Aseyev, V. O., Tenhu, H. & Winnik, F. M. Temperature dependence of the colloidal stability of neutral amphiphilic polymers in water. *Adv. Polym. Sci.* **196,** 1–85 (2006).
19. Weder, C. Polymers react to stress. *Nature* **459,** 45–46 (2009).
20. Bertrand, O. & Gohy, J. Photo-responsive polymers: synthesis and applications. *Polym. Chem.* **8,** 52–73 (2017).
21. Chen, W. & Du, J. Ultrasound and pH Dually Responsive Polymer Vesicles for Anticancer Drug Delivery. *Sci. Rep.* **3,** 2162 (2013).
22. Zeng, H., Zhang, Y., Mao, S., Nakajima, H. & Uchiyama, K. A reversibly electro-controllable polymer brush for electro-switchable friction. *J. Mater. Chem. C* (2017). doi:10.1039/C7TC01624G
23. Park, I. K. *et al.* PH-responsive polymers as gene carriers. *Macromolecular Rapid Communications* **31,** 1122–1133 (2010).
24. Stubenrauch, K., Voets, I., Fritz-Popovski, G. & Trimmel, G. pH and ionic strength responsive polyelectrolyte block copolymer micelles prepared by ring opening metathesis polymerization. *J. Polym. Sci. Part A Polym. Chem.* **47,** 1178–1191 (2009).
25. Xu, Q., He, C., Xiao, C. & Chen, X. Reactive Oxygen Species (ROS) Responsive Polymers for Biomedical Applications. *Macromol. Biosci.* **16,** 635–646 (2016).
26. Bajpai, A. K., Bajpai, J., Saini, R. & Gupta, R. Responsive Polymers in Biology and Technology. *Polym. Rev.* **51,** 53–97 (2011).
27. Roy, D., Cambre, J. N. & Sumerlin, B. S. Future perspectives and recent advances in stimuli-responsive materials. *Progress in Polymer Science (Oxford)* **35,** 278–301 (2010).
28. Schattling, P., Jochum, F. D. & Theato, P. Multi-stimuli responsive polymers – the all-in-one talents. *Polym. Chem.* **5,** 25–36 (2014).
29. Cao, Z. Q. & Wang, G. J. Multi-Stimuli-Responsive Polymer Materials: Particles, Films, and Bulk Gels. *Chem. Rec.* 1398–1435 (2016). doi:10.1002/tcr.201500281
30. Zhuang, J., Gordon, M. R., Ventura, J., Li, L. & Thayumanavan, S. Multi-stimuli responsive macromolecules and their assemblies. *Chem. Soc. Rev.* **42,** 7421 (2013).

31. Ilmain, F., Tanaka, T. & Kokufuta, E. Volume transition in a gel driven by hydrogen bonding. *Nature* **349,** 400–401 (1991).
32. Huo, M., Yuan, J., Tao, L. & Wei, Y. Redox-responsive polymers for drug delivery: from molecular design to applications. *Polym. Chem.* **5,** 1519–1528 (2014).
33. Guragain, S., Bastakoti, B. P., Malgras, V., Nakashima, K. & Yamauchi, Y. Multi-Stimuli-Responsive Polymeric Materials. *Chem. - A Eur. J.* **21,** 13164–13174 (2015).
34. Chu, Z., Dreiss, C. A. & Feng, Y. Smart wormlike micelles. *Chem. Soc. Rev.* **42,** 7174 (2013).
35. Grubbs, R. B. & Sun, Z. Shape-changing polymer assemblies. *Chem. Soc. Rev.* **42,** 7436 (2013).
36. Kumar, A., Srivastava, A., Galaev, I. Y. & Mattiasson, B. Smart polymers: Physical forms and bioengineering applications. *Progress in Polymer Science (Oxford)* **32,** 1205–1237 (2007).
37. Gandhi, A., Paul, A., Sen, S. O. & Sen, K. K. Studies on thermoresponsive polymers: Phase behaviour, drug delivery and biomedical applications. *Asian J. Pharm. Sci.* **10,** 99–107 (2015).
38. De La Rosa, V. R. Poly(2-oxazoline)s as materials for biomedical applications. *J. Mater. Sci. Mater. Med.* **25,** 1211–1225 (2014).
39. Stuart, M. A. C. *et al.* Emerging applications of stimuli-responsive polymer materials. *Nat. Mater.* **9,** 101–113 (2010).
40. Bajpai, A. K., Shukla, S. K., Bhanu, S. & Kankane, S. Responsive polymers in controlled drug delivery. *Progress in Polymer Science (Oxford)* **33,** 1088–1118 (2008).
41. Du, F., Wang, Y., Zhang, R. & Li, Z. Intelligent nucleic acid delivery systems based on stimuli-responsive polymers. *Soft Matter* **6,** 835–848 (2010).
42. Zha, L., Banik, B. & Alexis, F. Stimulus responsive nanogels for drug delivery. *Soft Matter* **7,** 5908 (2011).
43. Kelley, E. G., Albert, J. N. L., Sullivan, M. O. & Epps, III, T. H. Stimuli-responsive copolymer solution and surface assemblies for biomedical applications. *Chem. Soc. Rev.* **42,** 7057 (2013).
44. Ward, M. A. & Georgiou, T. K. Thermoresponsive polymers for biomedical applications. *Polymers (Basel).* **3,** 1215–1242 (2011).
45. Ge, Z. & Liu, S. Functional block copolymer assemblies responsive to tumor and intracellular microenvironments for site-specific drug delivery and enhanced imaging performance. *Chem. Soc. Rev.* **42,** 7289 (2013).

46. Wei, M., Gao, Y., Li, X. & Serpe, M. J. Stimuli-responsive polymers and their applications. *Polym. Chem.* **8,** 127–143 (2017).
47. Edinger, D. & Wagner, E. Bioresponsive polymers for the delivery of therapeutic nucleic acids. *Wiley Interdiscip. Rev. Nanomedicine Nanobiotechnology* **3,** 33–46 (2011).
48. Chen, Z. *et al.* Fast and reversible thermoresponsive polymer switching materials for safer batteries. *Nat. Energy* **1,** 15009 (2016).
49. Cao, P., Mangadlao, J. D. & Advincula, R. C. Stimuli-Responsive Polymers and their Potential Applications in Oil-Gas Industry. *Polym. Rev.* **55,** 706–733 (2015).
50. Gibson, M. I. & O'Reilly, R. K. To aggregate, or not to aggregate? considerations in the design and application of polymeric thermally-responsive nanoparticles. *Chem. Soc. Rev.* **42,** 7204–7213 (2013).
51. Kouřilová, H., Spěváček, J. & Hanyková, L. 1H NMR study of temperature-induced phase transitions in aqueous solutions of poly(N-isopropylmethacrylamide)/poly(N-vinylcaprolactam) mixtures. *Polym. Bull.* **70,** 221–235 (2013).
52. Hanyková, L. *et al.* Phase transition in hydrogels of thermoresponsive semi-interpenetrating and interpenetrating networks of poly(N,N-diethylacrylamide) and polyacrylamide. *Eur. Polym. J.* **85,** 1–13 (2016).
53. Zhou, J., Wang, G., Hu, J., Lu, X. & Li, J. Temperature, ionic strength and pH induced electrochemical switching of smart polymer interfaces. *Chem. Commun.* 4820 (2006). doi:10.1039/b611405a
54. Flory, P. J. Statistical Mechanics of Dilute Polymer Solutions. *J. Chem. Phys.* **17,** 1347–1348 (1949).
55. Rusu, M., Wohlrab, S., Kuckling, D., Möhwald, H. & Schönhoff, M. Coil-to-Globule Transition of PNIPAM Graft Copolymers with Charged Side Chains: A 1H and 2H NMR and Spin Relaxation Study. *Macromolecules* **39,** 7358–7363 (2006).
56. Allen, G. & Baker, C. H. Lower Critical Solution Phenomena in Polymer-Solvent Systems. *Polymer (Guildf).* **6,** 181–191 (1965).
57. Freeman, P. I. & Rowlinson, J. S. Lower Critical Points in Polymer Solutions. *Polymer (Guildf).* **1,** 20–26 (1960).
58. Southall, N. T., Dill, K. A. & Haymet, A. D. J. A View of the Hydrophobic Effect. *J. Phys. Chem. B* **106,** 521–533 (2002).
59. Weber, C., Hoogenboom, R. & Schubert, U. S. Temperature responsive bio-compatible polymers based on poly(ethylene oxide) and poly(2-oxazoline)s. *Prog. Polym. Sci.* **37,**

686–714 (2012).

60. Dimitrov, I., Trzebicka, B., Mu, A. H. E. & Dworak, A. Thermosensitive water-soluble copolymers with doubly responsive reversibly interacting entities. *Prog. Polym. Sci.* **32,** 1275–1343 (2007).
61. Roy, D., Brooks, W. L. A. & Sumerlin, B. S. New directions in thermoresponsive polymers. *Chem. Soc. Rev.* **42,** 7214 (2013).
62. Aseyev, V., Tenhu, H. & Winnik, F. M. in *Advances in Polymer Science* 29–89 (2010). doi:10.1007/12_2010_57
63. Heskins, M. & Guillet, J. E. Solution Properties of Poly(N-isopropylacrylamide). *J. Macromol. Sci. Part A - Chem.* **2,** 1441–1455 (1968).
64. Halperin, A., Kroeger, M. & Winnik, F. M. Poly(N-isopropylacrylamide) Phase Diagrams: Fifty Years of Research. *Angew. Chemie - Int. Ed.* **54,** 15342–15367 (2015).
65. Schild, H. G. Poly(N-isopropylacrylamide): experiment, theory and application. *Prog. Polym. Sci.* **17,** 163–249 (1992).
66. Dai, S. & Chiu, K. Thermo- and photo-responsive polymeric systems. *Soft Matter* **5,** 2513–2533 (2009).
67. Schmaljohann, D. Thermo- and pH-responsive polymers in drug delivery. *Adv. Drug Deliv. Rev.* **58,** 1655–1670 (2006).
68. Fujishige, S., Kubota, K. & Ando, I. Phase transition of aqueous solutions of poly(N-isopropylacrylamide) and poly(N-isopropylmethacrylamide). *J. Phys. Chem.* **93,** 3311–3313 (1989).
69. Ito, D. & Kubota, K. Solution Properties and Thermal Behavior of Poly (N - n - propylacrylamide) in Water. *Macromolecules* **30,** 7828–7834 (1997).
70. Maeda, Y., Nakamura, T. & Ikeda, I. Changes in the Hydration States of Poly (N - n - propylmethacrylamide) and Poly (N -isopropylmethacrylamide) during Their Phase Transitions in Water Observed by FTIR Spectroscopy. *Macromolecules* **34,** 8246–8251 (2001).
71. Idziak, I., Avoce, D., Lessard, D., Gravel, D. & Zhu, X. X. Thermosensitivity of Aqueous Solutions of Poly(N,N -diethylacrylamide). *Macromolecules* **32,** 1260–1263 (1999).
72. Akiyama, Y., Shinohara, Y., Hasegawa, Y., Kikuchi, A. & Okano, T. Preparation of Novel Acrylamide-Based Thermoresponsive Polymer Analogues and Their Application as Thermoresponsive Chromatographic Matrices. *J. Polym. Sci. Part A-Polymer Chem.* **46,** 5471–5482 (2008).

73. Aoki, T., Muramatsu, M., Torii, T., Sanui, K. & Ogata, N. Thermosensitive Phase Transition of an Optically Active Polymer in Aqueous Milieu. *Macromolecules* **34,** 3118–3119 (2001).

74. Zou, Y., Brooks, D. E. & Kizhakkedathu, J. N. A Novel Functional Polymer with Tunable LCST. *Macromolecules* **41,** 5393–5405 (2008).

75. Huang, X., Du, F., Ju, R. & Li, Z. Novel Acid-Labile , Thermoresponsive Poly (methacrylamide) s with Pendent Ortho Ester Moieties a. *Macromol. Rapid Commun.* **28,** 597–603 (2007).

76. Huang, X., Du, F., Zhang, B. O., Zhao, J. & Li, Z. Acid-labile , Thermoresponsive (Meth) acrylamide Polymers with Pendant Cyclic Acetal Moieties. *J. Polym. Sci. Part A-Polymer Chem.* **46,** 4332–4343 (2008).

77. Starovoytova, L., Spěváček, J., Hanyková, L. & Ilavský, M. 1H NMR study of phase transition of uncharged and negatively charged poly(N-isopropylmethacrylamide) in D2O solutions. *Macromol. Symp.* **203,** 239–246 (2003).

78. Yuri E. Kirsh. *Water soluble poly-N-vinylamides: synthesis and physicochemical properties*. (Wiley & Sons, 1998).

79. Tager, A. A., Safronov, A. P., Berezyuk, E. A. & Galaev, I. Y. Lower critical solution temperature and hydrophobic hydration in aqueous polymer solutions. *Colloid Polym. Sci.* **272,** 1234–1239 (1994).

80. Vihola, H., Laukkanen, A., Valtola, L., Tenhu, H. & Hirvonen, J. Cytotoxicity of thermosensitive polymers poly (N -isopropylacrylamide), poly (N -vinylcaprolactam) and amphiphilically modified poly (N -vinylcaprolactam). *Biomaterials* **26,** 3055–3064 (2005).

81. Lau, A. C. W. & Wu, C. Thermally Sensitive and Biocompatible Poly(N-vinylcaprolactam): Synthesis and Characterization of High Molar Mass Linear Chains. *Macromolecules* **32,** 581–584 (1999).

82. Maeda, Y., Nakamura, T. & Ikeda, I. Hydration and Phase Behavior of Poly (N-vinylcaprolactam) and Poly (N-vinylpyrrolidone) in Water. *Macromolecules* **32,** 217–222 (2002).

83. Suwa, K. *et al.* Synthesis and functionalities of poly(N-vinylalkylamide). IV. Synthesis and free radical polymerization of N-vinylisobutyramide and thermosensitive properties of the polymer. *J. Polym. Sci. Part A Polym. Chem.* **35,** 1763–1768 (1997).

84. Sedlacek, O., Monnery, B. D., Filippov, S. K., Hoogenboom, R. & Hruby, M. Poly(2-oxazoline)s - Are they more advantageous for biomedical applications than other

polymers? *Macromol. Rapid Commun.* **33,** 1648–1662 (2012).

85. Hoogenboom, R. Poly(2-oxazoline)s: A polymer class with numerous potential applications. *Angew. Chemie - Int. Ed.* **48,** 7978–7994 (2009).
86. Christova, D., Velichkova, R., Loos, W., Goethals, E. J. & Du Prez, F. New thermo-responsive polymer materials based on poly(2-ethyl-2-oxazoline) segments. *Polymer (Guildf).* **44,** 2255–2261 (2003).
87. Hoogenboom, R. *et al.* Tuning the LCST of poly(2-oxazoline)s by varying composition and molecular weight: alternatives to poly(N-isopropylacrylamide)? *Chem. Commun. (Camb).* 5758–5760 (2008). doi:10.1039/b813140f
88. Alexandridis, P. & Hatton, T. A. Poly(ethylene oxide)-poly(propylene oxide)-poly(ethylene oxide) block copolymer surfactants in aqueous solutions and at interfaces: thermodynamics, structure, dynamics, and modeling. *Colloids Surfaces A Physicochem. Eng. Asp.* **96,** 1–46 (1995).
89. Alexandridis, P., Athanassiou, V. & Hatton, T. A. Pluronic-P105 PEO-PPO-PEO Block Copolymer in Aqueous Urea Solutions: Micelle Formation, Structure, and Microenvironment. *Langmuir* **11,** 2442–2450 (1995).
90. Kříž, J. & Dybal, J. Cooperative Preassociation Stages of PEO−PPO−PEO Triblock Copolymers: NMR and Theoretical Study. *J. Phys. Chem. B* **114,** 3140–3151 (2010).
91. Pitto-Barry, A. & Barry, N. P. E. Pluronic® block-copolymers in medicine: from chemical and biological versatility to rationalisation and clinical advances. *Polym. Chem.* **5,** 3291–3297 (2014).
92. Han, S., Hagiwara, M. & Ishizone, T. Synthesis of Thermally Sensitive Water-Soluble Polymethacrylates by Living Anionic Polymerizations of Oligo(ethylene glycol) Methyl Ether Methacrylates. *Macromolecules* **36,** 8312–8319 (2003).
93. Lutz, J. F. Thermo-switchable materials prepared using the OEGMA-platform. *Adv. Mater.* **23,** 2237–2243 (2011).
94. Lutz, J. F. & Hoth, A. Preparation of ideal PEG analogues with a tunable thermosensitivity by controlled radical copolymerization of 2-(2-methoxyethoxy)ethyl methacrylate and oligo(ethylene glycol) methacrylate. *Macromolecules* **39,** 893–896 (2006).
95. Lutz, J.-F., Weichenhan, K., Akdemir, Ö. & Hoth, A. About the Phase Transitions in Aqueous Solutions of Thermoresponsive Copolymers and Hydrogels Based on 2-(2-methoxyethoxy)ethyl Methacrylate and Oligo(ethylene glycol) Methacrylate. *Macromolecules* **40,** 2503–2508 (2007).

96. Maeda, Y. IR Spectroscopic Study on the Hydration and the Phase Transition of Poly(vinyl methyl ether) in Water. *Langmuir* **17,** 1737–1742 (2001).
97. Hanyková, L., Spěváček, J. & Ilavský, M. 1H NMR study of thermotropic phase transition of linear and crosslinked poly(vinyl methyl ether) in D2O. *Polymer (Guildf).* **42,** 8607–8612 (2001).
98. Aoshima, S., Oda, H. & Kobayashi, E. Synthesis of thermally-induced phase separating polymer with well-defined polymer structure by living cationic polymerization. I. Synthesis of poly(vinyl ether)s with oxyethylene units in the pendant and its phase separation behavior in aqueous solution. *J. Polym. Sci. Part A Polym. Chem.* **30,** 2407–2413 (1992).
99. Iwasaki, Y., Wachiralarpphaithoon, C. & Akiyoshi, K. Novel thermoresponsive polymers having biodegradable phosphoester backbones. *Macromolecules* **40,** 8136–8138 (2007).
100. Lee, S. B., Song, S.-C., Jin, J. & Sohn, Y. S. Structural and Thermosensitive Properties of Cyclotriphosphazenes with Poly(ethylene glycol) and Amino Acid Esters as Side Groups. *Macromolecules* **34,** 7565–7569 (2001).
101. Lee, B. H., Lee, Y. M., Sohn, Y. S. & Song, S. A Thermosensitive Poly(organophosphazene) Gel. *Macromolecules* **35,** 3876–3879 (2002).
102. Allcock, H. R., Pucher, S. R., Turner, M. L. & Fitzpatrick, R. J. Poly(organophosphazenes) with poly(alkyl ether) side groups: a study of their water solubility and the swelling characteristics of their hydrogels. *Macromolecules* **25,** 5573–5577 (1992).
103. Boutris, C., Chatzi, E. G. & Kiparissides, C. Characterization of the LCST behaviour of aqueous poly(N-isopropylacrylamide) solutions by thermal and cloud point techniques. *Polymer (Guildf).* **38,** 2567–2570 (1997).
104. Meier-Koll, A., Pipich, V., Busch, P., Papadakis, C. M. & Müller-Buschbaum, P. Phase separation in semidilute aqueous poly(N-isopropylacrylamide) solutions. *Langmuir* **28,** 8791–8798 (2012).
105. Guo, H. *et al.* Thermoresponsive Toughening in LCST-Type Hydrogels with Opposite Topology: From Structure to Fracture Properties. *Macromolecules* **49,** 4295–4306 (2016).
106. Lyngsø, J. *et al.* Small-angle X-ray scattering studies of thermoresponsive poly(N -isopropylacrylamide) star polymers in water. *Macromolecules* **48,** 2235–2243 (2015).
107. Yamauchi, H. & Maeda, Y. LCST and UCST behavior of poly(N-isopropylacrylamide)

in DMSO/water mixed solvents studied by IR and micro-raman spectroscopy. *J. Phys. Chem. B* **111,** 12964–12968 (2007).

108. Shiraga, K., Naito, H., Suzuki, T., Kondo, N. & Ogawa, Y. Hydration and hydrogen bond network of water during the Coil-to-Globule transition in poly(N -isopropylacrylamide) aqueous solution at cloud point temperature. *J. Phys. Chem. B* **119,** 5576–5587 (2015).
109. Spěváček, J., Dybal, J., Starovoytova, L., Zhigunov, A. & Sedláková, Z. Temperature-induced phase separation and hydration in poly(N-vinylcaprolactam) aqueous solutions: a study by NMR and IR spectroscopy, SAXS, and quantum-chemical calculations. *Soft Matter* **8,** 6110 (2012).
110. Spěváček, J. & Dybal, J. Temperature-Induced Phase Separation and Hydration in Aqueous Polymer Solutions Studied by NMR and IR Spectroscopy: Comparison of Poly(N -vinylcaprolactam) and Acrylamide-Based Polymers. *Macromol. Symp.* **336,** 39–46 (2014).
111. Bloksma, M. M. *et al.* Poly(2-cyclopropyl-2-oxazoline): From rate acceleration by cyclopropyl to thermoresponsive properties. *Macromolecules* **44,** 4057–4064 (2011).
112. Saeed, A., Georget, D. M. R. & Mayes, A. G. Solution thermal properties of a family of thermo-responsive N-isopropyl acrylamide-co-N-hydroxymethyl acrylamide copolymers - Aspects intrinsic to the polymers. *React. Funct. Polym.* **72,** 77–82 (2012).
113. Diab, C., Akiyama, Y., Kataoka, K. & Winnik, F. M. Microcalorimetric Study of the Temperature-Induced Phase Separation in Aqueous Solutions of Poly(2-isopropyl-2-oxazolines). *Macromolecules* **37,** 2556–2562 (2004).
114. Zhang, Q., Weber, C., Schubert, U. S. & Hoogenboom, R. Thermoresponsive polymers with lower critical solution temperature: from fundamental aspects and measuring techniques to recommended turbidimetry conditions. *Mater. Horiz.* **4,** 109–116 (2017).
115. Chen, J., Spěváček, J. & Hanyková, L. NMR Methods to Study Effects of Additives on Phase Separation of Thermoresponsive Polymer. *Macromol. Symp.* **339,** 24–32 (2014).
116. Kocak, G., Tuncer, C. & Bütün, V. pH-Responsive polymers. *Polym. Chem.* **8,** 144–176 (2017).
117. Bazban-Shotorbani, S. *et al.* Revisiting structure-property relationship of pH-responsive polymers for drug delivery applications. *J. Control. Release* **253,** 46–63 (2017).
118. Roy, S. G. & De, P. pH responsive polymers with amino acids in the side chains and their potential applications. *J. Appl. Polym. Sci.* **131,** 41084 (2014).

119. Pang, X. *et al.* pH-responsive polymer–drug conjugates: Design and progress. *J. Control. Release* **222,** 116–129 (2016).
120. Yin, J., Chen, Y., Zhang, Z. H. & Han, X. Stimuli-responsive block copolymer-based assemblies for cargo delivery and theranostic applications. *Polymers* **8,** (2016).
121. Mathew, A., Cho, K.-H., Uthaman, S., Cho, C. & Park, I. Stimuli-Regulated Smart Polymeric Systems for Gene Therapy. *Polymers (Basel).* **9,** 152 (2017).
122. Song, C.-C., Du, F.-S. & Li, Z.-C. Oxidation-responsive polymers for biomedical applications. *J. Mater. Chem. B* **2,** 3413–3426 (2014).

7 Appendix

7.1 List of other publications not included in the thesis

1. V. Patsula, E. Petrovský, J. Kovářová, R. Konefał, D. Horák „Monodisperse superparamagnetic nanoparticles by thermolysis of Fe(III) oleate and mandelate complexes", Colloid and Polymer Science, 2014, 292, 9, 2097-2110.
2. E. Jäger, R. K Donato, M. Perchacz, A. Jäger, F. Surman, A. Höcherl, R. Konefal, K. Donato, C. G. Venturini, V. Bergamo, H. S. Schrekker, A. M. Fuentefri, M. G. Raucci, L. Ambrosio, P. Stepanek "Biocompatible succinic acid-based polyesters for potential biomedical applications: fungal biofilm inhibition and mesenchymal stem cell growth" RSC Advances, 5, 104 (2015), 85756-85766
3. M. Rabyk, M. Hruby, M. Vetrik, J. Kucka, V. Proks, M. Parizek, R. Konefal, P. Krist, D. Chvatil, L. Bacakova, M. Slouf, P. Stepanek "Modified glycogen as construction material for functional biomimetic microfibers" Carbohydrate Polymers, 152, 2016, 271-279
4. S. Petrova, D. Klepac, R. Konefał, S. Kereiche, L. Kováčik, S. K. Filippov "Synthesis and solution properties of PCL-b-PHPMA diblock copolymers containing stable nitroxyl radicals" Macromolecules, 49, 15 (2016), 5407-5417
5. V. Patsula, L. Kosinová, M. Lovrić, L. Ferhatovic Hamzić, M. Rabyk, R. Konefal, A. Paruzel, M. Šlouf, V. Herynek, S. Gajović, D. Horák "Superparamagnetic Fe3O4 nanoparticles: synthesis by thermal decomposition of iron(III) glucuronate and application in magnetic resonance imaging" ACS Applied Materials & Interfaces, 8, 11 (2016), 7238-7247
6. O. Sedlacek, P. Cernoch, J. Kucka, R. Konefal, P. Stepanek, M. Vetrik, T. P. Lodge, M. Hruby "Thermoresponsive polymers for nuclear medicine: which polymer is the best?" Langmuir, 32, 24 (2016), 6115-6122
7. J. Trousil, S. K. Filippov, M. Hrubý, T. Mazel, Z. Syrová, D. Cmarko, S. Svidenská, J. Matějková, L. Kováčik, B. Porsch, R. Konefał, R. Lund, B. Nyström, I. Raška, P. Štěpánek "System with embedded drug release and nanoparticle degradation sensor showing efficient rifampicin delivery into macrophages" Nanomedicine: Nanotechnology, Biology and Medicine, 13, 1 (2017), 307-315
8. H. Mackova, Z. Plichta, H. Hlidkova, O. Sedlacek, R. Konefal, Z. Sadakbayeva, M.

Duskova-Smrckova, D. Horák, S. Kubinova, “Reductively degradable poly(2-hydroxyethyl methacrylate) hydrogels with oriented porosity for tissue engineering applications”, ACS Appl. Mater. Interfaces, 9, 12 (2017), 10544-10553

9. P. Bojarová, P. Chytil, B. Mikulová, L. Bumba, R. Konefal, H. Pelantová, J. Krejzová, K. Slamova, L. Petrásková, L. Kotrchová, J. Cvačka, T. Etrych, V. Kren, “ Glycan-decorated HPMA copolymers as high-affinity lectin ligands“, Polym. Chem., 8, 13 (2017), 1999-2004
10. M. Perchacz, R. Donato, L. Seixas, A. Zhigunov, R. Konefal, M. Serkis-Rodzeń, H. Benes, “Ionic liquid-silica precursors via solvent-free sol-gel process and their application in epoxy-amine network: a theoretical-experimental study”, ACS Applied Materials & Interfaces, 9, 19, (2017), 16474-16487
11. J. Brus, M. Urbanová, J. Czernek, M. Pavelkova, K. Kubova, J. Vyslouzil, S. Abbrent, R. Konefal, J. Horsky, D. Vetchy, J. Vysloužil, P. Kulich, “Structure and dynamics of alginate gels cross-linked by polyvalent ions probed via solid state NMR spectroscopy”, Biomacromolecules, 18, 8, (2017), 2478-2488
12. M. Holubova, R. Konefał, Z. Moravkova, A. Zhigunov, J. Svoboda, O. Pop-Georgievski, J. Hromadkova, O. Groborz, P. Stepanek, M. Hruby, “Carbon nanospecies affecting amyloid formation”, RSC Advances, 7, 85, (2017), 53887-53898
13. M. Studenovsky, L. Sivak, O. Sedlacek, R. Konefal, V. Horkova, T. Etrych, M. Kovar, B. Rihova, M. Sirova, “Polymer nitric oxide donors potentiate the treatment of experimental solid tumours by increasing drug accumulation in the tumour tissue”, Journal of Controlled Release, 269, (2018), 214-224
14. A. Jäger, E. Jäger, F. C. Giacomelli, F. Nallet, M. Steinhart, J.-L. Putaux, R. Konefal J. Spěváček, K. Ulbrich, P. Štěpánek, “Structural changes on polymeric nanoparticles induced by hydrophobic drug entrapment”, Colloids and Surfaces A-Physicochemical and Engineering Aspects, 538, (2018), 238-249

Additionally active participation in 11 international conferences, and co-author of other 19 presentations at scientific meetings.